THESIS

MECHANISMS OF SUPERCONDUCTIVITY IN DEGENERATE SEMICONDUCTORS

YASUTAMI TAKADA

Department of Physics
Faculty of Science
University of Tokyo

MECHANISMS OF SUPERCONDUCTIVITY IN DEGENERATE SEMICONDUCTORS

A Dissertation

Presented to

the Faculty of Science

the University of Tokyo

In Partial Fulfillment of the Requirements

for the Degree of Ph.D. in Physics

---

by

Yasutami TAKADA

December 1978

ACKNOWLEDGEMENTS

The author would like to express his sincerest gratitude to Professor Yasutada Uemura for his kind advices and continual guidance. He is greatly indebted to Professor T. Ando for a number of comments and stimulating discussions. He is also grateful to Professor S. Kawaji for kindly showing him his experimental results prior to publication and for valuable discussions. He is pleased to acknowledge useful discussions with Professor H. Kamimura, Professor K. Nakao, Professor M. Tsukada, Dr. F. J. Ohkawa, Dr. Y. Kuramoto, Dr. H. Aoki and all the members of the research group under Professor Y. Uemura and Professor H. Kamimura. His thanks are also extended to Professor R. Aoki for giving him some information about $SrTiO_3$. Especial thanks are due to Miss Y. Yamazaki and Mrs. N. Kashiwabara for typing his thesis. Finally, he wishes to thank his parents for many years of upbringing and encouragements.

BIOGRAPHICAL NOTE

The author was born in Awaji Island in Hyogo Prefecture on the ninth of October, 1950. He graduated from the University of Tokyo in 1974 and has received his M. Sc. degree in Physics from the University of Tokyo in 1976.

LIST OF PAPERS SUBMITTED FOR THE REQUIREMENT OF THE DEGREE

(1) "Plasmon Mechanism of Superconductivity in Two- and Three-Dimensional Electron Systems", Y. Takada, *J. Phys. Soc. Japan* 45, 786 (1978).

(2) "Theory of Superconductivity in Polar Semiconductors and its Application to Semiconducting $SrTiO_3$", Y. Takada, to be submitted to *Phys. Rev.* B.

(3) "First-Principle Calculation of Superconducting Transition Temperature of MOS Inversion Layers", Y. Takada, to be submitted to *J. Phys. Soc. Japan.*

LIST OF RELATED PAPERS ADDED FOR REFERENCES

(1) "Acoustic Plasmon and Possibility of Superconductivity in MOS Structures", Y. Takada and Y. Uemura, *Proceedings of the 13-th International Conference on Physics of Semiconductors, Rome*, 1976, *p.* 754.

(2) "Subband Structures of *N*-Channel Inversion Layers on *III-V* Compounds — A Possibility of the Gate Controlled Gunn Effect —", Y. Takada and Y. Uemura, *J. Phys. Soc. Japan* 43, 139 (1977).

(3) "Acoustic Plasmons in MOS Inversion Layers", Y. Takada, *J. Phys. Soc. Japan* 43, 1627 (1977).

(4) "Stress Effects on Electronic Properties of Silicon Inversion Layers", Y. Takada and T. Ando, *J. Phys. Soc. Japan* 44, 905 (1978).

(5) "Effects of Screening and Neutral Impurity on Mobility in Silicon Inversion Layers under Uniaxial Stress", Y. Takada, *J. Phys. Soc. Japan* 46, 114 (1979).

CONTENTS

INTRODUCTION

Phenomena of superconductivity are very interesting from both physical and technological points of view. Microscopically, these phenomena stem from the condensation of a macroscopic number of electron pairs. This electron pair is usually believed to be formed by an attractive interaction brought about by the virtual exchange of phonons between the electrons. In metallic superconductors, this phonon mechanism of superconductivity is confirmed experimentally. In addition, theoretical calculations can reproduce the observed superconducting transition temperature T_c well.

In low-carrier-concentration systems such as degenerate semiconductors, however, the situation is a little different from that in metals. The Fermi energy ε_f becomes of the order of the Debye energy ω_D. Since the conventional method to calculate T_c in metallic superconductors makes full use of the smallness of the parameter ω_D/ε_f, we cannot apply this conventional method to the discussion of superconductivity in degenerate semiconductors immediately. In particular, the idea of the Coulomb pseudopotential μ^* adopted in the usual theory of superconductivity in metals does not seem to be appropriate to the case of $\omega_D \simeq \varepsilon_f$.

Thus in this thesis, we develop a new numerical method of calculating T_c in which the effect of the Coulomb interaction on superconductivity is taken into account much more accurately than in the method hitherto applied to the calculation of T_c.

The method presented here opens several new aspects of the mechanisms of superconductivity. The effect of the plasmon on superconductivity is studied quantitatively and the possibility of the plasmon mechanism of superconductivity is considered for the first time. The change of the contribution of phonons to superconductivity with the increase of the parameter ω_D/ε_f is examined. Superconductivity in multi-carrier systems is discussed in order to make a quantitative study of the acoustic plasmon mechanism of superconductivity. The interrelation of the phonon, the plasmon, and the acoustic plasmon mechanisms of superconductivity is also clarified.

The present thesis is organized as follows. In chapter I, we formulate the new method to calculate T_c from the first principles. Only the weak-coupling approximation is employed in the derivation of the present method and T_c can be determined without any adjustable parameters like μ^*. In the latter part of this chapter, this method is applied to a quantitative investigation of the role of the plasmon in superconductivity in the electron-gas system. In contrast with the case of phonons, the plasmon induces a long-range attractive interaction between electrons. When the carrier density of the system is low enough to give the r_s-parameter of the system larger than about six, this attractive interaction becomes so large that even the

electron-gas system is suggested to become superconducting only with the aid of the plasmon. The bound state of the Cooper pair in this plasmon mechanism is a little different from that in the phonon mechanism. This difference is shown by a simple physical picture. In the end of this chapter, we make a discussion on the validity of the plasmon mechanism of superconductivity from various points of view and come to the conclusion that the electron-gas system with $r_s \gtrsim 6$ has a superconducting instability with the aid of the plasmon, provided that the system is not in the ordered states with diagonal long-range order like the Wigner-lattice one, but in the normal metallic state with a definite Fermi surface.

Chapter II is devoted to the investigation of superconductivity in polar semiconductors. A few workers have already studied this problem, but none of them have noticed the importance of the plasmon in these materials. Thus we include the contribution of the plasmon and examine the interplay of the plasmon and the polar optic phonon in the superconductivity. This general theory is applied to the explanation of the superconductivity in semiconducting $SrTiO_3$. $SrTiO_3$ is a highly polarizable material and the static dielectric constant becomes as large as 10^4 at low temperatures. By doping, we can have an n-type semiconducting $SrTiO_3$ whose carrier concentration n can be varied from 10^{18}cm^{-3} to $6\times10^{20}\text{cm}^{-3}$. Superconductivity is observed in this material and the dependence of T_c on n and also on the stress is known to be peculiar: As n is increased, T_c has a maximum of the order of 0.3 K at $n \sim 10^{20}\text{cm}^{-3}$. Under the hydrostatic pressure, T_c

decreases, while T_c increases when the uniaxial stress of the order of 1 kb along the [100] direction is applied. In the present thesis, this behavior is explained in the plasmon-ferroelectric soft phonon mechanism of superconductivity. The observed curve of T_c as a function of n and the stress is reproduced quite well by the first-principle calculation without any adjustable parameters. This fact seems to support the validity of the present theory.

In chapter III, the possibility of superconductivity in an inversion layer at the Metal-Oxide-Semiconductor (MOS) junction is investigated. In this MOS structure, the motion of electrons perpendicular to the interface is quantized. Thus the system has a two-dimensional character and the dispersion relation of the plasmon is proportional to $\sqrt{q}$ for small wave numbers q. Owing to this property, the contribution of the plasmon to superconductivity is larger in this system than in bulk ones, which suggests that an MOS system may be a good one for the observation of the plasmon mechanism of superconductivity. As an example of real systems, an n-channel inversion layer at the $Si(100)/SiO_2$ interface is treated and is predicted to have T_c in the plasmon mechanism of the order of 1 mK, when the carrier density is less than about $5\times10^{11}cm^{-2}$. In the latter part of this chapter, superconductivity in a two-subband system is discussed to investigate the effect of the acoustic plasmon which is the characteristic collective mode in such a multi-carrier system. The interplay of the plasmon and the acoustic plasmon is also clarified. Results in chapters II and III lead us to

the conclusion that in low-carrier-concentration systems, the effect of the plasmon on superconductivity should be taken into account. In particular, when each energy of the modes in the system is larger than the Fermi energy, the plasmon plays the main role in superconductivity and other modes such as phonons and acoustic plasmons, even if they exist, do not contribute much to superconductivity.

CHAPTER I

GENERAL ASPECTS OF MECHANISMS OF SUPERCONDUCTIVITY

Chapter I provides a basic knowledge about the mechanisms of superconductivity. Following the brief review of a general background of the thesis in §1, we describe the newly developed numerical method to solve the gap equation in §2. In the last part of this section, an analytically soluble model of the gap equation is introduced to elucidate some conditions of the occurrence of superconductivity. In §3, we investigate the possibility of superconductivity in the electron-gas system with the aid of the plasmon. One of the main interests of the present thesis is the role of the plasmon in superconductivity, the importance of which will be exemplified for real materials in chapters II and III.

§1. A Physical Background of the Thesis

1-1. Origins of Superconductivity

Phenomena of superconductivity like the infinite electric conductivity[1] and the Meissner effect[2] originate from the coherent quantum field on a macroscopic scale. The concept of the coherent quantum field was first suggested by London[3], later improved by Ginzburg and Landau[4], and established fairly well by the recent observation of the Josephson effect[5]. Bardeen, Cooper and Schrieffer (BCS)[6] revealed that the coherent state was due to the condensation of electron pairs (Cooper pairs[7]). The microscopic origin of the formation of the Cooper pair is believed to be an attractive interaction induced by the virtual exchange of phonons between electrons. This phonon mechanism of superconductivity is confirmed in many superconductors by the isotope effect[8] and the tunneling experiment[9].

1-2. Calculation of Superconducting Transition Temperature in Metals

Although the BCS theory has succeeded in explaining various properties of superconductivity, it may still be called a phenomenological theory for the problem to calculate the transition temperature T_c, because the coupling constant in the BCS Hamiltonian is the parameter to be determined by the observed T_c. In addition, the static interaction between electrons is negative in this Hamiltonian, while the stability condition for the

crystal[10] requires that it should be positive. If it were negative, the system would not be in the superconducting state, but in other ordered states such as a charge-density-wave (CDW) one.

An important contribution was made by Bogoliubov *et al.*[11] and also by Morel and Anderson[12] to this point. They showed that the effective interaction responsible for the formation of the Cooper pair was not a static interaction but a dynamical one. When one electron of the Cooper pair oscillates with a frequency near a resonant frequency of the lattice, the ions vibrate to overscreen the Coulomb repulsion to produce the attractive potential in the neighbourhood of the electron. The other electron of the pair sees this attractive potential, when it oscillates with the same frequency. Of course, there also occur the scatterings with the frequency much different from this resonant frequency, but the probability of occurring the scatterings of this kind is small. In this way, the Coulomb repulsion is reduced and this physics has been treated by the Coulomb pseudo-potential μ^*.[11,12] The above dynamical process can be simulated by the BCS Hamiltonian, so that various phenomena of super-conductivity are accounted for on the basis of this Hamiltonian.

In order to calculate T_c from the microscopic point of view, however, all these dynamical effects should be taken into account properly. Theories for this task were formulated by Eliashberg[13] and Nambu[14], and their results were improved by several authors.[12,15,16] Final completion has been given by McMillan,[17] who calculated T_c of various metals within the framework

of the strong-coupling theory with the use of adjustable parameters, μ^* and $\alpha^2(\Omega)F(\Omega)$ (the phonon density of states $F(\Omega)$ times an average of the square of the electron-phonon matrix elements $\alpha^2(\Omega)$, where Ω is the energy variable).

1-3. Role of Parameter ω_D/ε_f in Phonon Mechanism of Superconductivity

The parameter ω_D/ε_f is of the order of 10^{-2} in usual metals, where ω_D and ε_f are the Debye energy and the Fermi energy, respectively. Therefore the Cooper pair is mainly formed by the electrons very close to the Fermi surface. Since the degrees of freedom of these electrons are restricted to two owing to the presence of the Fermi surface, the relative motion of the pair has a two-dimensional character. Thanks to this fact, a bound pair can be created even by a weak short-range attractive potential, because two-dimensional systems have a bound state even in a very shallow attractive potential well, in contrast with the three-dimensional ones.

Further, the small ω_D/ε_f value makes the calculation of T_c easy in several points. First, the electron-phonon vertex corrections can be neglected, as pointed out by Migdal,[18] since the lowest-order correction to the bare vertex is $\lambda\omega_D/\varepsilon_f$ with the usual definition of the dimensionless electron-phonon coupling constant λ and is negligible even when λ is of the order of unity. Secondly, the gap equation is tractable even in the strong-coupling form owing to the fact that the self-energy part of the single-particle Green's function and also the gap function are independent of the momentum variable, that is, they depend only

on the energy variable ω when $\omega_D/\varepsilon_f \ll 1$. The last point is connected with the calculation of the kernel in the gap equation. The effect of the phonon-mediated interaction on the kernel does not vanish only near the Fermi surface, while that of the Coulomb interaction extends beyond the Fermi energy. Thus in case of $\omega_D/\varepsilon_f \ll 1$, it is effective in the solution of the gap equation to treat these two interactions separately. From such a treatment, the idea of the Coulomb pseudo-potential μ^* was born.

1-4. Comments on McMillan's Work

As reviewed in 1-3, the theory of McMillan made full use of the smallness of the parameter ω_D/ε_f. Thus, when we deal with the case of $\omega_D \sim \varepsilon_f$, we cannot adopt his method immediately and should pay some special attentions to both the physics of the mechanism itself and the method of the calculation of T_c. As for the Coulomb interaction, McMillan assumed that it did not supply any help for the formation of the Cooper pair. He, therefore, treated the effect of the Coulomb repulsion rather crudely by introducing one adjustable parameter μ^*. Other effects of the Coulomb interaction were considered at most to renormalize the energy bands and the electron-phonon matrix elements.[19] It must be noted here that McMillan's method cannot be regarded as the first-principle calculation in the strict sense, since μ^* is usually chosen to be able to account for the observed T_c.

McMillan also noticed that T_c was not expected

to exceed 30 K in the phonon mechanism. This led several people to search the nonphonon mechanism of superconductivity, because the original BCS theory does not exclude the possibility of other mechanisms of superconductivity. An example of such theoretical attempts is the exciton mechanism in one-dimensional polymeric systems,[20,21] in a thin metallic film sandwiched between layers of a highly polarizable material,[22] and in a thin metallic film coated on a simiconductor with a high dielectric constant.[23] Another example is the acoustic plasmon mechanism which has been discussed in a transition metal with s- and d-electrons,[24-27] and in a semimetal, or a degenerate semiconductor with an electron-hole system.[28] These authors predicted that T_c was as high as 100 K for these mechanisms. However, we cannot accept these results readily, because they calculated T_c with the use of similar methods to the McMillan's one in spite of the fact that the energies of the exciton and the acoustic plasmon are both as large as ε_f. Thus a further investigation is necessary to treat these cases

1-5. A New Numerical Method to Solve the Gap Equation

In this thesis, we develop a new numerical method to solve the gap equation which is applicable to a wide range of ω_0/ε_f, where ω_0 is the energy of the mode to be exchanged virtually between electrons of the Cooper pair. In this method, we employ only one approximation, *i.e.*, the weak-coupling approximation. Since the idea of μ^* does not seem to hold for the case of $\omega_0 \sim \varepsilon_f$,

the Coulomb interaction is treated much more rigorously in this method than in the conventional one, so that no adjustable parameters like μ^* are introduced. In this sense, the present method enables us to make a quantitative study of T_c of superconductivity from the first principles, even when ω_0/ε_f is not small compared with unity. As to the weak-coupling approximation, we cannot justify the validity to use it in every case. However, we can check the applicability of this approximation by comparing T_c obtained in the present method with ω_0 in each case.

With the help of this new method, the present thesis aims at studying the following four subjects about the mechanisms of superconductivity. The first subject is to evaluate the effect of the Coulomb interaction, in particular, that of the plasmon on superconductivity precisely. The problem has never been studied in details since the appearance of the BCS theory. The second subject is to investigate the change of the contribution of phonons as the parameter ω_D/ε_f is increased to be of the order of unity. The third one is to examine the superconductivity in a multi-carrier system. The effect of the acoustic plasmon in a multi-carrier system is studied as an example of the nonphonon mechanism of superconductivity. This study may also throw light on the problem to obtain a high T_c superconductor. The fourth subject is to make the interrelation of several mechanisms clear, so that we can discuss the mechanisms to determine T_c quantitatively in a real superconductor.

1-6. Superconductivity in Degenerate Semiconductors

Semiconductors provide a very good system for the theoretical study of the subjects described in 1-5, although T_c of these materials is in general low and the observed T_c is at most in the range of 0.1 K.[29-31] The physical properties of semiconductors in the normal state such as the band structure are understood better than those of metals. The carrier concentration n of the system can be changed over a wide range, as shown in the examples discussed later. Thanks to this feature, we can make a systematic study of T_c with the change of ω_D/ε_f, since the parameter ω_D/ε_f can be varied, for example, from about 0.1 to 10, in these systems. The controllability of n also gives us a great help for the determination of the main active modes to cause the superconductivity in these materials. Besides, semiconductors are more favorable systems to obtain a multi-carrier system than metals.

A similar study has already been done by M.L. Cohen[29] for several semiconductors. He studied the superconductivity in multi-valley semiconductors and emphasized the importance of the role of inter-valley phonon scatterings in these systems. His method to solve the gap equation is analogous to the present method, but it seems that it does not take a proper account of a mode having the energy of the order of ε_f. This will be made clearer in the following section (2-1).

1-7. Semiconducting $SrTiO_3$ and MOS Inversion Layers

Among various degenerate semiconductors, the systems we will treat in the thesis are the following two systems; semiconducting $SrTiO_3$ and inversion layers of Metal-Oxide-Semiconductor (MOS) junctions. The normal properties of these systems have been studied well, both experimentally and theoretically. The carrier concentration n can be changed over a very wide range. In the former case, n is varied from 10^{18} cm^{-3} to 6×10^{20} cm^{-3} by doping, while in the latter one, n is from 10^{11} cm^{-2} to 10^{13} cm^{-2} by changing the gate voltage.

$SrTiO_3$ is a highly polar material and is observed to have an n-dependent T_c of the order of 0.1 K for n in the range from 8.5×10^{18} cm^{-3} to 3.0×10^{20} cm^{-3}. [30,32] Since none of other materials have shown the superconducting behavior at such a low n, it is supposed that the mechanism to cause the superconductivity in this material is very interesting. A detailed discussions of this material are given in chapter II. We can reproduce the experimental curve of T_c as a function of n fairly well by the first-principle calculation. The observed effects of uniaxially applied stresses on T_c are also explained quantitatively. It should be noted again that the quantitative calculation is made without any adjustable parameters.

MOS systems are treated from various reasons, although there is no definite experimental evidence of superconductivity at present. [33] Firstly, an n-channel inversion layer at the $Si(100)/SiO_2$ interface is a much simpler and a better known system than semiconducting $SrTiO_3$ and has been investigated

so well[34] that T_c can be predicted without any ambiguous parameters. The second reason is related to the quasi-two-dimensionality of the MOS system. In a two-dimensional system, the dispersion relation of the plasmon for small wave numbers q is proportional to $\sqrt{q}$ [35] and is different from that in bulk systems. We, thus, investigate how this property is reflected in the contribution of the plasmon to superconductivity. Thirdly, a multi-carrier system can be realized easily in the MOS system by controlling the gate voltage[36] and the applied stress.[37] Thus the MOS structure provides a very good system for the presence of the acoustic plasmon mechanism of superconductivity. Quantitative discussions on the prediction of T_c in this system will be given in chapter III.

§2. Gap Equation

2-1. Preliminaries

Following the introduction of 1-5, the method to treat the gap equation is developed in detail in §2. In the first place, we relate the microscopic interaction to the kernel in the gap equation by an analogous way to that of Kirzhnits *et al.*[38] The kernel thus obtained is compared with that of Cohen[29] in the end of this subsection.

A. Hamiltonian

We consider electrons in an n-type degenerate semiconductor with the valley degeneracy g_v, although the results obtained here apply also to holes in a p-type semiconductor. The Hamiltonian of this system† is written by

$$H = H_e + H_{ph}, \tag{2.1}$$

with

$$H_e = \sum_{i=1}^{g_v} \sum_{p\sigma} \epsilon_p C^\dagger_{ip\sigma} C_{ip\sigma} + \frac{1}{2} \sum_{ii'} \sum_{pp'\sigma\sigma'} \sum_{q\neq 0} V^0(q) C^\dagger_{ip\sigma} C^\dagger_{i'p'\sigma'} C_{i'p'-q\sigma'} C_{ip+q\sigma}, \tag{2.2}$$

and

$$H_{ph} = \sum_{q\nu} \omega_\nu(q) (a^\dagger_{q\nu} a_{q\nu} + \frac{1}{2}) + \sum_{ii'} \sum_{pp'\sigma\nu} g_{ip,i'p',\nu} (a_{p+q_i-p'-q_{i'},\nu} + a^\dagger_{-p-q_i+p'+q_{i'},\nu}) \times C^\dagger_{ip\sigma} C_{i'p'\sigma}, \tag{2.3}$$

---

† In this thesis, we use the units in which $c = \hbar = k_B = 1$.

where $C_{ip\sigma}$ is the anihilation operator of the electron of the momentum p with respect to the bottom of the valley and the spin σ in the i-th valley whose single-particle energy ε_p is supposed to be independent of i, $V^0(q)$ is the Fourier transform of the Coulomb interaction given by

$$V^0(q) = 4\pi e^2/\kappa q^2, \tag{2.4}$$

with the dielectric constant κ, $a_{q\lambda}$ is the anihilation operator of the phonon of the wave vector q and the ν-th kind, $\omega_\nu(q)$ is its energy, $g_{ip,i'p',\nu}$ is the matrix element of the electron-phonon interaction, and Q_i is the wave vector of the bottom of the i-th valley. In eq.(2.2), the inter-valley exchange Coulomb interactions are neglected, because the Fermi wave number $p_f \equiv (3\pi^2 n/g_v)^{1/3}$ with the carrier concentration n is less than 10^7 cm^{-1} in usual degenerate semiconductors to make $p_f/|Q_i| \lesssim 0.1$, from which the inter-valley exchange Coulomb interactions are less than 10^{-2} of the direct ones.

B. Basic equation

The anomalous Green's function, $F_i(p,i\omega_p)$, defined by

$$F_i(p,i\omega_p) = -\int_0^{1/T} d\tau\, e^{i\omega_p\tau} \langle T_\tau C_{ip\uparrow}(\tau) C_{i-p\downarrow}(0)\rangle, \tag{2.5}$$

with the usual definition of T_τ and $C_{ip\sigma}(\tau)$, satisfies the following gap equation at $T = T_c$:

$$F_i(p,i\omega_p) = -G_i(p,i\omega_p)\,G_i(-p,-i\omega_p)\,T\sum_{\omega_{p'}}\sum_{i'p'} I_{ii'}(p,p';i\omega_p,i\omega_{p'})\,F_{i'}(p',i\omega_{p'}), \quad (2.6)$$

with $\omega_p \equiv \pi T(2p+1)$, where p is an integer, $G_i(p,i\omega_p)$ is the single-particle Green's function, and $I_{ii'}(p,p';i\omega_p,i\omega_{p'})$ is the irreducible interaction of two particles which changes two electrons in the i'-th valley into those in the i-th one. In order to proceed further, the weak-coupling approximation is employed. Since we treat the case of $\omega_D/\varepsilon_f \sim 1$, the quasi-particle picture cannot be used when the interaction is strong, but for a weak interaction, $G_i(p,i\omega_p)$ can be written in the form of

$$G_i(p,i\omega_p) = \frac{1}{i\omega_p - \epsilon_p} \quad . \quad (2.7)$$

The weak-coupling approximation also permits us to consider the irreducible interaction to be of the form of

$$I_{ii'}(p,p';i\omega_p,i\omega_{p'}) = V_{ii'}(p-p',i\omega_p-i\omega_{p'}) \quad . \quad (2.8)$$

This is because the contributions from complicated vertex corrections are higher-order corrections of a weak interaction and may be neglected even when $\omega_D/\varepsilon_f \sim 1$.

With the use of eqs. (2.7) and (2.8), eq. (2.6) can be transformed into the form convenient to find the numerical solution for T_c. Performing the frequency sum in eq. (2.6) and making the analytic continuation from $i\omega_p$ to $\omega+i0^+$ to use the retarded

Green's function denoted by the superscript R, we can obtain the following equation:

$$F^R(p,\omega) = \frac{1}{\omega^2 - \epsilon_p^2 + i0^+} \int_0^\infty \frac{d\omega'}{\pi} \sum_{i'p'} \mathrm{Im} F^R(p',\omega') \Big\{ (1-2f(\omega')) V^0(p-p') \delta_{ii'}$$

$$+ \int_0^\infty \frac{d\Omega}{\pi} \mathrm{Im} V^R_{ii'}(p-p',\Omega) \Big[(f(-\omega')+n(\Omega)) \cdot \Big(\frac{1}{\omega+\omega'+\Omega+i0^+} + \frac{1}{\Omega+\omega'-\omega-i0^+} \Big)$$

$$+ (f(\omega')+n(\Omega)) \cdot \Big(\frac{1}{-\omega-\Omega+\omega'-i0^+} + \frac{1}{\omega-\Omega+\omega'+i0^+} \Big) \Big] \Big\}, \tag{2.9}$$

where $f(\omega')$ and $n(\Omega)$ are the Fermi and Bose distribution functions, respectively, and the following relation is used:

$$V^R_{ii'}(q,\omega) = V^0(q)\delta_{ii'} - \int_0^\infty \frac{d\Omega}{\pi} \cdot \frac{2\Omega}{\omega^2 - \Omega^2 + i0^+} \mathrm{Im} V^R_{ii'}(q,\Omega), \tag{2.10}$$

This comes from the facts that $V^R_{ii'}(q,\omega)$ is analytic in the upper ω-plane and that $V^R_{ii'}(q,\omega) = V^R_{ii'}(q,-\omega^*)^*$. Since F^R_i does not depend on i, the suffix i for F^R_i is deleted in eq.(2.9).

The kernel in the integral equation (2.9) is complicated a little, but when we take the imaginary part of both sides of eq.(2.9) and then integrate by the variable ω, we can have a much simpler equation as

$$\Delta(p) = -\sum_{i'p'} \frac{\Delta(p')}{2|\epsilon_{p'}|} \Big\{ (1-2f(|\epsilon_{p'}|)) \cdot \Big(V^0(p-p')\delta_{ii'} + \int_0^\infty \frac{2}{\pi} d\Omega \frac{\mathrm{Im} V^R_{ii'}(p-p',\Omega)}{\Omega + |\epsilon_p| + |\epsilon_{p'}|} \Big)$$

$$+ \int_0^\infty \frac{2}{\pi} d\Omega \, \mathrm{Im} V^R_{ii'}(p-p',\Omega) \cdot (f(|\epsilon_{p'}|)+n(\Omega))$$

$$\times \Big[\frac{1}{|\epsilon_p| + |\epsilon_{p'}| + \Omega} + \frac{\theta(|\epsilon_{p'}|-\Omega)}{|\epsilon_{p'}| - \Omega + |\epsilon_p|} + \frac{\theta(\Omega - |\epsilon_{p'}|)}{|\epsilon_{p'}| - \Omega - |\epsilon_p|} \Big] \Big\}, \tag{2.11}$$

where $\theta(x)$ is the Heaviside function, and $\Delta(p)$ is defined by

$$\Delta(p) \equiv 2|\epsilon_p| \int_0^\infty \frac{d\omega}{\pi} \, \mathrm{Im}\, F^R(p,\omega) , \tag{2.12}$$

In deriving eq.(2.12), Im $F^R(p,\omega)$ is approximated by $\pi\Delta(p)\delta(\omega-|\varepsilon_p|)/2|\varepsilon_p|$, since the quasi-particle picture holds well in the weak-coupling superconductors.

The last three terms in eq.(2.11) may be neglected, if we take the following points into consideration. The contribution of Im $V^R_{ii'}(p-p',\Omega)$ vanishes except that Ω is near the energies of the modes such as phonons and the plasmon. On the other hand, T_c is much smaller than these energies in the weak-coupling superconductor. Thus the contribution of $n(\Omega)\cdot$Im $V^R_{ii'}(p-p',\Omega)$ is always negligible. The term

$$\mathrm{Im}\, V^R_{ii'}(p-p',\Omega) f(|\epsilon_{p'}|)\left[\frac{1}{|\epsilon_p|+|\epsilon_{p'}|+\Omega} + \frac{\theta(|\epsilon_{p'}|-\Omega)}{|\epsilon_{p'}|-\Omega+|\epsilon_p|} + \frac{\theta(\Omega-|\epsilon_{p'}|)}{|\epsilon_{p'}|-\Omega-|\epsilon_p|}\right] \tag{2.13}$$

is also small, because $f(|\varepsilon_{p'}|)$ is not small only for $\varepsilon_{p'} \sim 0$, but when $|\varepsilon_{p'}|$ is very small, the term (2.13) becomes to be

$$-2\,\mathrm{Im}\, V^R_{ii'}(p-p',\Omega) f(|\epsilon_{p'}|)\,|\epsilon_{p'}| / (|\epsilon_p|+\Omega)^2 \approx 0 .$$

In this way, the gap equation to be solved becomes

$$\Delta(p) = -\sum_{p'} \frac{\Delta(p')}{2\epsilon_{p'}} \tanh\frac{\epsilon_{p'}}{2T_c} \cdot V_{pp'} , \tag{2.14}$$

with the pairing interaction $V_{pp'}$, defined by

$$V_{pp'} = V^0(p-p') + \sum_{i'} \int_0^\infty \frac{2}{\pi} d\Omega \, \frac{\mathrm{Im}\, V^R_{ii'}(p-p',\Omega)}{\Omega + |\epsilon_p| + |\epsilon_{p'}|} . \tag{2.15}$$

When the single-particle energy ϵ_p has the form of

$$\epsilon_p = p^2/2m^* - \epsilon_f \,, \tag{2.16}$$

with the effective mass m* and the Fermi energy ϵ_f, eq.(2.14) changes into

$$\Delta(\omega) = -\int_{-\epsilon_f}^{\infty} \frac{d\omega'}{2\omega'} \tanh\frac{\omega'}{2T_c}\,\Delta(\omega')\,K(\omega,\omega') \,, \tag{2.17}$$

where the momentum variable, p, is related to the energy variable, ω, through $p = \sqrt{2m^*(\omega+\epsilon_f)}$, and the kernel, $K(\omega,\omega')$, is defined by

$$K(\omega,\omega') = \frac{m^* p'}{2\pi^2}\cdot\frac{1}{pp'}\int_{|p-p'|}^{p+p'} \frac{q\,dq}{2}\, V_{pp'} \,. \tag{2.18}$$

Equation (2.18) can be rewritten as

$$K(\omega,\omega') = \frac{m^*}{4\pi^2 p}\int_{|p-p'|}^{p+p'} q\,dq \int_0^{\infty} \frac{2}{\pi}\,d\Omega\, \frac{|\omega|+|\omega'|}{\Omega^2+(|\omega|+|\omega'|)^2}\, V^R(q,i\Omega) \,, \tag{2.19}$$

with

$$V^R(q,i\Omega) \equiv \sum_{i'} V^R_{ii'}(q,i\Omega) \,. \tag{2.20}$$

C. Comparison with Cohen's kernel

Equation (2.18), or (2.19), relates the microscopic interaction $V^R_{ii'}(q,i\Omega)$ to the kernel $K(\omega,\omega')$. This kernel is just the same form as that obtained by Kirzhnits *et al.*,[38] but is

different from that of Cohen.[29] Cohen's kernel, $K^{Cohen}(\omega,\omega')$, was given by

$$K^{Cohen}(\omega,\omega')=\sum_{i'}\frac{m^*}{2\pi^2\rho}\int_{|p-p'|}^{p+p'}\frac{qdq}{2}V^R_{ii'}(q,\omega'-\omega). \qquad (2.21)$$

The difference between $K(0,\omega')$ and $K^{Cohen}(0,\omega')$ is calculated to be

$$K(0,\omega')-K^{Cohen}(0,\omega')$$
$$=\sum_{i'}\frac{m^*}{4\pi^2 p_f}\int_{|p_f-p'|}^{p_f+p'}qdq\int_0^\infty\frac{d\Omega}{\pi}\,Im\,V^R_{ii'}(q,\Omega)\left(\frac{1}{\Omega+|\omega'|}+\frac{1}{|\omega'|-\Omega}\right), \qquad (2.22)$$

which shows that for $|\omega'| \sim 0$, the difference is negligibly small, while for larger $|\omega'|$, in particular, for $|\omega'|$ near the energies of the modes such as phonons and the plasmon, the difference is large. The same is also applied to the variable ω. In general, this difference has a large effect on T_c, when the superconductivity is brought about by the mode having a large energy. Thus, the results obtained by Cohen should be checked for superconductors with the Debye energy ω_D of the order of ε_f. The difference of the conclusions arisen from the use of the different kernels will be illustrated in chapter II by the study of the superconductivity in $SrTiO_3$.

2-2. Method of Numerical Calculation

In the present subsection, we describe the numerical method

to solve the gap equation (2.17) with the kernel (2.18), or (2.19).

A. Modification of gap equation

Since it is hard to determine T_c and the corresponding gap function $\Delta(\omega)$ at the same time, the first step to solve eq.(2.17) is to modify it into the form which permits us to treat $\Delta(\omega)$ and T_c separately. For this purpose, we take the procedure proposed by Zubarev,[39] which is valid in the weak-coupling superconductor. The equation for the function $\phi(x)$, defined by

$$\phi(x) \equiv \Delta(x)/\Delta(0), \tag{2.23}$$

with the variable $x \equiv \omega/\varepsilon_f$ is given by eq.(2.17) as

$$\phi(x) = -\int_{-1}^{\infty} \frac{dx'}{2x'} \tanh(\varepsilon_f x'/2T_c)\,\phi(x')\,K(x,x'). \tag{2.24}$$

Since $\phi(0)$ is unity by its definition, we obtain

$$1 = -\int_{-1}^{\infty} \frac{dx}{2x} \tanh(\varepsilon_f x/2T_c)\,\phi(x)\,K(0,x). \tag{2.25}$$

By combining these two equations, we get

$$\phi(x) = K(x,0)/\lambda_0 - \int_{-1}^{\infty} \frac{dx'}{2|x'|}\,\phi(x')\tanh(\varepsilon_f|x'|/2T_c) \times [K(x,x') - K(x,0)\,K(0,x')/\lambda_0], \tag{2.26}$$

with

$$\lambda_0 \equiv K(0,0). \tag{2.27}$$

In eq.(2.26), the singularity at x' = 0 disappears. This permits us to replace $\tanh(\varepsilon_f|x'|/2T_c)$ by unity with a logarithmic accuracy and $\phi(x)$ is determined by

$$\phi(x) = K(x,0)/\lambda_0 - \int_{-1}^{\infty} \frac{dx'}{2x'} \phi(x') [K(x,x') - K(x,0) K(0,x')/\lambda_0]. \tag{2.28}$$

With this $\phi(x)$, T_c can be obtained with the use of eq.(2.25) which is rewritten as

$$1 = -\lambda_0 \int_{-1}^{1} \frac{dx}{2x} \tanh(\epsilon_f x/2T_c) - \int_{-1}^{1} \frac{dx}{2|x|} \tanh(\epsilon_f|x|/2T_c) \cdot [K(0,x)\phi(x) - \lambda_0] - \int_{1}^{\infty} \frac{dx}{2x} \tanh(\epsilon_f|x|/2T_c)\, \phi(x) K(0,x).$$

(2.29)

As before, $\tanh(\varepsilon_f|x|/2T_c)$ can be replaced by unity in the second and third terms in eq. (2.29) and the first term can be integrated easily. Thus we get the equation for T_c as

$$T_c = 1.134\, \epsilon_f \exp\left\{ \frac{1}{\lambda_0} + \int_{-1}^{\infty} \frac{dx}{2|x|} [\phi(x) K(0,x)/\lambda_0 - \theta(1-|x|)] \right\}. \tag{2.30}$$

B. Change into matrix equation

The gap equation (2.17), or (2.28), is usually solved by an iteration method,[17] but here, we change the integral equation into the matrix one and solve it by the calculation of the inverse matrix. The integral in eq.(2.28) is performed by taking x_m for the upper limit of the integral and breaking up the

interval $(-1, x_m)$ into small ones, (x_i, x_{i+1}). The spacing, δ_i, varies with $\bar{x}_i \equiv (x_i + x_{i+1})/2$: For $|\bar{x}_i| \sim 0$, δ_i is 10^{-4}, and for $|\bar{x}_i|$ larger than 0.1, $\delta_i = |\bar{x}_i|/10$. The gap function $\phi(x)$ is assumed to be constant, ϕ_i, in the interval (x_i, x_{i+1}) and eq. (2.28) leads to the following equation for $\Phi \equiv (\phi_i)$:

$$\Phi = \Phi_0 - J \Phi , \tag{2.31}$$

with

$$\Phi_0 \equiv (K_{i0} / \lambda_0) , \tag{2.32}$$

and

$$J \equiv ([K_{ij} - K_{i0} K_{0j} / \lambda_0] \cdot (x_{j+1} - x_j)/2|\bar{x}_j|) , \tag{2.33}$$

where the subscript, 0, is so chosen that $\bar{x}_0 = 0$ and K_{ij} is defined by

$$K_{ij} \equiv \frac{1}{x_{j+1} - x_j} \int_{x_j}^{x_{j+1}} dx' \, K(\bar{x}_i, x') . \tag{2.34}$$

Equation (2.31) is solved to be

$$\Phi = (1 + J)^{-1} \Phi_0 , \tag{2.35}$$

with the unit matrix 1 and T_c is obtained as a function of x_m as

$$T_c = 1.134 \, \epsilon_f \exp\left\{ \frac{1}{\lambda_0} + \sum_j \frac{x_{j+1} - x_j}{2|\bar{x}_j|} [K_{j0} \phi_j / \lambda_0 - \theta(1 - |\bar{x}_j|)] \right\} , \tag{2.36}$$

with the use of eq. (2.30). As x_m is increased, T_c increases in general, but the change of T_c with x_m is negligibly small for x_m

larger than 10^3. In the following calculations, x_m is taken to be 10^4 and the size of the matrix J is 177×177.

C. Numerical computation of kernel

The most difficult problem arises from the calculation of K_{ij}, given by eq.(2.34) with the definition of K(x,x') in eq.(2.19). Since $pK(\omega,\omega') = p'K(\omega',\omega)$, we obtain an equation of

$$K_{ji} = \bar{P}_i \; K_{ij} \; / \; \bar{P}_j \tag{2.37}$$

with $\bar{p}_i \equiv p_f\sqrt{1+x_i}$ and we can reduce our computational time to the half. We, nevertheless, have to compute K_{ij} for about 16000 points in all. This is practically impossible, because it consumes too much time to carry it out. Accordingly, Kirzhnits *et al.*[38] did not enter into the task of the numerical solution. This problem would have been presumably the reason why Cohen used his kernel $K^{Cohen}(\omega,\omega')$, defined by eq.(2.21), even though it was not correct. The kernel $K^{Cohen}(\omega,\omega')$ can be calculated much more easily than $K(\omega,\omega')$.

In order to overcome this difficulty, we notice the fact that $V^R_{ii'}(q,i\omega)$, and consequently $K(\omega,\omega')$, vary very slowly with ω and ω', although the effective interaction $V^R_{ii'}(q,\omega)$ changes very much at ω near the resonant frequencies of the modes such as the phonons and the plasmon. Thanks to this property, we can take the following strategy: We first choose as a set of $\{K_{ij}\}$ each element of which is evaluated rigorously, that is,

$$K_{ij} = \frac{m^* e^2}{\pi k \bar{P}_i}\left[\frac{2\bar{P}_i}{P_{j+1}+P_j} + \frac{x_{j+1}-\bar{x}_i}{x_{j+1}-x_j}\ln\left|\frac{P_{j+1}+\bar{P}_i}{P_{j+1}-\bar{P}_i}\right| + \frac{\bar{x}_i - x_j}{x_{j+1}-x_j}\ln\left|\frac{P_j+\bar{P}_i}{P_j-\bar{P}_i}\right|\right]$$
$$+ \frac{m^*}{4\pi^2\bar{P}_i}\int_0^\infty \frac{2}{\pi}d\Omega \; \frac{|\bar{\omega}_i|+|\bar{\omega}_j|}{\Omega^2+(|\bar{\omega}_i|+|\bar{\omega}_j|)^2}\left\{\int_{|P_{j+1}-\bar{P}_i|}^{P_{j+1}+\bar{P}_i} q\,dq \; \tilde{V}^R(q,i\Omega)\right.$$

$$+\frac{1}{\omega_{j+1}-\omega_j}\Big[-\int_{p_j}^{p_{j+1}} dq\cdot(q+\bar{p}_i)\cdot(q^2-p_j^2)\,\tilde{V}^R(q+\bar{p}_i,i\Omega)$$
$$+(1-\delta_{ij})\int_{p_j}^{p_{j+1}} dq\cdot(q-\bar{p}_i)\cdot(q^2-p_j^2)\cdot\tilde{V}^R(|q-\bar{p}_i|,i\Omega)$$
$$+\delta_{ij}\int_{2\bar{p}_i-p_i}^{p_{i+1}} dq\cdot(q-\bar{p}_i)\cdot(q^2-p_i^2)\cdot\tilde{V}^R(q-\bar{p}_i,i\Omega)+4\delta_{ij}\int_0^{\bar{p}_i-p_i} q^2dq\,\bar{p}_i\,\tilde{V}^R(q,i\Omega)\Big]\Big\}, \tag{2.38}$$

where $\omega_i \equiv \varepsilon_f x_i$, $p_j \equiv p_f\sqrt{1+x_j}$ and

$$\tilde{V}^R(q,i\Omega) \equiv V^R(q,i\Omega) - V^0(q). \tag{2.39}$$

Then we calculate the rest of K_{ij} by the interpolation of them.

After several trials to obtain a proper set of $\{K_{ij}\}$, it is found that every eighth point of i and j should be chosen for the set and that every point near the Fermi surface and almost all the diagonal points, *i.e.*, the points of $i = j$ should be added to them. As a result, the number of elements of $\{K_{ij}\}$ becomes about three hundred and it takes *ca.* 250 seconds to compute every element of the matrix J with the use of HITAC 8800/8700 at the Computer Centre of the University of Tokyo.

2-3. Analytic Solution

In this subsection, we give a few examples of the approximate solution of the gap equation in order to clarify the physics of the mechanisms of superconductivity, in particular, the importance of considering the effective interaction dynamically. The first

example is due to Morel and Anderson[12] and the second one is proposed in this thesis to improve their model. The latter model is applied to the electron-phonon system. The relation between the kernel, defined by eq.(2.18), and the dimensionless electron-phonon coupling constant λ, defined as usual, is obtained and the maximum T_c is examined under several assumptions. In the last part of this subsection, we comment on the requirements for the mode with the energy of the order of ε_f to cause superconductivity and also for the single-particle state to show a superconducting behavior.

A. Morel-Anderson model

In the conventional theory of superconductivity, the effective interaction $V^R(q,\omega)$ is devided into two parts. One is the contribution of the Coulomb interaction and the other is that of phonons. These two will be denoted by $V^C(q,\omega)$ and $V^{ph}(q,\omega)$, respectively. In accordance with this, the kernel, defined by eq.(2.18), is separated into two as

$$K^C(\omega,\omega') = \frac{m^*}{4\pi^2 p}\int_{|p-p'|}^{p+p'} q\,dq\left[V^0(q)+\int_0^\infty \frac{2}{\pi}d\Omega\,\frac{\mathrm{Im}V^C(q,\Omega)}{\Omega+|\omega|+|\omega'|}\right], \tag{2.40}$$

and

$$K^{ph}(\omega,\omega') = \frac{m^*}{4\pi^2 p}\int_{|p-p'|}^{p+p'} q\,dq\int_0^\infty \frac{2}{\pi}d\Omega\,\frac{\mathrm{Im}V^{ph}(q,\Omega)}{\Omega+|\omega|+|\omega'|}. \tag{2.41}$$

These kernels are usually approximated as

$$K^{C}(\omega,\omega') = \mu\,\theta(\epsilon_f - |\omega|)\,\theta(\epsilon_f - |\omega'|), \tag{2.42}$$

and

$$K^{ph}(\omega,\omega') = -\lambda\,\theta(\omega_D - |\omega|)\,\theta(\omega_D - |\omega'|), \tag{2.43}$$

respectively, where the Coulomb parameter μ is given by

$$\mu = \frac{m^*}{4\pi^2 p_f}\int_0^{2p_f} q\,dq\; V^{C}(q,0), \tag{2.44}$$

and λ is defined with the use of the Eliashberg's function[13] $\alpha^2(\omega)F(\omega)$ as

$$\lambda = 2\int_0^{\infty}\frac{d\omega}{\omega}\,\alpha^2(\omega)\,F(\omega), \tag{2.45}$$

with

$$\alpha^2(\omega)\,F(\omega) \equiv -\frac{m^*}{4\pi^2 p_f}\int_0^{2p_f} q\,dq\;\frac{1}{\pi}\,\mathrm{Im}\,V^{ph}(q,\omega). \tag{2.46}$$

Putting $K(\omega,\omega') \equiv K^{C}(\omega,\omega') + K^{ph}(\omega,\omega')$, defined by eqs.(2.42) and (2.43), into eq.(2.28) and noticing $\lambda_0 \equiv \mu - \lambda$, we obtain $\phi(x)$ readily as

$$\phi(x) = \begin{cases} 1, & \text{for } |x| \le x_0, \\ \dfrac{\mu^*}{\mu^* - \lambda}, & \text{for } x_0 \le |x| \le 1, \\ 0, & \text{for } x > 1, \end{cases} \tag{2.47}$$

where $x_0 \equiv \omega_D/\varepsilon_f$ is assumed to be less than unity and the Coulomb pseudo-potential μ^* is given by

$$\mu^* = \mu \,/\, [\, 1 + \mu \ln 1/x_0 \,]. \tag{2.48}$$

With the use of this $\phi(x)$ and eq.(2.30), T_c is calculated to be

$$\begin{aligned} T_c &= 1.134\, \varepsilon_f \exp\left\{ \frac{1}{\mu - \lambda}\left[1 + \frac{\mu^*}{\mu^* - \lambda} \mu \ln\frac{1}{x_0} \right] - \ln\frac{1}{x_0} \right\} \\ &= 1.134\, \omega_D \exp\left\{ - \frac{1}{\lambda - \mu^*} \right\}, \end{aligned} \tag{2.49}$$

which is just the result obtained by Morel and Anderson.

The example presented here elucidates the physics as to how the occurrence of superconductivity is compatible with the stability condition for the crystal[10] which requires that μ should be larger than λ. The kernel $K(\omega,\omega')$ is always positive when μ is larger than λ, but this does not cause any difficulties. The important point is how the kernel $K(\omega,\omega')$ changes with the change of the energy variables ω and ω'. The phonons make the kernel small, if $|\omega|$ and $|\omega'|$ are both smaller than ω_D, while the kernel becomes large, when $|\omega|$ and/or $|\omega'|$ are in the range from ω_D to ε_f. The gap function also changes in accordance with this behavior of the kernel. In particular, it should be noted that the gap function does not vanish even for the energy variable ω larger than ω_D. When the Cooper pair is scattered into this energy region where only the Coulomb repulsion is present, the phase of the coherent oscillation of the pair is changed by a factor of π, as indicated by the change in the sign of the gap

function in eq.(2.47). Owing to this effect, the effective Coulomb repulsion is reduced from μ to μ^* and the effective interaction between the electrons of the Cooper pair can be evaluated by $\lambda - \mu^*$. Therefore, even though λ is smaller than μ, superconductivity arises if λ is larger than μ^*.

The above discussion shows explicitly that the gap function in the part of $|\omega| \geqq \omega_D$ also plays an important role in the occurrence of superconductivity. Consequently, we have to calculate this part of the gap function accurately as well as the part of $|\omega| < \omega_D$ in order to obtain a correct μ^*, that is, in order to evaluate T_c from the first principles. In this respect, both the BCS theory[6] and the McMillan's theory[17] are incomplete, because in their theories, the gap function was assumed to vanish when the energy variable exceeds ω_D and μ^* was introduced as an adjustable parameter.

B. New model

As clarified in 2-3.A, the appearance of superconductivity does not depend on whether the kernel at the Fermi surface is negative, or not, but on how the kernel $K(\omega,\omega')$ changes with the energy variables ω and ω'. Thus we have to treat a more realistic kernel than the Morel-Anderson model in order to obtain a deeper knowledge of the mechanism of superconductivity. For such a purpose, a model for the kernel is proposed here as

$$K(x,x') = [\lambda_0 + F(x) + F(x')]\,\theta(1-|x|)\,\theta(1-|x'|), \qquad (2.50)$$

where F(x) is free from all the restrictions except that F(0) = 0. When we substitute this kernel into eq.(2.28), the gap function is easily solved to be

$$\Phi(x) = \left[1 - \frac{1 + \langle F \rangle}{\langle F^2 \rangle - \lambda_0} F(x) \right] \theta(1-|x|), \tag{2.51}$$

with the notation $\langle A \rangle$, defined by

$$\langle A \rangle \equiv \int_{-1}^{1} \frac{dx}{2|x|} A(x). \tag{2.52}$$

The condition for the appearance of superconductivity is given by

$$\langle F^2 \rangle > \lambda_0, \tag{2.53}$$

and T_c is solved to be

$$T_c = 1.134 \epsilon_f \exp\left[-(1+\langle F \rangle)^2 / (\langle F^2 \rangle - \lambda_0) \right]. \tag{2.54}$$

When F(x) is proportional to $|x|^{\alpha}$ with a positive α, $\langle F^2 \rangle$ is calculated to be $F(1)^2/2\alpha$, which leads the condition (2.53) to

$$[K(1,0) - K(0,0)]^2 > 2\alpha K(0,0). \tag{2.55}$$

According to this inequality, it is favorable for the presence of superconductivity to have a small α for a positive K(0,0), which means that the kernel should change steeply near the Fermi surface as the energy variable is increased.

C. Application to electron-phonon systems

We apply the model mentioned above to the electron-phonon system defined by the Hamiltonian (2.1). The effective interaction $V^R(q,\omega)$ in this system may be written as

$$V^R(q,\omega) = V^0(q) / \varepsilon^R(q,\omega), \tag{2.56}$$

with the dielectric function $\varepsilon^R(q,\omega)$, which is assumed to be

$$\varepsilon^R(q,\omega) = 1 + V^0(q)\Pi(q,\omega) + \sum_\nu \frac{f_\nu(q)}{\omega_\nu(q)^2 - \omega^2 - i0^+} \tag{2.57}$$

where $\Pi(q,\omega)$ is the electronic polarization function, and $f_\nu(q)$ is related to the oscillator strength of the ν-th phonon and can be calculated with the use of the electron-phonon interaction $g_{ip,i'p',\nu}$. Equation (2.56) with eq.(2.57) gives the contribution of the phonons to Im $V^R(q,\omega)$ as

$$\mathrm{Im}\, V^{ph}(q,\omega) = -\frac{\pi}{2} V^0(q) \sum_\nu \frac{\delta(\omega - \tilde{\omega}_\nu(q))}{\tilde{\omega}_\nu(q)} \tilde{f}_\nu(q), \tag{2.58}$$

where $\tilde{\omega}_\nu(q)$ and $\tilde{f}_\nu(q)$ are the quantities renormalized by the Coulomb interactions. For $\omega \ll \varepsilon_f$, the kernel defined by eq.(2.18) becomes

$$K(x,0) \simeq \lambda_0 + F(x), \tag{2.59}$$

with

$$\lambda_0 \equiv \mu - \frac{m^*}{4\pi^2 p_f} \int_0^{2p_f} q\,dq\, V^0(q) \sum_\nu \tilde{f}_\nu(q) / \tilde{\omega}_\nu^2(q), \tag{2.60}$$

and

$$F(\omega) = \frac{m^*}{4\pi^2 p_f} \int_0^{2p_f} q\,dq\, V^0(q) \sum_\nu \frac{\tilde{f}_\nu(q)}{\tilde{\omega}_\nu^2(q)} \cdot \frac{|\omega|}{|\omega| + \tilde{\omega}_\nu(q)} \tag{2.61}$$

where μ is defined by eq.(2.44). When $\tilde{\omega}_\nu(q)$ does not depend on q, λ_0 and $F(\omega)$ have the following forms as

$$\lambda_0 = \mu - \sum_\nu \lambda_\nu \,, \tag{2.62}$$

and

$$F(\omega) = \sum_\nu \lambda_\nu \frac{|\omega|}{|\omega| + \tilde{\omega}_\nu} \,, \tag{2.63}$$

respectively, with the definition of λ_ν as

$$\lambda_\nu \equiv \frac{m^*}{4\pi^2 p_f} \int_0^{2p_f} q\,dq\, V^0(q)\, \tilde{f}_\nu(q) / \tilde{\omega}_\nu^2 \,. \tag{2.64}$$

In the following, we assume that only one branch of phonons is present. For $|\omega|$ much smaller than $\tilde{\omega}_\nu$, $F(\omega)$ becomes

$$F(\omega) \simeq \frac{\lambda_\nu}{\tilde{\omega}_\nu} |\omega| \,, \tag{2.65}$$

which tells us that λ_ν can be readily known from $F(\omega)$, although the static interaction λ_0 does not give us a definite value of λ_ν. This again shows the importance of treating the effective interaction dynamically. Inequality (2.53) with $F(x)$, given by

$$F(x) = \lambda_\nu \frac{|x|}{|x| + x_\nu}, \qquad x_\nu \equiv \tilde{\omega}_\nu / \epsilon_f, \tag{2.66}$$

reads that

$$\lambda_\nu g(x_\nu) > \mu - \lambda_\nu, \tag{2.67}$$

and the transition temterature is obtained as

$$T_c = 1.134\, \tilde{\omega}_\nu \exp\left[-1/\lambda_{BCS}\right], \tag{2.68}$$

where the function g(x) is defined by

$$g(x) = \ln \frac{1+x}{x} - \frac{1}{1+x}, \tag{2.69}$$

and the BCS coupling constant λ_{BCS} is given by

$$\lambda_{BCS} = \left(\lambda_\nu^2 g(x_\nu) + \lambda_\nu - \mu\right) / \left[\left(1 + \lambda_\nu \ln \frac{1+x_\nu}{x_\nu}\right)^2 - \left(\lambda_\nu^2 g(x_\nu) + \lambda_\nu - \mu\right) \ln 1/x_\nu\right]. \tag{2.70}$$

Inequality (2.67) suggests that for the presence of superconductivity, λ_ν and $\epsilon_f/\tilde{\omega}_\nu$ should be large. If we can change $\tilde{\omega}_\nu$ independently of λ_ν and assume $\mu = \lambda_\nu$, the maximum T_c is obtained as

$$T_c^{max} \simeq 1.134\, \epsilon_f \exp\left[-4 \frac{1+\mu}{\mu}\right], \tag{2.71}$$

for $x_\nu \simeq \exp(-2-1/\mu)$. Since the typical value of μ is 0.5, T_c^{max} becomes of the order of 1 K for the case of $\varepsilon_f \sim 10$ eV.

Now, we make some comments on the above discussions. Although all the results are obtained under the assumption that $\tilde{\omega}_\nu(q)$ is independent of q, we have to take its q-dependence into account in real materials. In addition, $\tilde{\omega}_\nu(q)$ cannot be changed without changing $\tilde{f}_\nu(q)$ in actual situations. Further, although we have assumed that only one mode is present in the system, it is often the case that several modes are present. Equation (2.62) for λ_0 implies that every mode works additionally, but T_c cannot be determined only by the quantities at the Fermi surface. Thus the interplay of several modes is the problem to be studied more carefully. All these problems are investigated numerically in the following sections on the basis of the method described in the previous subsection.

D. Discussions on mechanisms of superconductivity and single-particle states

Here, we make a qualitative discussion on the requirement for the mode with the energy ω_0 of the order of ε_f to bring about superconductivity. As eq.(2.64) indicates, a large ω_0 leads to a small λ and is disadvantageous for superconductivity. Physically, when ω_0/ε_f is increased, the degrees of freedom of the relative motion of the Cooper pair increase from two to three and the binding energy of the pair decreases for the short-range attraction. As a result, in order for a mode of $\omega_0 \sim \varepsilon_f$ to contribute to superconductivity, the mode should induce either a very strong

short-range attraction or a long-range one. When the latter condition is satisfied, the mode has a strong coupling constant for small q and makes λ in eq.(2.64) large by the contribution of the region of $q \sim 0$.

We should not misunderstand that for the case of $\omega_0 \sim \varepsilon_f$, electrons of $|\varepsilon_p| \sim \varepsilon_f$ have a large contribution to the macroscopic coherent field ψ. Even in such a case, ψ is constructed only by electrons of $|\varepsilon_p| \sim 0$. One way to understand this is to remember that in usual weak-coupling superconductors, ψ can be characterized only by the energy gap at $T = 0$, $\Delta_0 \equiv 1.75\ T_c$, and that the Debye energy ω_D does not appear. Another is to observe that in the superconducting state, ε_p changes into $\varepsilon_p\sqrt{1 + \Delta(p)^2/\varepsilon_p^2}$ with the gap function $\Delta(p)$, defined by eq.(2.12), which shows that only the electrons for $|\varepsilon_p| < \Delta_0$ experience a great change by the phase transition. The role of the gap function $\Delta(p)$ for $|\varepsilon_p| >> \Delta_0$ is not to make the single-particle state of its own change, but to help the electrons near the Fermi surface become superconducting, as discussed in 2-3.A. This is the reason why the BCS theory explains phenomena of superconductivity well, although it is not correct in the sense that the gap function does not vanish only near the Fermi surface in the BCS theory.

The foregoing discussion imposes a restriction to the single-particle states near the Fermi surface. Since a macroscopic number of pairs is necessary to construct ψ, a number of the single-particle states near the Fermi surface should be macroscopically large, as is the case with the normal metallic phase. In order to illustrate this, we consider the CDW state,

in which the single-particle energy ε_p^{CDW} is given by

$$\varepsilon_p^{CDW} = sgn(\varepsilon_p)\sqrt{\Delta_{CDW}^2 + \varepsilon_p^2}\,, \tag{2.72}$$

where Δ_{CDW} is the energy gap in the CDW state, ε_p is defined by eq.(2.16), and the function sgn(x) is defined as

$$sgn(x) = \begin{cases} 1\,, & x > 0\,, \\ -1\,, & x < 0\,. \end{cases} \tag{2.73}$$

Since we choose eq.(2.72) for the single-particle energy instead of eq.(2.16), we have to return to the gap equation (2.14). Because of $|\varepsilon_p^{CDW}| \sim \Delta_{CDW}$ near the Fermi surface, the pairing interaction $V_{p,p'}$, given by eq.(2.15), is independent of p and p'. That is, $V_{p,p'}$ does not show any change as p and p' are changed. As we have learned in the present subsection, such an interaction does not cause superconductivity and the CDW state does not show a superconducting behavior. This argument also applies to any single-particle state in which a number of the levels near the Fermi level is not macroscopic.

§3. Roles of Plasmon in Superconductivity

3-1. Introduction

A. Motivation

Since the BCS theory, the Coulomb interaction has not usually been considered to give any contribution to the formation of the Cooper pair, because it is repulsive. As a result, the treatment of this interaction has been much simpler than that of the phonon-mediated interaction in the theory of superconductivity. All the effects of the Coulomb interaction are estimated by one adjustable parameter μ^*, as we have pointed out in §1.

To the author's knowledge, however, it has not proved conclusively that the Coulomb interaction alone never gives rise to superconductivity. On the contrary, the electron-gas system without phonons has a possibility to be superconducting with the aid of the plasmon, since the dynamical interaction, which we should consider for the formation of the pair, is actually attractive at the frequency ω near that of the plasmon ω_p for small wave numbers. Cohen, who did not employ the idea of μ^* and treated the Coulomb interaction more seriously,[29] also speculated that the plasmon might have some effects on the occurrence of superconductivity,[40] although he did not consider that the plasmon alone could cause superconductivity. Cohen's method, however, does not seem to be applicable to this problem owing to $\omega_p \sim \varepsilon_f$, as mentioned in 2-1.C. Therefore, we should make a more detailed investigation into the plasmon mechanism of superconductivity in the electron-gas system having only the Coulomb interactions with the use of the new method in 2-2.

B. Plasmon mechanism of superconductivity

When we consider the plasmon mechanism of superconductivity, we readily notice a difference between this mechanism and the phonon one. Phonons are the vibrations of the lattice system, while the plasmon originates from the electron system itself, which means that the superconductivity arises from the internal force in the plasmon mechanism. This, however, will not cause any difficulties, considering that the internal force gives rise to superfluidity in ^{3}He in which the paramagnon plays an important role.[41] In addition, according to the theory of Bohm and Pines,[42] an assembly of electrons with the Coulomb interactions can be divided into two components. One is the part of the collective fields (plasmon) and the other is that of individual particles which interact with the collective fields and with one another via short-range screened Coulomb repulsions. If we consider the Cooper pair of the individual particles in the polarizable medium of the collective fields, the situation is just the same as that in the phonon mechanism.

We, nevertheless, has to recognize another difference. In usual materials, ω_p/ε_f is of the order of unity. This is a marked difference from the phonon mechanism in metals in which ω_D/ε_f is very small. Further, in contrast with the phonon mechanism, the range of the attractive interaction is long in the plasmon mechanism and this will produce a new type of the bound state of the pair. As we have discussed in 2-3.D, these two problems are related to each other and the long-range nature of the attractive interaction helps in constructing the pair when $\omega_p/\varepsilon_f \sim 1$. In order to make this point clearer, the present section

is devoted to the plasmon mechanism of superconductivity in the electron-gas system described by the Hamiltonian H_e, given by eq. (2.2).

C. Organization of §3

This section proceeds as follows. In 3-2, calculations of T_c in the plasmon mechanism of superconductivity are done with the use of the effective interaction in the plasmon-pole approximation[43,44] and also in the RPA. The physical picture of this mechanism is considered in 3-3, in which particular attention is paid to the long-range property of the plasmon-mediated attraction. In 3-4, we discuss the problems as to the validity of the plasmon mechanism of superconductivity from various points of view. The topics to be treated are the numerical evaluation of the effects of vertex corrections and strong coupling, the consideration of the disadvantageous effects like the disorders in actual materials and a presence of other ordered states such as the Wigner-lattice state,[45] and the discussion on the possibility to find a real system in which the plasmon has a very large contribution to the superconductivity.

3-2. Calculation without Vertex Corrections

Since we have no information about the plasmon mechanism of superconductivity at present, we begin to study this mechanism of superconductivity with the use of the lowest-order approximation to the effective interaction for the sake of simplicity. In the

first part of this subsection, we employ the plasmon-pole approximation[43,44] to obtain analytic solutions with the use of the method described in 2-3.B. Then we show the numerical results in this approximation and also in the RPA.

A. Plasmon-pole approximation

In the plasmon-pole approximation, the excitation spectrum of the system is replaced by a single mode $\tilde{\omega}_p(q)$ which approaches to ω_p for small q and Im $V^R(q,\omega)$ has the form:

$$\mathrm{Im}\, V^R(q,\omega) = -\pi \omega_p^2 \delta(\omega^2 - \tilde{\omega}_p^2(q))\, V^0(q), \tag{3.1}$$

with

$$\omega_p \equiv \sqrt{4\pi n e^2/\kappa m^*}, \tag{3.2}$$

where the factor in front of the delta-function is determined with the aid of the f-sum rule. When eq. (3.1) is substituted into the Kramers-Kronig relation (2.10) and ω is taken to be zero, we obtain the relation between $\tilde{\omega}_p(q)$ and ω_p as

$$\tilde{\omega}_p(q) = \omega_p / \sqrt{1 - V^R(q,0)/V^0(q)}. \tag{3.3}$$

There are several ways to give the static interaction $V^R(q,0)$, but for the time being, we take $V^R(q, 0)$ to be the Thomas-Fermi approximation:

$$V^R(q,0) = 4\pi e^2/\kappa (q^2 + q_{TF}^2), \tag{3.4}$$

with the inverse of the Thomas-Fermi screening length q_{TF}, defined by

$$q_{TF} = \sqrt{4 g_v e^2 m^* p_f / \pi \kappa} \quad . \tag{3.5}$$

B. Analytic results

When eq.(3.1) with eqs.(3.3) and (3.4) is put into eq.(2.18), the kernel can be integrated easily and every element of K_{ij}, defined by eq.(2.34), can be obtained without resort to the interpolation method, discussed in 2-2.C. An example of the calculated kernel K(x,x') is shown in Fig. 3.1 by the solid line. Although the Coulomb kernel has usually been approximated by a constant as indicated by eq.(2.42), the actual kernel is far from a constant even near the Fermi surface. In order to see the origin of this difference, the approximate form of K(x,x') is calculated for small |x| and |x'| as

$$K(x,x') = \frac{q_{TF}^2}{8 g_v p_f^2} \ln \frac{q_{TF}^2 + 4 p_f^2}{q_{TF}^2} + \frac{\sqrt{3}\, q_{TF}}{8 g_v p_f} (|x| + |x'|) \ln \frac{4}{|x - x'|} \tag{3.6}$$

The second term in eq.(3.6) stems from the plasmon and makes the kernel vary rather steeply. Because of the long-range nature of the plasmon-mediated attraction, there is a logarithmic singularity at $x = x' \neq 0$. This singularity is taken into account in the gap equation by the procedure, described in 2-2, in which K(x,x') is integrated by x' as shown in eq.(2.34).

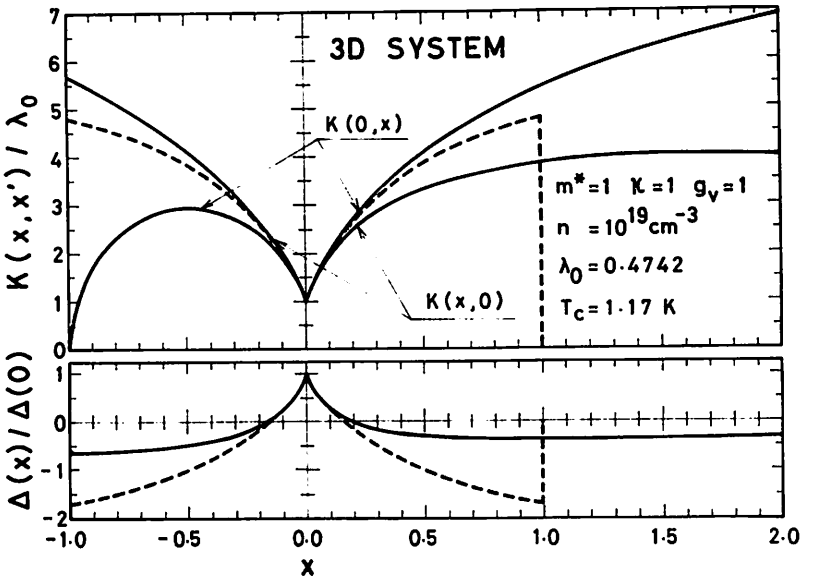

Fig.3.1. An example of the calculated kernel K(x,x') and the corresponding gap function Δ(x). Solid curves represent the results in the plasmon-pole approximation, given by eqs.(3.1)-(3.4), while broken curves show those obtained by the approximate procedure, given in eqs.(2.50)-(2.54), with the use of F(x) defined in eq.(3.7).

Now, we apply the criteria for superconductivity obtained in 2-3.B to the present case. Considering the behavior of $K(x,x')$ in eq.(3.6), we can take $F(x)$ as

$$F(x) = \frac{\sqrt{3}\, q_{TF}}{8 g_v p_f} |x| \ln \frac{4}{|x|} = 0.176 \frac{\sqrt{r_s}}{g_v^{1/3}} |x| \ln \frac{4}{|x|} , \tag{3.7}$$

where r_s parameter is defined as usual by

$$r_s = \frac{m^* e^2}{\kappa} \left(\frac{3}{4\pi n} \right)^{1/3} . \tag{3.8}$$

An example of the kernel obtained by eq.(2.50) and the gap function $\phi(x)$ given by eq.(2.51) with $F(x)$ in eq.(3.7) is plotted in Fig. 3.1 by the broken lines. Inequality (2.53) gives the condition for the appearance of superconductivity as

$$r_s \gtrsim 6 , \tag{3.9}$$

for the case of $g_v = 1$.

Compared with eq.(2.65), eq.(3.7) also gives us the dimensionless coupling constant λ_p for the plasmon mechanism as

$$\lambda_p \propto g_v^{1/3} r_s , \tag{3.10}$$

with the use of the relation of

$$\omega_p / \epsilon_f = 0.940\, g_v^{2/3} \sqrt{r_s} . \tag{3.11}$$

Equation (3.10) indicates that the plasmon contributes to the superconductivity for every r_s, although in the usual metals whose largest r_s value is 5.62 in Cs, the contribution is not so large as to cause superconductivity. Therefore, in the usual superconductors in which r_s values are in the range from 1.6 to 2.7,[46] the role of the plasmon is at most to give some help to phonons and is included in the adjustable parameter μ^* effectively.

C. Numerical results

Now, we turn to the numerical solutions. An example of the gap function $\phi(x) \equiv \Delta(x)/\Delta(0)$ is shown in Fig. 3.1 by the solid line which corresponds to the kernel in Fig. 3.1. The results of T_c are plotted in Fig. 3.2 as a function of r_s for several values of m^*, κ, and g_v. All these curves of T_c behave in the similar way: As r_s is increased, T_c increases abruptly first and then decreases gradually. The reason of this behavior will be clarified in 3-3. In order to estimate the BCS coupling constant λ_p^{BCS} of this mechanism, we express T_c in the form:

$$T_c = 1.134\, \omega_p \exp\left(-1/\lambda_p^{BCS}\right). \qquad (3.12)$$

The results of λ_p^{BCS} are illustrated as a function of r_s for a few values of g_v in Fig. 3.3 by solid lines, while the broken line represents the approximate one of λ_p^{BCS} with the use of eq.(2.54) and F(x) defined by eq.(3.7). With the increase of

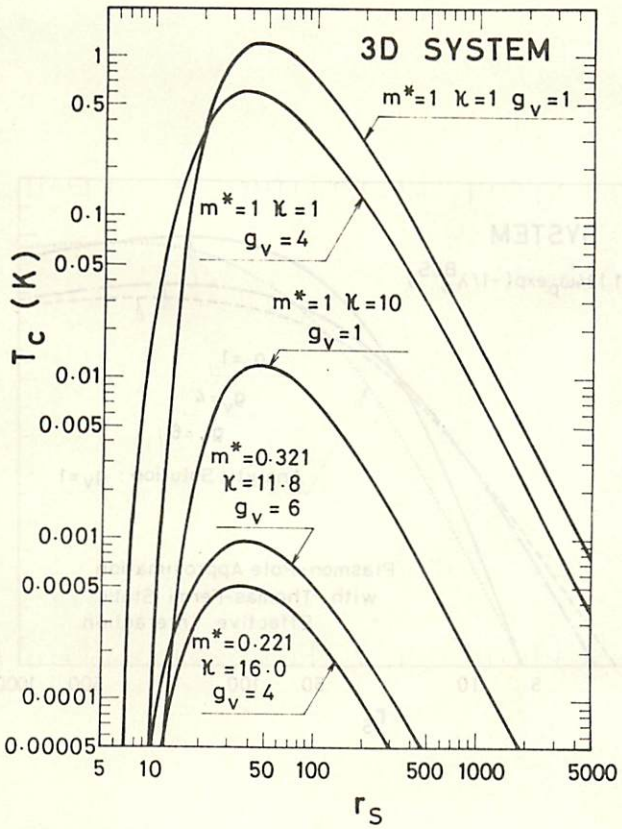

Fig.3.2. Calculated results of T_c for several values of m*, κ, and g_v in the plasmon-pole approximation with the use of the static effective interaction in the Thomas-Fermi approximation. The case of m*= 0.321 m_e, κ = 11.8, and g_v = 6 treats n-type Si, while that of m*= 0.221 m_e, κ = 16.0, and g_v= 4 deals with n-type Ge.

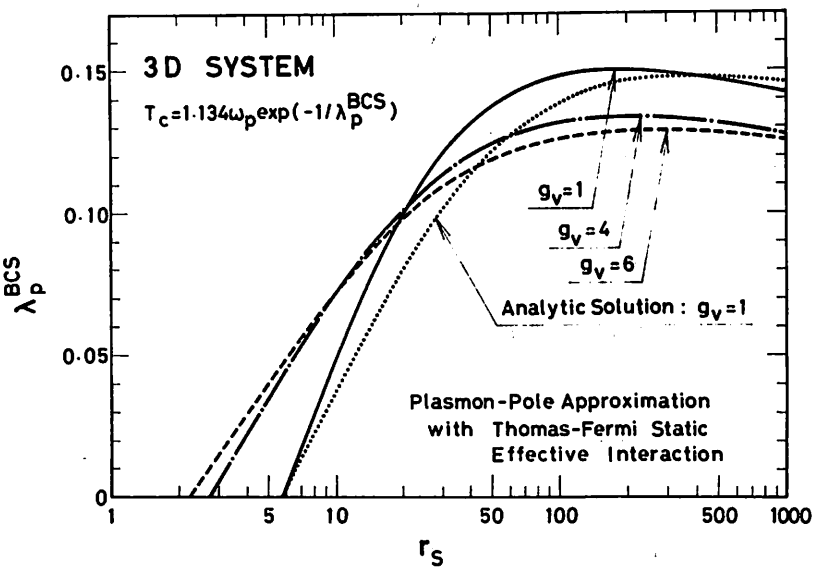

Fig.3.3. Calculated results of the BCS coupling constant in the plasmon mechanism of superconductivity for the cases of $g_v = 1$, 4, and 6 with the use of the plasmon-pole approximation. The dotted curve shows the result obtained by the analytically soluble model described in 2-3.B with F(x) in eq.(3.7). When r_s is decreased, λ_p^{BCS} becomes negative, which means the absence of the superconductivity in this mechanism.

r_s, λ_p^{BCS} increases first, but when r_s becomes larger than 50, λ_p^{BCS} is nearly constant. This leads us to the relation of $T_c \propto \omega_p$ for $r_s \gtrsim 50$. In any case, the magnitude of λ_p^{BCS} never becomes greater than 0.15 and the weak-coupling approximation seems to be satisfied.

Figure 3.3 also gives us a knowledge as to which part of the kernel is important to the formation of the Cooper pair in the plasmon mechanism. The approximate analytic model, described in 2-3.B, is shown to work very well, though it is quite simple. In this model, F(x) is defined with the use of the changing rate of the kernel near the Fermi surface and plays the most important role in the determination of T_c. Therefore the shape of the kernel near the Fermi surface is very important to this mechanism of superconductivity.

The importance of the kernel in the vicinity of the Fermi surface is also indicated by the shape of the gap function. An example of the gap function is given in Fig.3.1 in which $\Delta(x)/\Delta(0)$ is positive only when $|x| \equiv |\varepsilon_p/\varepsilon_f|$ is less than *ca.* 0.2. According to the discussion about the sign of $\Delta(x)/\Delta(0)$ in 2-3.A, the plasmon-mediated attractive potential has a large effect on the kernel near the Fermi surface, or more precisely, the kernel in the region where $\Delta(x)/\Delta(0)$ is positive.

In order to understand the reason why the scatterings within the region near the Fermi surface are important even in this plasmon mechanism, let us examine the meaning of the pairing interaction $V_{pp'}$, defined by eq.(2.15). When one Cooper pair characterized by momentum p, that is, a pair constructed by an

electron with p and another one with -p is scattered into another pair characterized by p', the effective interaction between the electrons is given by $V^R(p-p',\Omega)$, if the electrons are oscillating with the frequency Ω during the scattering process. However, $V^R(p-p',\Omega)$ is not the pairing potential for the pair scattered from p to p', because the oscillation of the electrons can occur with any Ω. After we take all these dynamical (Ω-dependent) effects into account, we obtain $V_{pp'}$, given by eq.(2.15), for the pairing potential.

In the present case, the plasmon exists only for small wave numbers, so that the plasmon contributes to the pairing interaction only when p is nearly equal to p', namely only when the forward scattering occurs. Thus, when we consider the Cooper pair at the Fermi surface, only the scatterings in the region near the Fermi surface have an effect of the plasmon-mediated attractive interaction. In this way, the long-range nature of this attractive potential limits the scatterings of the Cooper pairs mainly to the vicinity of the Fermi surface, even if ω_p is larger than ε_f.

D. Calculation in the RPA

The excitation mode $\tilde{\omega}_p(q)$ in eq.(3.1) should approach to $q^2/2m^*$ for very large q, but $\tilde{\omega}_p(q)$ defined by eqs.(3.3) and (3.4) does not share this property. In order to improve this point, the static interaction $V^R(q,0)$ in eq.(3.3) is evaluated in the RPA as

$$V^R(q,0) = V^0(q) / \left[1 + \frac{1}{2} \frac{q_{TF}^2}{q^2} \left(1 + \frac{4p_f^2 - q^2}{4p_f q} \ln \left| \frac{2p_f + q}{2p_f - q} \right| \right) \right]. \quad (3.13)$$

The calculated results of T_c in the present approximation is plotted in Fig. 3.4 as a function of the carrier concentration n for the case of $g_v = 1$ by the dotted curve. For the sake of comparison, the results in the former approximation, described in 3-2.A, and in the RPA are also shown by the broken and the solid curves, respectively. The effective interaction, $V^R(q,i\Omega)$, in the RPA is given by[47]

$$V^R(q,i\Omega) = V^0(q) / \left[1 + Q_0(q,i\Omega) \right], \quad (3.14)$$

where the function $Q_0(q,i\Omega)$ is defined by

$$Q_0(q,i\Omega) \equiv V^0(q) \Pi(q,i\Omega)$$

$$= \frac{1}{2} \cdot \frac{q_{TF}^2}{q^2} \left[1 + \frac{1 - z^2 + u^2}{4z} \ln \frac{(1+z)^2 + u^2}{(1-z)^2 + u^2} - u \tan^{-1} \frac{2u}{u^2 + z^2 - 1} \right]. \quad (3.15)$$

Here, $\Pi(q,i\Omega)$ is the electronic polarization function, $z \equiv q/2p_f$, $u \equiv \Omega/qv_f$ with the Fermi velocity v_f, and the branch of the function $\tan^{-1} z$ is so chosen that $0 \leq \tan^{-1} z < \pi$. In Fig. 3.4, T_c and n are represented in the scales of m^*/κ^2 and $(m^*/\kappa)^3$, respectively. This is because in the electron-gas system, the physical quantities having the dimensions of energy and length can be measured in the units of the effective Rydberg and the

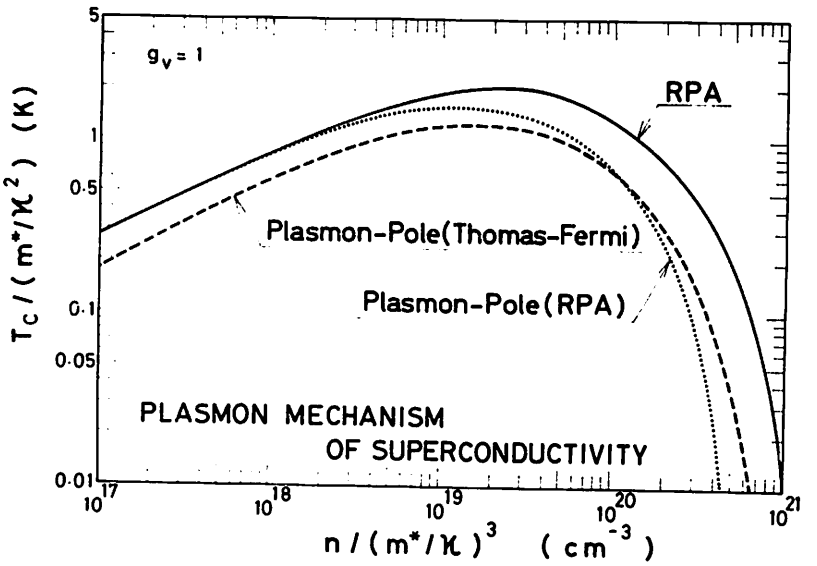

Fig.3.4. Transition temperature T_c scaled by the effective Rydberg as a function of n scaled by the inverse of the effective Bohr radius cubed, where m* is measured in the unit of m_e. Solid, broken and dotted lines correspond to the results in the RPA, the plasmon-pole approximation with the Thomas-Fermi static interaction, and that with the static RPA interaction, respectively.

effective Bohr radius, respectively.

Figure 3.4 shows that the change of T_c with the choice of the approximations is small, which indicates that for the calculation of T_c in the plasmon mechanism of superconductivity, the region of large q in the effective interaction is not important. For low n, the calculated curve of T_c increases in proportion to $\sqrt{n}$, which means that T_c is proportional to ω_p in this region of n. The maximum value of T_c becomes of the order of m^*/κ^2 degrees Kelvin at $r_s \sim 40$, where m^* is measured in the unit of the mass of a free electron which will be denoted by m_e.

3-3. Physical Picture of Plasmon Mechanism of Superconductivity

The analysis of 3-2 suggests that the plasmon has a rather large contribution to superconductivity. In particular, the electron-gas system with a low carrier concentration is expected to be superconducting with the aid of the plasmon. These results, however, cannot be accepted readily, because the approximations to the effective interaction employed there may not work well for the discussion on the superconductivity in such a low-carrier-concentration system. Thus in order to proceed further, we must have a more definite physical picture about the plasmon mechanism of superconductivity. In this subsection, we first review the bound state of the Cooper pair in the phonon mechanism of superconductivity in metals for the sake of comparison and then consider the case of the plasmon

mechanism of superconductivity.

A. Bound state in phonon mechanism

In the phonon mechanism of superconductivity, the BCS theory revealed that the effective potential for a Cooper pair which took every dynamical process into account could be represented by $V_{ph}(r)$ as

$$V_{ph}(r) = \begin{cases} -V_0, & r < r_0, \\ 0, & r > r_0, \end{cases} \tag{3.16}$$

with a positive V_0 and the range r_0 of the order of p_f^{-1}. The wave function $\phi(r)$ of the Cooper pair in the center-of-mass coordinate system under the potential (3.16) is obtained by

$$\phi(r) \equiv \oint \frac{d\omega}{2\pi i} \sum_p e^{ipr} F^C(p,\omega), \tag{3.17}$$

where $F^C(p,\omega)$ is the anomalous Green's function defined in 2-1 and the superscript C denotes the causal form. At T = 0, $\phi(r)$ is calculated to be

$$\phi(r) = \frac{m^*}{4\pi^2 r} \int_{-\epsilon_f}^{\infty} d\xi_p \frac{\Delta(p) \sin pr}{\sqrt{\xi_p^2 + \Delta(p)^2}}, \tag{3.18}$$

with $\Delta(p)$ defined by eq.(2.12). Since $\Delta(p)$ does not vanish only near the Fermi surface and is constant in the phonon mechanism, eq.(3.18) is estimated for large r as

$$\phi(r) = 1.764\, T_c \frac{m^* p_f}{2\pi^2} \cdot \frac{\sin p_f r}{p_f r} K_0(r/\pi\xi_0), \tag{3.19}$$

where the coherence length ξ_0 is given by

$$\xi_0 \equiv 0.180\, v_f / T_c, \tag{3.20}$$

with the Fermi velocity v_f and $K_0(z)$ is the zeroth-order modified Bessel function of the second kind. Equation (3.19) can be understood as the product of the wave function of the free particle with the wave number p_f and the "envelope function" $K_0(r/\pi\xi_0)$. Because of $\omega_D/\varepsilon_f \ll 1$, the degrees of freedom for the relative motion of the pair are two. This fact is reflected in the "envelope function" $K_0(r/\pi\xi_0)$ which is the characteristic for a two-dimensional motion in a square-well potential.

B. Bound state in plasmon mechanism

Now, we consider the plasmon mechanism in the electron-gas system. In any kind of approximations to the effective interaction, the dielectric function $\varepsilon(q,\omega)$ has the form for $\omega \gg qv_f$ as

$$\varepsilon(q,\omega) \simeq 1 - \omega_p^2/\omega^2, \tag{3.21}$$

while when q is much larger than p_f,

$$\varepsilon(q,\omega) \simeq 1, \tag{3.22}$$

for any value of ω. Thus the effective potential $V_{pl}(r)$ for the Cooper pair which exchanges the plasmon virtually, that is, which oscillates coherently with the frequency ω near ω_p, is assumed to be

$$V_{pl}(r) = \begin{cases} e^2/\kappa r, & r < r_p, \\ -e^2/\kappa_p r, & r > r_p, \end{cases} \tag{3.23}$$

where r_p and κ_p may be taken tentatively as

$$r_p \sim v_f/\omega_p, \tag{3.24}$$

and

$$\kappa_p/\kappa \sim \omega_p^2/\epsilon_f^2, \tag{3.25}$$

respectively. This potential $V_{pl}(r)$ corresponds to $V_{ph}(r)$ in the phonon mechanism, but the difference is clear: The former has a long-range attraction, while the latter has a short-range one. Thanks to this long-range nature, the bound state exists under the potential $V_{pl}(r)$ for any values of κ_p/κ and r_p, even if the parameter ω_p/ϵ_f is large to make the degrees of freedom three. In order to make this point clearer, the motion of the pair is solved variationally. The Hamiltonian for the relative motion of the pair is written by

$$H = -\frac{1}{m^*}\left(\frac{\partial^2}{\partial x^2} + \frac{\partial^2}{\partial y^2} + \frac{\partial^2}{\partial z^2}\right) + V_{pl}(r). \tag{3.26}$$

The wave function $\phi(r)$ can be obtained by eq.(3.18) with $\Delta(p)$ given in 3-2. In contrast with the previous case, $\Delta(p)$ changes even in the vicinity of the Fermi surface, as we have seen in Fig.3.1. Owing to this fact, $K_0(r/\pi\xi_0)$ in eq.(3.19) changes into another form and $\phi(r)$ may be approximated as

$$\phi(r) = \sqrt{\frac{1+a^2p_f^2}{\pi a^3}} \cdot \frac{\sin p_f r}{p_f r} \cdot e^{-r/a}, \tag{3.27}$$

where the parameter a will be determined variationally by $\partial\langle\phi|H|\phi\rangle/\partial a = 0$. If the total energy $\langle\phi|H|\phi\rangle$ is less than the kinetic energy of the free particles p_f^2/m^*, the electrons near the Fermi surface are bound together and the superconducting phase will appear. The parameter a can be solved rather easily and the approximate solution for a is given by

$$a/a^* = \frac{1}{a^* p_f} \exp\left[\left(1+\frac{\kappa_p}{\kappa}\right) I(2p_f r_p) + 1\right]. \tag{3.28}$$

The corresponding binding energy $\Delta \equiv |\langle\phi|H|\phi\rangle - p_f^2/m^*|$ is given by

$$\Delta/E^* = 4a^* p_f \frac{\kappa}{\kappa_p} \exp\left[-\left(1+\frac{\kappa_p}{\kappa}\right) I(2p_f r_p) - 1\right], \tag{3.29}$$

where $a^* \equiv \kappa/m^*e^2$, $E^* \equiv m^*e^4/2\kappa^2$, and $I(x)$ is defined by

$$I(x) = \int_0^x \frac{1-\cos t}{t}\, dt, \tag{3.30}$$

which is well-approximated by $x^2/4$ for $x \lesssim 3$. With the use of eqs.(3.24) and (3.25), eqs.(3.28) and (3.29) can be rewritten as

$$a/a^* \sim 80\, g_v^{1/3} r_s\, e^{4.5/g_v^{4/3} r_s}, \tag{3.31}$$

and

$$\Delta/E^* \sim \frac{0.06}{g_v^{5/3} r_s^2}\, e^{-4.5/g_v^{4/3} r_s}, \tag{3.32}$$

respectively. Since ap_f is calculated to be

$$ap_f \sim 150\, e^{4.5/g_v^{4/3} r_s}, \tag{3.33}$$

the important region for the formation of the pair is the long-range part of the attraction, that is, $q \ll p_f$. In this region, the effective interaction in any approximation is much the same as that in the RPA. Thus the results of T_c in any approximation are not expected to change very much. This will be assured in 3-4.B by the numerical evaluation of the gap equation.

As is consistent with the result of T_c in Fig. 3.2, the binding energy Δ in eq.(3.32) has an optimum r_s. Since Δ is proportional to $\kappa/\kappa_p \cdot \exp(-p_f^2 r_p^2)$, this behavior can be understood by the changes of r_p and κ_p with the increase of r_s. The region of the repulsive potential, $r_p p_f$, changes as

$$r_p p_f \sim 2.1/\, g_v^{2/3} \sqrt{r_s}, \tag{3.34}$$

and the strength of the attraction, κ/κ_p, varies as

$$\kappa/\kappa_p \sim 1.1/\, g_v^{4/3} r_s. \tag{3.35}$$

When r_s is increased, the repulsive region increases. On the other hand, the plasmon energy becomes so high that the attraction becomes weak. These two opposite effects make Δ have an optimum r_s. It should be noted here that because of the large $r_p p_f$ for small r_s, the approximation used in the derivation of eqs.(3.28) and (3.29) is rather poor. This is probably the main reason why the bound pair can be formed even in small r_s, in contrast with the results in 3-2.

In many-valley semiconductors, *i.e.*, in the system with large g_v, both $r_p p_f$ and κ/κ_p become small, as indicated in eqs. (3.34) and (3.35). Accordingly, the plasmon mechanism of superconductivity in these systems is more favorable for small r_s, whereas it becomes unfavorable for large r_s. This behavior is illustrated well in Fig.3.3 in which λ_p^{BCS} becomes large for large g_v when r_s is small, while the contrary is the case for large r_s.

C. Comment on single-particle states

An additional comment on the single-particle state is necessary in the plasmon mechanism of superconductivity, although we have already made some of them in 2-3.D. In order to enjoy the plasmon-mediated attractive interaction between the electrons of the pair, that is, in order to feel the effective interaction $V_{pl}(r)$, defined by eq.(3.23), each electron of the pair should oscillate coherently, which requires that the wave function of one electron of the pair should overlap with that of the other electron in the attractive potential region. Thus the wave function should extend over a very long range, because the

attractive potential is a long-range one in the plasmon mechanism. This condition for the wave function can be changed into that for the mean-free-path of electrons ℓ. Namely, ℓ should be at least larger than the shortest wavelength of the plasmon which can be estimated by r_p, given in eq.(3.24).

As mentioned in 2-3.D, the macroscopic coherent field is constructed by the electrons near the Fermi surface irrespective of the ratio of the energy of the intervening mode (plasmon in the present case) to ε_f. Thus, the electrons near the Fermi surface should meet the above condition. For these electrons, ℓ is given by the product of v_f and the life time of the single-particle state. The life time τ originates from both the impurity scatterings and electron-electron scatterings. With this τ, the condition of $\ell > r_p$ is reduced to that of $\omega_p\tau > 1$. Physically, if τ is shorter than ω_p^{-1}, the coherent oscillation of the pair is interrupted, so that the plasmon-mediated attractive interaction is not felt sufficiently. When we consider the phase transition from the normal metallic state to the superconducting one, the condition of $\tau > \omega_p^{-1}$ seems to be satisfied. Detailed discussions are given in the next subsection.

3-4. Discussions

A. Introduction

We have investigated the possibility of the plasmon mechanism of superconductivity in the electron-gas system by the application of the new numerical method to solve the gap equation. One of the results thus obtained is that for the case of $g_v = 1$, the plasmon

alone cannot bring about superconductivity when r_s is less than 6. This fact assures us of the validity of the conventional treatment of superconductivity in metals in which phonons are of the primary importance and every Coulombic effect including the contribution from the plasmon is dealt with by one adjustable parameter μ^*. We, at the same time, have obtained the result in which for lower carrier densities than those in metals, the superconducting state will appear with the aid of the long-range attractive interaction induced by the plasmon.

In such a low-carrier-density system, however, there remain several problems before we arrive at the final conclusion. In order to grasp what are the fundamental problems, let us return to the gap equation (2.6) which does not include any approximations. According to this equation, we can see that all the problems originate from two parts. One is the approximation to the single-particle Green's function $G_i(p,i\omega_p)$ and the other is that to the irreducible interaction $I_{ii'}(p,p';i\omega_p,i\omega_{p'})$. In principle, these two are connected with each other and the approximations to them should be done self-consistently. In this sense, the calculations in 3-2 are consistent, because the single-particle Green's function is approximated by the bare one and the vertex corrections are neglected everywhere. In order to take higher-order corrections into account, we must have a clear physical idea about the single-particle state. When the state for $T \gtrsim T_c$ is assured to be normal and thus a well-defined Fermi sphere is present, $G_i(p,i\omega_p)$ can be approximated by

$$G_i(p,i\omega_p) = \frac{1}{Z_c}\cdot\frac{1}{i\omega_p - \frac{1}{2m_c^*}(p^2-p_f^2)}\ , \tag{3.36}$$

where z_c and m_c^* are the renormalization factor and the renormalized effective mass at the Fermi surface, respectively. Then the self-consistent process reads that the calculations of z_c, m_c^* and higher-order vertex corrections to $I_{ii}(p,p';i\omega_p, i\omega_{p'})$ should be carried out consistently.

In the first part of this subsection, we make several arguments about the effects of vertex corrections and strong coupling under the assumption of $G_i(p,i\omega_p)$ in the form of eq.(2.7), or eq.(3.36). Secondly, we discuss the validity of this picture of the single-particle state. Lastly, we make some comments on the possibility to observe the plasmon mechanism of superconductivity in real materials. The valley degeneracy g_v is assumed to be unity in the following calculations and suffix i is deleted in I_{ii} and G_i.

B. Vertex corrections

The simplest way to include the vertex corrections is the Hubbard approximation.[48] The dielectric function in this approximation $\varepsilon_H(q,i\Omega)$ is

$$\varepsilon_H(q,i\Omega) = 1 + Q_0(q,i\Omega) / [1 - G_H(q) Q_0(q,i\Omega)], \quad (3.37)$$

where $Q_0(q,i\Omega)$ is defined in eq.(3.15) and the Hubbard's local-field correction $G_H(q)$ is given by

$$G_H(q) = q^2 / 2(q^2 + p_f^2 + q_{TF}^2). \quad (3.38)$$

The vertex correction $\Gamma_H(q,i\Omega)$ which is consistent with $\varepsilon_H(q,i\Omega)$ is obtained as

$$\Gamma_H(q,i\Omega) = 1 / [1 - G_H(q) Q_0(q,i\Omega)]. \quad (3.39)$$

Then the irreducible interaction $I(p,p';i\omega_p, i\omega_{p'})$ is given by

$$I(p,p';i\omega_p, i\omega_{p'}) = V^0(q)\Gamma_H^2(q,i\Omega)/\varepsilon_H(q,i\Omega), \tag{3.40}$$

with $q \equiv p - p'$ and $i\Omega \equiv i\omega_p - i\omega_{p'}$. It must be noted here that this interaction is different from that in the self-energy part of the single-particle Green's function which is given by $V^0(q)\Gamma_H(q,i\Omega)/\varepsilon_H(q,i\Omega)$. An example of the calculated kernels and the corresponding gap functions in the RPA and the Hubbard approximation is shown in Fig. 3.5, in which $z_c = m_c^*/m^* = 1$ is assumed. In spite of the large difference in the calculated kernels at the Fermi surface, the results of T_c are much the same, *i.e.*, T_c is determined almost by the changing rate of the kernel near the Fermi surface. Since this changing rate comes mainly from the plasmon, vertex corrections have only a small effect on T_c.

The electron-electron ladder diagrams, which are not included in the Hubbard approximation, should be taken into account for large r_s to have a correct short-range behavior of the pair correction function.[49] These diagrams can be treated by the scheme of Singwi *et al.*,[50] in which the local-field correction $G_s(q)$ is approximately represented by

$$G_s(q) = A\cdot(1 - e^{-Bq^2}), \tag{3.41}$$

where A and B are tabulated for r_s = 1, 2, ···, 6 in the paper of Vashishta and Singwi[51] and these results can be simulated well by the relation of

$$A = 0.7085 + 0.1363\ln r_s + 0.0975(\ln r_s)^2, \tag{3.42}$$

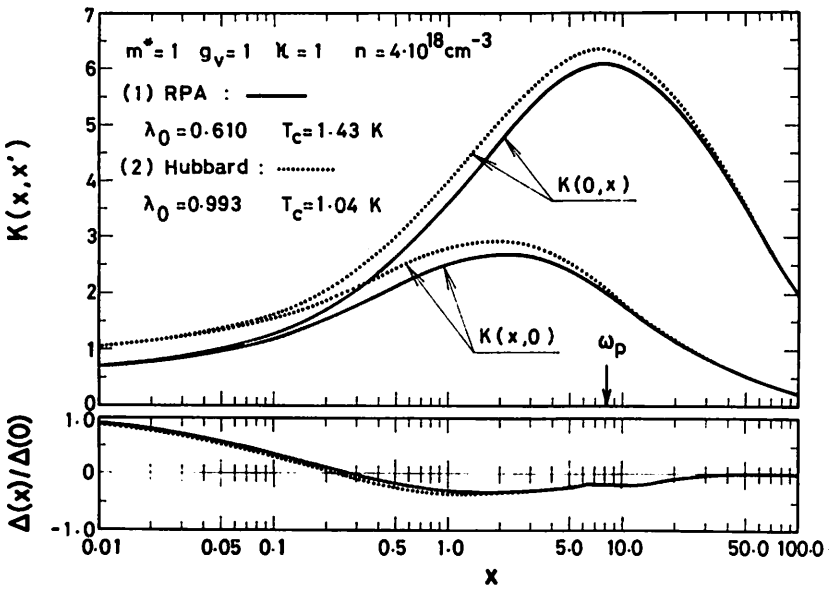

Fig.3.5. An example of calculated kernels and the corresponding gap functions. Solid and dotted lines correspond to the results in the RPA and the Hubbard approximation, respectively.

and

$$B = 0.3788 - 0.0688 \ln r_s . \tag{3.43}$$

The irreducible interaction in this approximation is obtained by the same form as that in eq.(3.40), in which $G_H(q)$ should be exchanged by $G_S(q)$. Some diagrams which are included in this approximation are shown in Fig. 3.6(a). The BCS coupling constant λ_p^{BCS}, which is defined in eq.(3.12), is calculated under the assumption of $z_C = m_C^*/m^* = 1$. The result is plotted in Fig. 3.7, in which the results in the RPA, the plasmon-pole approximation with the use of the Thomas-Fermi static interaction, and the Hubbard approximation are also shown. These results are essentially the same, in particular, for large r_s.

C. Strong-coupling effect

Now, we discuss the effects of z_C and m_C^*. When eq.(3.36) is used for $G(p,i\omega_p)$ instead of eq.(2.7), the kernel $K(\omega,\omega')$, defined by eq.(2.18), changes into $K^*(\omega,\omega')$ as

$$K^*(\omega,\omega') = \frac{1}{z_C^2} \cdot \frac{m_C^*}{m^*} \cdot K(\omega,\omega') . \tag{3.44}$$

In case of the phonon mechanism in metals, m_C^*/m^* is equal to z_C because of $\omega_D/\varepsilon_f \ll 1$ and eq.(3.44) is reduced to $K^*(\omega,\omega') = K(\omega,\omega')/z_C$, which is the familiar form in the strong-coupling theory.[13-17] In the present case, however, m_C^*/m^* is less than z_C. In the actual calculation, the values of z_C and m_C^*/m^* are, tentatively, borrowed from the results of Overhauser,[44] who,

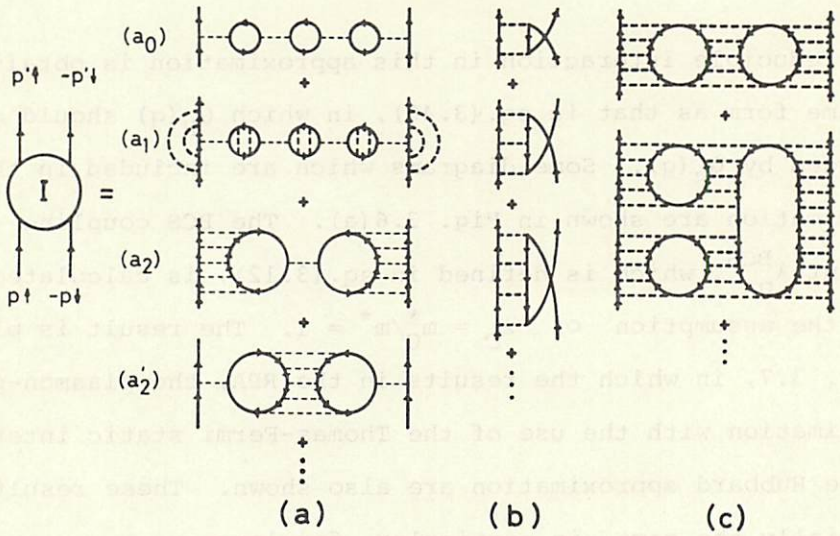

Fig.3.6. Some diagrams which contribute to the irreducible interaction $I(p,p';i\omega_p, i\omega_{p'})$. Diagrams of the type (a_0) are included in the RPA, while those of the type (a_1) are in the Hubbard approximation. Types such as (a_2) and (a_2') are approximately taken into account by the scheme of Singwi *et al*. Types of (b) and (c) are the contributions of the paramagnon effect and the fluctuation effect, respectively. A rough estimate of the type (b) is considered in 3-4.D. Type (c) is not important in a three-dimensional system and is neglected in §3, but in a two-dimensional system, it becomes important. Discussions of this type of diagrams are given in 9-2 briefly.

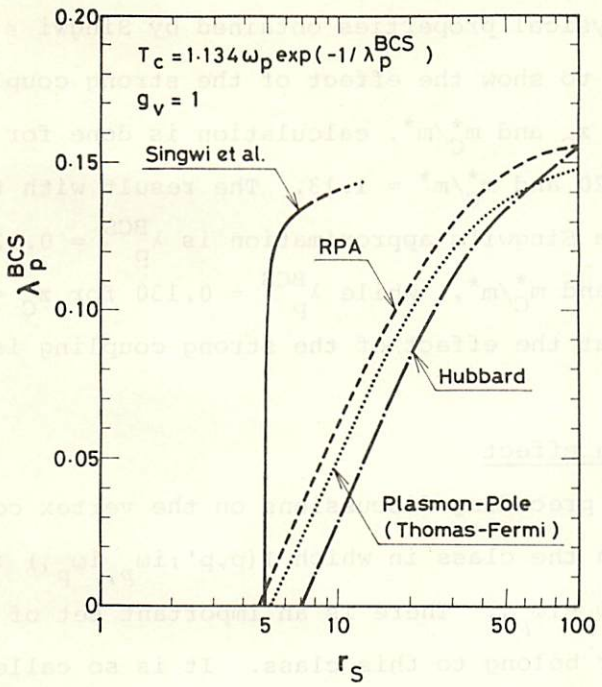

Fig.3.7. Comparison of the BCS coupling constants calculated in various approximations, that is, the scheme of Singwi *et al.*, the Hubbard approximation, the RPA, and the plasmon-pole approximation with the static screening in the Thomas-Fermi approximation. Since the validity of the extrapolated formulae for A and B, given in eqs. (3.42) and (3.43), respectively, is not known, the result in the scheme of Singwi *et al.* for $r_s > 10$ is not shown in the figure.

in the plasmon-pole approximation, tried to simulate the results of several physical properties obtained by Singwi *et al.*[50,51] As an example to show the effect of the strong coupling, that is, the effect of z_c and m_c^*/m^*, calculation is done for $r_s = 6$, in which $z_c = 2.20$ and $m_c^*/m^* = 1.13$. The result with the kernel $K(\omega,\omega')$ in the Singwi's approximation is $\lambda_p^{BCS} = 0.120$ for these values of z_c and m_c^*/m^*, while $\lambda_p^{BCS} = 0.130$ for $z_c = m_c^*/m^* = 1$. This means that the effect of the strong coupling is small.

D. Paramagnon effect

All the preceding discussions on the vertex corrections are concerned with the class in which $I(p,p';i\omega_p, i\omega_{p'})$ is a function of $p-p'$ and $i\omega_p - i\omega_{p'}$. There is an important set of diagrams which does not belong to this class. It is so called the paramagnon effect[52] and this produces a unfavorable effect on the s-wave coupling of the Cooper pair. In case of a short-range interaction as in ^{3}He, this effect is so strong that the spin-singlet state does not occur.[41] The diagrams of this effect are shown in Fig. 3.6(b) and it is very difficult to sum up these diagrams. We, therefore, make a rough estimate of the contribution from this set of the diagrams $I^{paramagnon}(p,p';i\omega_p, i\omega_{p'})$. When the interaction V_s appeared in these diagrams is approximated to be q- and ω-independent, the diagrams can be summed as

$$I^{paramagnon}(p,p';i\omega_p,i\omega_{p'}) = \frac{1}{2}V_s^2\Pi(p+p',i\omega_p+i\omega_{p'})/[1-\tfrac{1}{2}V_s\Pi(p+p',i\omega_p+i\omega_{p'})], \tag{3.45}$$

where $\Pi(q,i\omega_q)$ is the electronic polarization function in the RPA, given in eq.(3.15). Since the typical value of the static interaction V_s is

$$V_s \frac{m^* p_f}{2\pi^2} \sim \frac{1}{2}, \tag{3.46}$$

and $\Pi(p+p',i\omega_p+i\omega_{p'})$ can be estimated as

$$\Pi(p+p',i\omega_p+i\omega_{p'}) \simeq \Pi(2p_f, i2\epsilon_f) = \frac{1}{2}\cdot\frac{m^* p_f}{2\pi^2}, \tag{3.47}$$

the value of $I^{\text{paramagnon}}(p,p';i\omega_p, i\omega_{p'})m^* p_f/2\pi^2$ is estimated to be 0.07. This is about one tenth of the effective interaction in the RPA and is negligibly small.

E. Problems about the ground state in the jellium model

Thus far, we have discussed the phase transition from the normal metallic state to the superconducting one with the aid of the plasmon, which has ended in the positive conclusion. The true ground state, however, may be other ordered ones such as the Wigner-lattice state[45] in an assembly of electrons in a uniform background of neutralizing positive charges (jellium model), when r_s is large. If other states might occur for $r_s < 6$, the system may not experience the plasmon mechanism of superconductivity when the carrier concentration is varied. Therefore, we review other ordered states here.

The Wigner's idea that the electrons in the jellium model crystallize out at sufficiently low carrier densities is generally

accepted, although no conclusive calculations have been done to determine the critical value r_s^W of the r_s parameter at which the electron gas condenses into the Wigner lattice. Many people[53,54] have applied various methods to estimate r_s^W. Their results spread over a wide range and the largest one reaches 700,[54] from which we can say at least that the Wigner-lattice state will not appear if $r_s \lesssim 10$.

In order to compare the condensation energy between the Wigner-lattice and the superconductivity, the melting temperature T_m of the Wigner lattice is estimated to be

$$T_m/E^* \sim \frac{1}{\Gamma_0}\cdot\frac{2}{r_s}\ , \quad \text{for } r_s > r_s^W, \tag{3.48}$$

where E^* is the effective Rydberg and Γ_0 is typically of the order of 100.[55] Since the superconducting transition temperature T_c, which is estimated by Δ in eq.(3.32), is smaller than T_m, the Wigner-lattice state is more stable for $r_s > r_s^W$.

Thus, what remains to consider about the Wigner-lattice is a possibility of the superconductivity in the Wigner-lattice state, since the plasmon is also present in this state. However, the wave function of each electron is localized in this state and the superconductivity does not occur, as we have discussed in 3-3.C. This leads to the complete absence of the superconductivity for $r_s > r_s^W$. This problem can also be seen from another point of view. As r_s is increased, the single-particle state ψ_p characterized by the momentum p has a shorter life time τ_p due to the electron-electron scatterings. Accordingly, the

Fermi surface becomes blurred and it is not well-defined at all for $r_s \sim r_s^W$, so that $\tau_{p\simeq p_f}$ becomes of the order of ω_p^{-1}. When the life time of the quasi-particle is so short, the plasmon mechanism of superconductivity does not occur, as discussed in 3-3.C.

In connection with the superconductivity in a Wigner-lattice state, we make a few comments on the speculation by Bagchi,[56] who suggested that since the static dielectric function for small q was negative in the Wigner-lattice state, other conduction electrons, introduced into the lattice, would form the Cooper pair. First, he considered two kinds of electrons, while we discuss a single kind of electrons. His situation is just the same as that of electrons in the lattice of ions and there is nothing new. Secondly, when another kind of electrons is introduced into the Wigner-lattice state, the system will be changed in order not to make the static dielectric constant negative.

As for a candidate for the ordered state in the jellium model for large r_s, a ferromagnetic state is also investigated, which is related to the paramagnon effect. Several authors[57,58] studied this problem and found that this state would not appear if r_s was smaller than 10,[57] or 19.[58]

To sum up, there is no conclusive knowledge about the ground state in the jellium model with large r_s, but if we take an optimistic point of view, it seems safe to assume that for $6 \lesssim r_s \lesssim 10$, the system is in the normal metallic state with a well-defined Fermi surface for $T > T_c$ and that it becomes superconducting with the aid of the plasmon for $T < T_c$.

F. Effects of disorder

We have to recognize several discrepancies between the jellium model and real materials. Above all, there are various kinds of disorder in real systems. If the fluctuation of the potential coming from ions is very large, each electron will localize at the potential minima, as pointed out by Anderson.[59] This causes a fatal influence on the plasmon mechanism of superconductivity.

Even when the effects of disorder are not so strong that they can be treated in terms of the impurity scattering by electrons, the superconductivity in the plasmon mechanism might be damaged. In case of the phonon mechanism, the pair will oscillate coherently even for the very short relaxation time τ of the impurity scatterings, for example, $\tau \sim \varepsilon_f^{-1}$, because the range of the attraction is short and there are no impurities practically in that small region.

In the plasmon mechanism, however, the range of the plasmon-mediated attraction is long and there will be not a few impurities within the range. In the presence of impurities, the dielectric function for small q has the following form[60] instead of eq. (3.21):

$$\varepsilon(q,\omega) \simeq 1 - \frac{\omega_p^2}{\omega(\omega + i/\tau)} \quad . \tag{3.49}$$

Equation (3.49) requires the condition of

$$\omega_p \tau \ll 1 \, , \tag{3.50}$$

in order to make the same discussions as those in 3-3.B. Therefore, the plasmon mechanism is affected more strongly by impurities than the phonon one in which non-magnetic impurities hardly affect the superconductivity.[61]

G. Final conclusions and discussions

Now, we sum up the foregoing discussions on the plasmon mechanism of superconductivity in the electron-gas system. In the first place, the plasmon has an effect to make the system superconducting. The effect increases with the decrease of the carrier concentration, but it is not so strong as to overcome the effect of the short-range Coulomb repulsion in usual metals ($r_s \lesssim 5$). When the carrier concentration is decreased further, the plasmon brings about superconductivity, provided that the system is in the normal metallic state with a well-defined Fermi surface for $T > T_c$. In this case, the calculation of T_c can be made rather accurately in the RPA, because the important interaction for the plasmon mechanism comes from the region of small q and $\omega \sim \omega_p$. In such a region, every vertex correction is small and the interaction is weak enough to make the strong-coupling effect small.

Since it is rather a strong restriction for the system with $r_s > 6$ that it should be in the normal metallic state for $T > T_c$, it is a very subtle problem whether we can observe the plasmon mechanism of superconductivity in real materials. However, we come to know both favorable and unfavorable factors for the presence of the plasmon mechanism of superconductivity,

which provides us a hint to find out the system having the property that the contribution of the plasmon to the superconductivity is reinforced, or that the disadvantageous factors are suppressed.

The first system that we can point out to satisfy this requirement is a polar semiconductor in which the static dielectric constant ε_0 is large, while the optic one ε_∞ is small. Because of the large ε_0, the Wigner crystallization and the Anderson localization are difficult to occur and the life time due to both the impurities scatterings and the electron-electron scatterings is long owing to $\tau \propto 1/\varepsilon_0^2$. On the other hand, the contribution of the plasmon to the superconductivity does not change, if the energy of the optic mode ω_ℓ is of the order of ω_p. This is because the plasmon-mediated attraction comes from the dynamical effect and the dielectric constant for this process is not ε_0 but ε_∞. Discussions on this material are done in chapter II.

The suppression of the electron-localization can be also done by the introduction of other kind of carriers, since the static dielectric constant becomes large. From this reason, superconductivity in multi-carrier systems is treated in chapter III. It is also the purpose of this chapter that we deal with a two-dimensional (2D) system in which the dispersion relation of the plasmon for small q is proportional to $\sqrt{q}$. According to the discussions in 3-3.B, one of the reasons why the binding energy of the pair is rather small is that ω_p/ε_f becomes too large for low-carrier-density systems. In 2D systems, however,

ω_p is always small for small q and the contribution of the plasmon is expected to be large. In this way, 2D systems deserve a special attention.

Lastly, we make a comment on the observation of the plasmon mechanism. Even when a material with a low carrier concentration shows a superconducting behavior, there always exist phonons in real systems. Therefore, we cannot ascribe the superconductivity to the plasmon immediately and we must know the interrelation between the plasmon and other modes such as phonons in the superconductivity. This is also one of the main problems in the following chapters.

CHAPTER II

SUPERCONDUCTIVITY IN SEMICONDUCTING $SrTiO_3$

Chapter II treats the superconductivity observed in an n-type semiconducting $SrTiO_3$. We make a general survey of this system in §4. Since this material is a polar crystal, a general theory of superconductivity in polar semiconductors is presented in §5. In §6, we apply this theory to this material to determine the mechanism of superconductivity in this system.

§4. General Survey

4-1. Introduction

Superconductivity in semiconductors has been treated in much the same way as that in metals.[29-31,62] The contribution of the plasmon has not been considered to be large and all the effects of the Coulomb interaction have been estimated by one parameter μ^*. However, the analysis in the previous chapter shows that the plasmon plays rather an important role in superconductivity in low-carrier-concentration systems such as degenerate semiconductors. Thus, we have to reexamine the superconductivity in these materials by taking the effect of the plasmon into account more precisely.

As the first example of such a study, we deal with polar semiconductors in the present chapter in which the longitudinal optical (LO) phonons couple strongly to electrons through the electric field of the polarization wave. Gurevich *et al.*[62] examined this problem and obtained the conclusion that the superconductivity could occur only if the Fermi energy ε_f was much higher than the energy of the LO phonon ω_ℓ. This result is reexamined and the correct condition for the presence of superconductivity in polar semiconductors is investigated in §5.

We apply the general discussion on the superconductivity in polar semiconductors to semiconducting $SrTiO_3$. This material is observed to show a superconducting behavior in very low carrier concentrations. The details of this material are summarized in the following subsections. The calculated results of T_c are

compared with the experimental ones in §6, from which the mechanism of superconductivity and the role of the plasmon are clarified.

4-2. $SrTiO_3$

A. Pure crystal

$SrTiO_3$ is a representative material of perovskite-type compounds and has many interesting properties. When the crystal of $SrTiO_3$ is pure, it is an insulator having an energy gap around 3.3 eV.[63] The phonon, characterized by Γ_{25}, condenses at the R-point at the temperature of *ca.* 105 K and a cubic-to-tetragonal structural phase transition takes place.[64] Although a ferroelectric transition does not occur, the static dielectric constant ε_0 increases with the decrease of the temperature, as high as 10^4 at $T \simeq 4$ K.[65,66] This is related to a low-lying transverse optic (TO) mode at the Γ-point.[67] This ferroelectric (FE) soft mode has been observed by various methods.[68-71] Stress effects on this phonon are also investigated. Hydrostatic pressures harden the FE soft mode,[72,73] while uniaxial stresses soften it to bring about a ferroelectric state.[74,75]

B. Properties in the normal state

When $SrTiO_3$ is doped with Nb or La, or reduced in vacuum or low-pressure hydrogen atmosphere, it becomes an n-type semiconductor, in which the electron concentration n can be varied very widely from $10^{18}cm^{-3}$ to $10^{21}cm^{-3}$.[76,77] The band structure of this material was calculated by several people.[78-80] All

these works show that the conduction bands are composed of the titanium t_{2g} bands, but can be classified into two, according to positions of the energy minimum in the conduction band. One is a many-valley model whose minima are at the X-points, which was first proposed by Kahn and Leyendecker.[78] The other is a warped band model at the Γ-point which Mattheiss obtained by the APW calculations.[79] In order to determine which model is correct, various experiments have been done on the transport properties.[77,81-84] At first, the former model was supported, in particular, by the measurement of the magnetoresistance.[77,81] Piezoresistive properties, however, indicated that the minimum of the conduction band was at the Γ-point.[83] Moreover, the recent experiment on the magnetoresistance supported the theoretica results of Mattheiss strongly.[84]

C. Superconductivity

Semiconducting $SrTiO_3$ exhibits superconducting behaviors, when n is in the range from $8.5\times10^{18}cm^{-3}$ to $3.0\times10^{20}cm^{-3}$.[30,32] The curve of T_c as a function of n has a peculiar feature: T_c first increases, reaches its maximum of 0.3 K at $n \simeq 10^{20}cm^{-3}$ and then decreases with the increase of n, as shown in Fig.4.1. Stresses also produce very interesting and unusual effects on T_c. Pfeiffer *et al.*[85] discovered that T_c decreases with the increase of the hydrostatic pressure by an amount approximately two to five times greater than the corresponding effect in usual metallic superconductors, while T_c is sometimes increased by the application of the uniaxial stress along the [100] direction. These behaviors

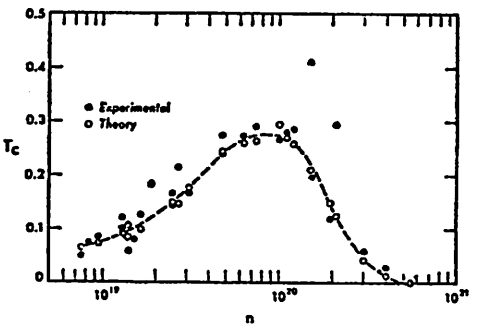

Fig.4.1. Observed T_c in the n-type semiconducting $SrTiO_3$ as a function of the carrier concentration n. Plain solid circles represent the experimental data, while the open circles show the calculated results obtained by Koonce *et al.*

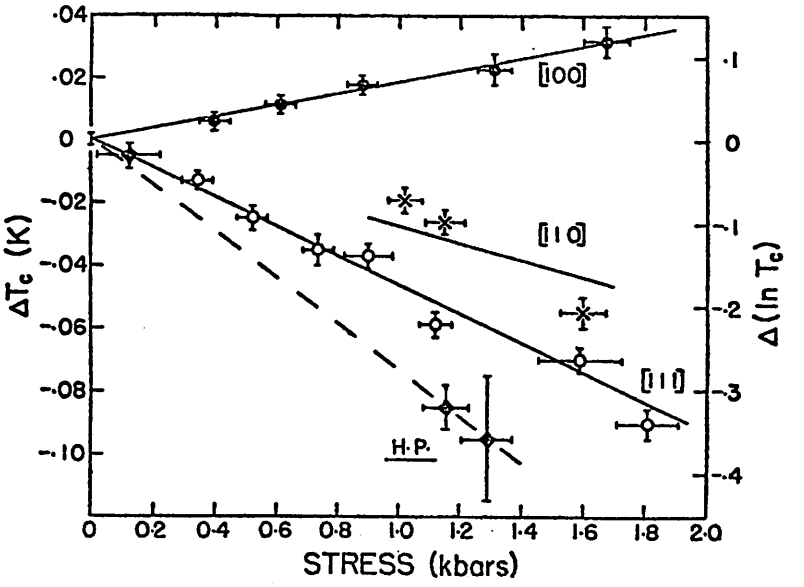

Fig.4.2 (a)

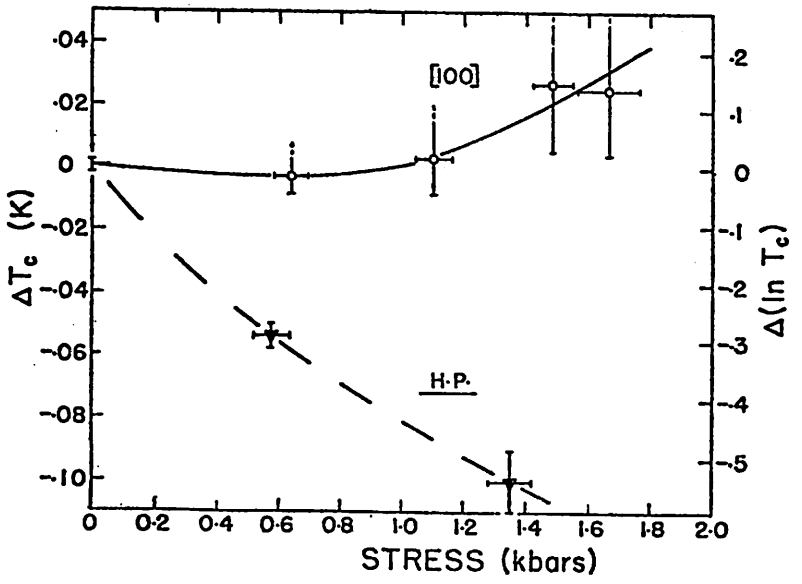

Fig.4.2 (b)

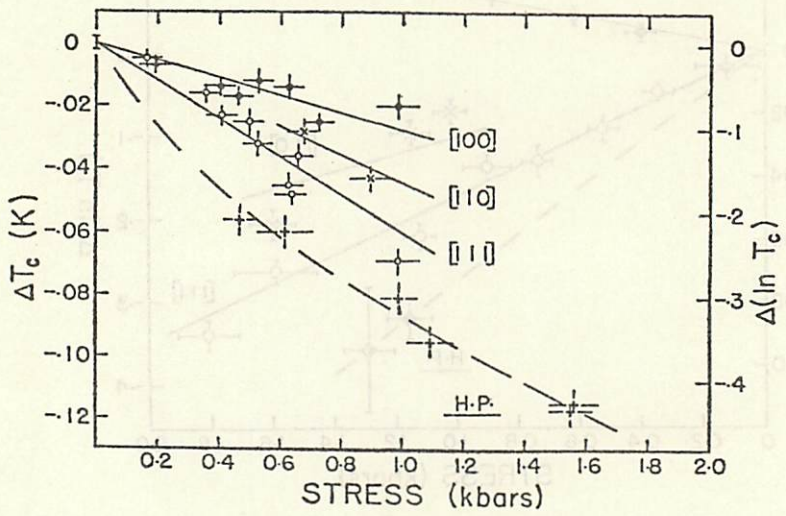

Fig.4.2 (c)

Fig.4.2. Stress effects on the superconducting transition temperature ΔT_c measured in $SrTiO_3$ under the hydrostatic pressure, the uniaxial stresses along [100], [110], and [111] directions, which are indicated by H.P., [100], [110], and [111], respectively. The carrier concentration is $2.5\times10^{19}cm^{-3}$ for (a) and (b), while it is $6.3\times10^{19}cm^{-3}$ for (c). Sample (a) is prepared by the doping of Nb, while those of (b) and (c) are the self-reduction. In the materials with nearly cubic symmetry as in the present case, there is no qualitative difference between the data of H.P. and those of [111], so that in the later calculations, we do not consider the case of [111].

are illustrated in Fig.4.2.

There have been several studies on the explanation of the superconductivity.[30.86-88] The most comprehensive investigation was done by Koonce and Cohen[30] with the use of Cohen's theory of superconductivity in degenerate semiconductors.[29] They adopted the many-valley model of Kahn and Leyendecker[78] and emphasized the importance of the inter-valley phonon scatterings. Appel[86] laid stress on the soft optic phonon connected with the 105 K structural phase transition, while Zinamon[87] assumed that the intra-valley acoustic phonon was responsible for the superconductivity. Each of these works accounted for the observed dependence of T_c on n with the use of the deformation potential as an adjustable parameter, but each mechanism is not convincing by the following three reasons. First, the many-valley model does not seem to be correct, which eliminates the mechanism of Koonce and Cohen.[30] Secondly, all the authors except Koonce and Cohen did not solve the gap equation correctly and used the idea of the Coulomb pseudo-potential μ^*, which does not seem appropriate in the present system. Besides, we cannot accept the calculation of Koonce and Cohen readily, because according to the discussion in 2-1.C, Cohen's theory does not seem to work well in the present system in which the mode to bring about superconductivity has the energy of the order of ε_f. The last reason is that it is not clear whether any of these mechanisms can explain the unusual pressure effects on T_c.

In the present chapter, the model for the conduction band calculated by Mattheiss[79] is assumed, so that the valley

degeneracy g_v is taken to be unity. The mechanism to cause the superconductivity is considered to be the combination of the plasmon and the FE soft phonon which enters into the theory through the dynamical dielectric constant of the electron-phonon system for a polar semiconductor. The experimental curve of T_c as a function of n and the stress is reproduced quite well without any adjustable parameters. The details are described in §6.

§5. General Theory of Superconductivity in Polar Semiconductors

In this section, we make a general study of the superconductivity in polar semiconductors. The curve of T_c as a function of n is calculated in 5-2 for several values of ε_0, ε_∞, and ω_ℓ in order to investigate the interplay of the LO phonon and the plasmon in the superconductivity, where ε_0 and ε_∞ are the static and the optic dielectric constant, respectively, and ω_ℓ is the energy of the LO phonon. In 5-3, we discuss the physics of the interplay and show that the parameter $\omega_\ell/\omega_{p\infty}$ plays an important role in the interplay, where the plasmon energy $\omega_{p\infty}$ is defined with respect to ε_∞ as

$$\omega_{p\infty} = \sqrt{4\pi e^2 n/\epsilon_\infty m^*}, \tag{5.1}$$

with the effective mass m*.

5-1. Effective Interaction

We consider an n-type isotropic polar semiconductor with $g_v = 1$. In this system, besides the bare Coulomb interaction $V^\infty(q)$, given by

$$V^\infty(q) = 4\pi e^2/\epsilon_\infty q^2, \tag{5.2}$$

the interaction coming from the virtual exchange of the optic phonon $W_\ell(q,\omega)$, expressed by

$$W_\ell(q,\omega) = V^\infty(q)\,(1-\varepsilon_\infty/\varepsilon_0)\,\frac{\omega_\ell^2}{\omega^2-\omega_\ell^2+i0^+} \tag{5.3}$$

contributes to the electron-electron interaction. The parameters ε_0, ε_∞ and ω_ℓ are supposed to be independent of q in this section.

As we have studied in §3, the RPA works rather well in the calculation of T_c in the plasmon mechanism of superconductivity even in low-carrier-concentration systems. This will also be the case with the present system, since the important contribution of the optic phonon-mediated interaction comes from the region of small q. Thus, we employ the RPA and the retarded effective electron-electron interaction $V^R(q,\omega)$ is calculated to be

$$V^R(q,\omega) = [\,V^\infty(q)+W_\ell(q,\omega)\,]\,/\,[\,1+\Pi(q,\omega)\{V^\infty(q)+W_\ell(q,\omega)\}\,]$$

$$\equiv 4\pi e^2/q^2\,\varepsilon(q,\omega) \tag{5.4}$$

where the dielectric function in the electron-optic phonon system $\varepsilon(q,\omega)$ is given by

$$\varepsilon(q,\omega) = \varepsilon_\infty + Q_e(q,\omega) + (\varepsilon_0-\varepsilon_\infty)\,\frac{\omega_t^2}{\omega_t^2-\omega^2-i0^+}, \tag{5.5}$$

with the electronic part $Q_e(q,\omega)$, defined by

$$Q_e(q,\omega) \equiv 4\pi e^2/q^2\cdot\Pi(q,\omega), \tag{5.6}$$

and the energy of the TO phonon ω_t which relates to ω_ℓ through

the Lyddane-Sachs-Teller relation[89] as

$$\omega_t^2 = \frac{\varepsilon_\infty}{\varepsilon_0}\,\omega_\ell^2 \,. \tag{5.7}$$

When the single-particle energy ε_p is assumed to be

$$\varepsilon_p = \frac{p^2}{2m^*} - \epsilon_f \,, \tag{5.8}$$

as in chapter I, the electronic polarization function $\Pi(q,\omega)$ is given in eq.(3.15).

5-2. Calculated Results of T_c

When the effective interaction $V^R(q,i\Omega)$, given by eq.(5.4), is substituted into eq.(2.18), T_c can be obtained readily with the use of the new numerical method described in 2-2. Figure 5.1 shows the calculated T_c as a function of n for several values of ω_ℓ, in which T_c and ω_ℓ are measured in the unit of the effective Rydberg m^*/ε_∞^2 and n is in the unit of $(m^*/\varepsilon_\infty)^3$, as in the case of the plasmon mechanism. The electron-optic phonon coupling constant is characterized by the parameter $1-\varepsilon_\infty/\varepsilon_0$ which is taken to be 2/3 in Fig.5.1. Fermi energies normalized by the effective Rydberg $\varepsilon_f/(m^*/\varepsilon_\infty^2)$ are 42.3 K, 196 K, and 911 K for $n/(m^*/\varepsilon_\infty)^3 = 10^{18}\text{cm}^{-3}$, 10^{19}cm^{-3}, and 10^{20}cm^{-3}, respectively, where m^* is measured in the unit of the mass of a free electron m_e. Every curve of T_c behaves much the same way as that in the plasmon mechanism. When n is very low to have ε_f much lower than ω_ℓ,

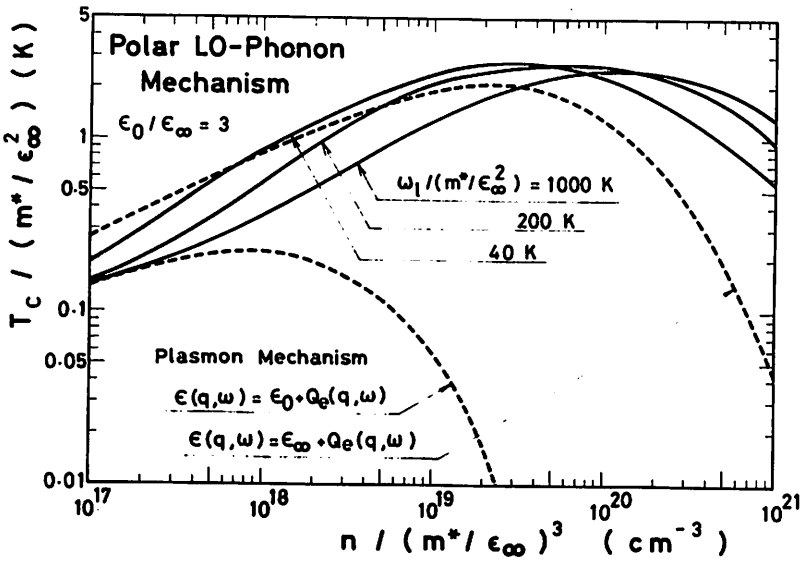

Fig.5.1. Calculated T_c scaled by the effective Rydberg m^*/ϵ_∞^2 as a function of n scaled by the inverse of the effective Bohr radius cubed $(m^*/\epsilon_\infty)^3$ for several values of the LO phonon energy ω_ℓ in polar semiconductors. The upper broken curve indicated by $\epsilon_\infty + Q_e(q,\omega)$ shows the result in which every effect of the LO phonon is neglected and therefore, only the plasmon with the optic dielectric constant ϵ_∞ contributes to the superconductivity. The lower broken one is the result given in the plasmon mechanism with the static dielectric constant ϵ_0. In this case, the dynamical effect of the LO phonon is neglected.

T_c approaches to that indicated by the lower broken curve which is obtained in the plasmon mechanism with the static dielectric constant ε_0, that is, which is calculated with the use of the dielectric function of

$$\epsilon(q,\omega) = \varepsilon_0 + Q_e(q,\omega). \tag{5.9}$$

This suggests that the polar phonon has only a small effect in this region of n. As n is increased to make ε_f the order of ω_ℓ, T_c becomes larger than that in the plasmon mechanism with the optic dielectric constant ε_∞, shown by the upper broken curve. With the further increase of n, T_c reaches its maximum of the order of $3\times(m^*/\varepsilon_\infty^2)$ K, and then decreases. The superconductivity continues to arise even when the $r_{s\infty}$ value, defined by

$$r_{s\infty} \equiv \frac{m^* e^2}{\varepsilon_\infty}\left(\frac{3}{4\pi n}\right)^{1/3}, \tag{5.10}$$

becomes less than 1.0. This should be compared with the case in the plasmon mechanism in which superconductivity does not appear for $r_{s\infty} < 6.0$. The optic phonon makes the system superconducting even in very high carrier concentrations.

The effect of the electron-polar phonon coupling constant $1-\varepsilon_\infty/\varepsilon_0$ on T_c is shown in Fig.5.2, in which $\omega_\ell/(m^*/\varepsilon_\infty^2)$ is taken to be 200 K. In the region of low n where the plasmon mechanism dominates, T_c is of the order of m^*/ε_0^2 and a system with low ε_0 has a higher T_c than one with high ε_0. On the other hand, for higher n, a system with high ε_0 is more favorable for the superconductivity, since it has all the larger electron-phonon coupling

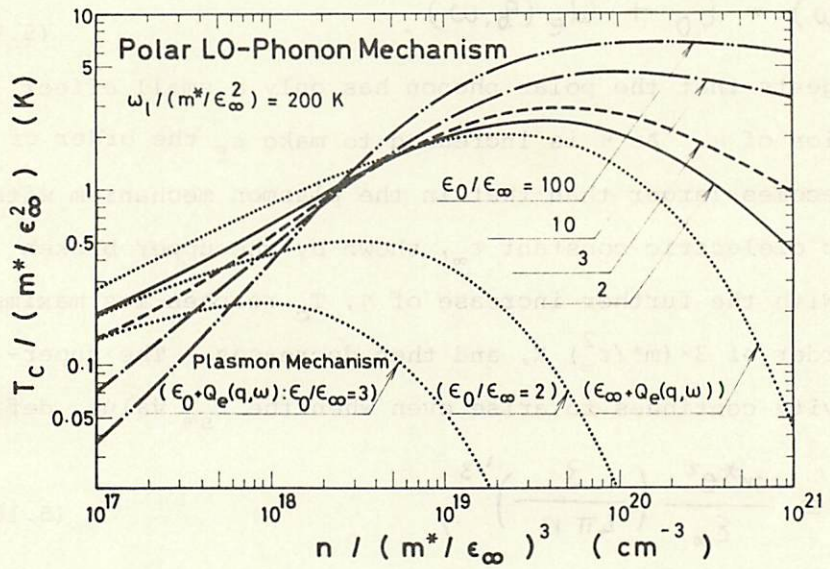

Fig.5.2. Dependence of T_c on the electron-LO phonon coupling constant characterized by $1-\epsilon_\infty/\epsilon_0$ in polar semiconductors. The uppermost dotted curve corresponds to the result in which every effect of the LO phonon is neglected and only the plasmon with ϵ_∞ has a contribution to the superconductivity. Other dotted curves show the results in the plasmon mechanism with ϵ_0.

constant.

5-3. Physics of Superconductivity in Polar Semiconductors

A. Modes in electron-polar LO phonon systems

In order to clarify the physics of the superconductivity in this system, we first investigate the modes of the system which can be obtained by the zeros of $\varepsilon(q,\omega)$. For small q, there are two modes, plasmon-like one and phonon-like one, approximately given by

$$\omega_{\pm}^2 = \frac{1}{2}\left\{ \omega_\ell^2 + \omega_{p\infty}^2 \pm \sqrt{(\omega_\ell^2 + \omega_{p\infty}^2)^2 - 4\omega_{p\infty}^2 \omega_t^2} \right\}. \qquad (5.11)$$

In case of high n, namely, $\omega_{p\infty} >> \omega_\ell$, ω_+ and ω_- are reduced to

$$\left.\begin{aligned} \omega_+ &\simeq \sqrt{\omega_{p\infty}^2 + \omega_\ell^2 - \omega_t^2} \simeq \omega_{p\infty}, \\ \text{and} \\ \omega_- &\simeq \omega_t, \end{aligned}\right\} \qquad (5.12)$$

respectively. On the other hand, in the system with low n to produce $\omega_{p\infty} << \omega_\ell$, they become to be

$$\left.\begin{aligned} \omega_+ &\simeq \sqrt{\omega_\ell^2 + (1-\varepsilon_\infty/\varepsilon_0)\,\omega_{p\infty}^2} \simeq \omega_\ell, \\ \text{and} \\ \omega_- &\simeq \omega_{p0}, \end{aligned}\right\} \qquad (5.13)$$

respectively, where ω_{p0} is defined by

$$\omega_{p0} \equiv \sqrt{\frac{\varepsilon_\infty}{\varepsilon_0}}\,\omega_{p\infty} = \sqrt{\frac{4\pi n e^2}{\varepsilon_0 m^*}} \quad . \tag{5.14}$$

B. Kernel in the gap equation

Now, we apply the approximate method, given in 2-3.B, to the present system. Assuming that

$$Q_e(q,0) \simeq \varepsilon_0 q_{TF}^2 / q^2 , \tag{5.15}$$

with

$$q_{TF} = \sqrt{4e^2 m^* p_f / \pi \varepsilon_0} , \tag{5.16}$$

as in the case of 3-2.A, we obtain the approximate form of the kernel (2.18) for small $x \equiv \omega/\varepsilon_f$ and $x' \equiv \omega'/\varepsilon_f$ as

$$K(x,x') = \frac{q_{TF}^2}{8p_f^2} \ln \frac{q_{TF}^2 + 4p_f^2}{q_{TF}^2} + \frac{1}{4}\cdot\frac{q_{TF}^2}{p_f^2}\cdot\frac{\varepsilon_0}{\varepsilon_\infty}\cdot\left(\frac{\varepsilon_f}{\omega_+}\cdot\frac{f_+}{\omega_+^2} + \frac{\varepsilon_f}{\omega_-}\cdot\frac{f_-}{\omega_-^2}\right)$$
$$\times (|x|+|x'|) \ln \frac{4}{|x-x'|} \tag{5.17}$$

where p_f is the Fermi wave number, $f_\pm$ are given by

$$f_+ = \frac{\omega_+^2(\omega_+^2 - \omega_t^2)}{\omega_+^2 - \omega_-^2} , \tag{5.18}$$

and

$$f_- = \frac{\omega_-^2(\omega_t^2 - \omega_-^2)}{\omega_+^2 - \omega_-^2} \tag{5.19}$$

respectively. The values $f_{\pm}$ are examples of $\tilde{f}_{\nu}(q)$ appeared in eq.(2.58).

For the case of $\omega_{p\infty} >> \omega_{\ell}$, eq.(5.17) is reduced to

$$K(x,x') = \frac{q_{TF}^2}{8p_f^2} \ln \frac{q_{TF}^2+4p_f^2}{q_{TF}^2} + \frac{\sqrt{3}}{8}\frac{q_{TF}}{p_f}\sqrt{\frac{\varepsilon_0}{\varepsilon_\infty}}\left[1+\left(\frac{\varepsilon_\infty}{\varepsilon_0}\right)^2\left(1-\frac{\varepsilon_\infty}{\varepsilon_0}\right)\frac{\omega_\ell^3}{\omega_{p\infty}^3}\right] \times (|x|+|x'|)\ln\frac{4}{|x-x'|}, \tag{5.20}$$

while for $\omega_{p\infty} << \omega_{\ell}$, K(x,x') has the form of

$$K(x,x') = \frac{q_{TF}^2}{8p_f^2} \ln \frac{q_{TF}^2+4p_f^2}{q_{TF}^2} + \frac{\sqrt{3}}{8}\frac{q_{TF}}{p_f}\left[1+\sqrt{\frac{\varepsilon_0}{\varepsilon_\infty}}\left(1-\frac{\varepsilon_\infty}{\varepsilon_0}\right)\frac{\omega_{p\infty}}{\omega_\ell}\right] \times (|x|+|x'|)\ln\frac{4}{|x-x'|}. \tag{5.21}$$

C. Physical interpretation

If we compare the above kernel with that in the plasmon mechanism, given by eq.(3.6), we can immediately notice that the essential mechanism to bring about the bound pair is the same. The only effect of the optic phonon is to increase the contribution of the plasmon to the superconductivity. As a result, the overall behavior of the curve of T_c as a function of n in this mechanism is the same as that in the plasmon one, as we have already seen in Figs.5.1 and 5.2. For low n, the kernel, given by eq.(5.21), approaches to that in the plasmon mechanism with ε_0, whereas eq.(5.20) indicates that for large $\varepsilon_0/\varepsilon_\infty$, the system becomes superconducting even when n is very large.

The maximum T_c appears when $\omega_{p\infty}$ is of the order of ω_{ℓ}, *i.e.*, $\omega_+ \simeq \omega_-$. Physically, when the frequencies $\omega_{\pm}$ are different very

much, the Cooper pair oscillates coherently with one of these frequencies which produces a larger attraction. As a result, the other mode is not excited by the pair and cannot contribute to the formation of the pair. In order to enjoy the full contribution from both of the modes, the frequencies of these modes are required to be almost the same. This argument suggests that even when several modes are present in the system, they cannot be treated by the addition of the contribution of each mode.

D. Comparison with the result of Gurevich, Larkin and Firsov

Gurevich *et al.*[62] discussed this problem and obtained the condition for the appearance of superconductivity in this system as

$$1-\frac{\varepsilon_\infty}{\varepsilon_0}-\frac{1}{1+\alpha \ln \varepsilon_f/\omega_l}>0, \tag{5.22}$$

with

$$\alpha \simeq \frac{1}{16}\frac{\varepsilon_0}{\varepsilon_\infty}\cdot\frac{q_{TF}^2}{p_f^2}\ln\frac{\varepsilon_\infty p_f^2}{\varepsilon_0 q_{TF}^2}. \tag{5.23}$$

According to the inequality (5.22), superconductivity arises only when

$$\varepsilon_0 \gg \varepsilon_\infty, \tag{5.24}$$

and

$$\varepsilon_f \gg \omega_l. \tag{5.25}$$

Since $SrTiO_3$ does not satisfy the condition (5.25), all the workers[30,86-88] who treated this problem before did not think that the optic phonon in $SrTiO_3$ was very important in the superconductivity.

The result of Gurevich *et al.* is totally different from that in 5-2. This difference comes mainly from the neglect of the contribution of the plasmon. Experimental facts are necessary to determine which theory is correct. As we will see in the next section, the theory proposed here, that is, the plasmon-polar phonon mechanism of superconductivity, seems to be supported by the experiment of the superconductivity in $SrTiO_3$.

§6. Application to Semiconducting $SrTiO_3$

In this section, we apply the general theory in §5 to $SrTiO_3$ and disclose the mechanism of the superconductivity in this material. In 6-1, the model of the system is described. The calculated results of T_c in the plasmon-polar phonon mechanism are shown in 6-2 and compared with the experiment.[30,32] The stress effects on T_c are evaluated to account for the experiment[85] in 6-3. Contributions of other modes are examined numerically in 6-4. Summary and discussions are given in 6-5.

6-1. Model of the System

Below 105 K, $SrTiO_3$ has a tetragonal structure with c/a = 1.0006[90] and anisotropic behaviors are observed in various physical properties. For example, the dispersion relation of the ferroelectric (FE) soft mode $\omega_t(q)$ is anisotropic and depends strongly on q.[68,71,75] The Fermi surface is also highly anisotropic according to the warped-band model of Mattheiss,[79] which is observed experimentally.[84]

In the actual calculations, however, the anisotropy is not considered for the sake of simplicity. The single-particle energy ε_p is assumed to be parabolic, as shown in eq.(5.8). The effective mass m* is taken to be the density-of-states mass m_D^*. The results of m_D^* calculated by Mattheiss showed a nonparabolic effect, but its effect was small. With the tenfold increase of n, m_D^* was increased by about 10 %. On the average, m_D^* was of the order of 1.7 m_e. The recent experiments of the electron tunneling[82]

and the magnetoresistance[84] supported this value of m_D^*. The static dielectric constant ε_0 and $\omega_t(q)$ are determined by

$$\epsilon_0 \equiv (\epsilon_x \epsilon_y \epsilon_z)^{1/3}, \tag{6.1}$$

and

$$\omega_t(q) \equiv (\omega_x(q)\omega_y(q)\omega_z(q))^{1/3}, \tag{6.2}$$

respectively, where ε_α and $\omega_\alpha(q)$ are the static dielectric constant and the dispersion relation of the FE soft mode along the α-axis ($\alpha = x, y$, or z), respectively. The z-axis is taken along the c-axis. With the use of these values of $\omega_t(q)$ and ε_0, the dielectric function of the system is given by

$$\epsilon(q,\omega) = \epsilon_\infty + Qe(q,\omega) + [\epsilon_0(q) - \epsilon_\infty] \frac{\omega_t^2(q)}{\omega_t^2(q) - \omega^2 - i0^+}, \tag{6.3}$$

where $\varepsilon_0(q)$ is related to $\omega_t(q)$ for small q as

$$\epsilon_0(q) = \epsilon_0 \omega_t^2(0) / \omega_t^2(q) \tag{6.4}$$

which can be obtained by the extension of the Lyddane-Sachs-Teller relation to the case of small q.[86,87,89] There are optic modes other than the FE soft mode in this material, but they are neglected in eq.(6.3), since the mode strengths for these modes are less than 10^{-3} of that for the FE soft mode.[69]

6-2. Calculated Results in Plasmon-FE Phonon Mechanism

When the experimental values of $\varepsilon_\infty = 5.2$,[91] $\varepsilon_0 = 23000$[65,71,75] and $\omega_t(q)$, given by[65,66,71]

$$\omega_t(q) = 6.34 + 1.40 \times 10^{-13} q_0^2 \quad (cm^{-1}), \tag{6.5}$$

are substituted into eq.(6.3), T_c can be readily obtained by the numerical method in 2-2. The dispersion relation (6.5) of $\omega_t(q)$ is just the same as employed by Appel.[86] Since the observed m_D^* varies in a very wide range from 1.1 m_e to 14 m_e,[77,81,82,84] T_c is calculated for several values of m* and the results are shown in Fig.6.1. The experimental points in the figure are quoted from Koonce *et al.*[30] (Fig.4.1) and these points can be reproduced quite well with the use of m* in the range from 1.5 m_e to 2.0 m_e, which is in good agreement with the "adjusted" result of Mattheiss.[79]

The behavior of T_c is similar to that obtained in 5-2, but the change of T_c with n is steeper in this case. This reflects the fact that in contrast with the case of §5, $\varepsilon_0(q)$ decreases with q and therefore the averaged static dielectric constant $\bar{\varepsilon}_0$, estimated by $\bar{\varepsilon}_0 \simeq \varepsilon_0(p_f)$, decreases with the increase of n. It should be noted here that if the contribution from the plasmon is not considered, superconductivity does not appear in this region of n, that is, in the region of $6 < r_{s\infty} < 20$, where $r_{s\infty}$ is defined by eq.(5.10) with m* = 1.8 m_e.

In order to obtain a better knowledge of the effect of the FE soft mode on the superconductivity, the change of T_c with $\omega_t(0)$

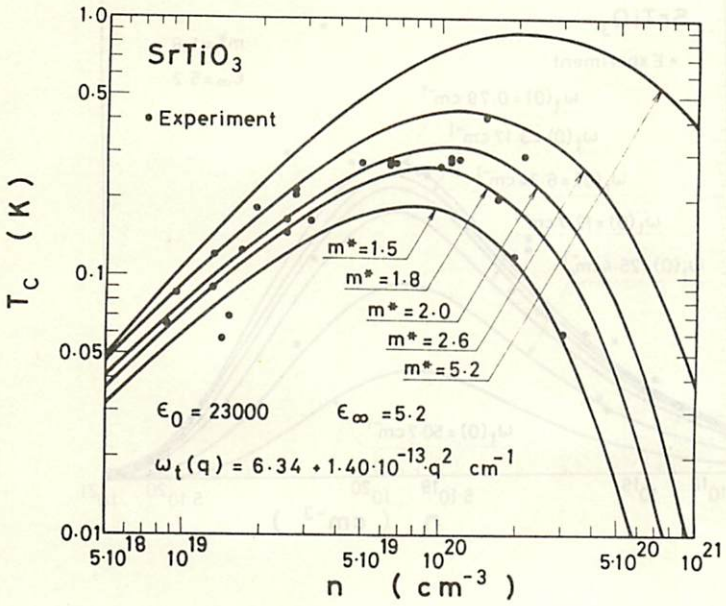

Fig.6.1. Calculated results of T_c as a function of the carrier density n for several values of m* in the plasmon-FE phonon mechanism. Experimental points are quoted from those in Fig.4.1.

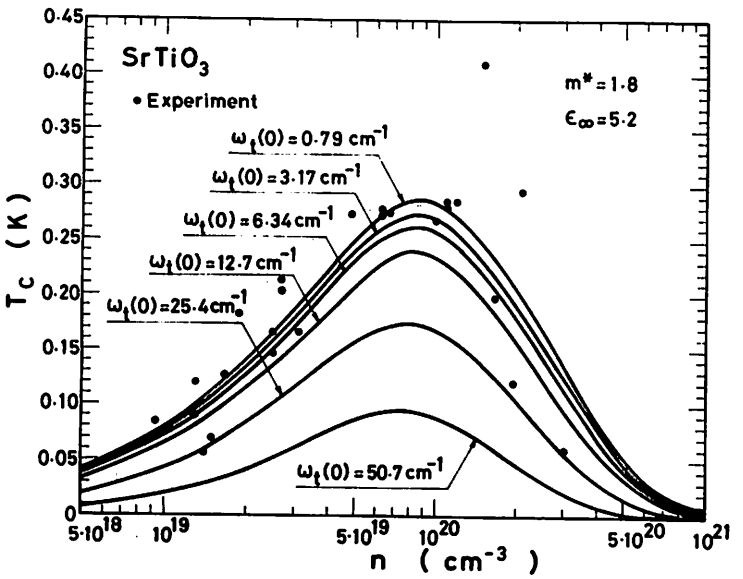

Fig.6.2. Effect of the softening of the FE phonon on T_c. Experimental points are borrowed from those in Fig.4.1.

is investigated in Fig.6.2, in which $m^* = 1.8\ m_e$, $\varepsilon_\infty = 5.2$, $\omega_t(q)$ is so chosen that

$$\omega_t(q) = \omega_t(0) + 1.40 \times 10^{-13} q^2 \quad (cm^{-1}) , \tag{6.6}$$

and ε_0 is determined by

$$\varepsilon_0 = 23000 \cdot (\omega_{t0}(0) / \omega_t(0))^2 , \tag{6.7}$$

with $\omega_{t0}(0) = 6.34\ cm^{-1}$. The crystal becomes more polarizable with the decrease of $\omega_t(0)$, which is taken into account by eq.(6.7). As $\omega_t(0)$ is decreased, T_c increases because of the increase of the electron-phonon coupling constant $1-\varepsilon_\infty/\varepsilon_0(q)$. However, if $\omega_t(0)$ is less than $15\ cm^{-1}$, the change of T_c is small and the electron concetration to give the maximum T_c hardly changes with $\omega_t(0)$. Thus, even if we employ the other observed value of $\omega_t(0)$ instead of $\omega_t(0) = 6.34\ cm^{-1}$, for example, $\omega_t(0) = 15.3\ cm^{-1}$ measured by Yamada and Shirane,[71] or $\omega_t(0) = 12.2\ cm^{-1}$ observed by Uwe and Sakudo,[75] the conclusion that the superconductivity in semiconducting $SrTiO_3$ can be accounted for by the plasmon-FE phonon mechanism of superconductivity is unchanged.

The FE soft mode has a rather large width γ,[71,75] so that the effect of γ on T_c is studied by changing $\omega_t^2(q)/(\omega_t^2(q)-\omega^2-i0^+)$ in eq.(6.3) into $\omega_t^2(q)/(\omega_t^2(q)-\omega^2-i\omega\gamma)$. The calculated T_c is plotted in Fig.6.3 for the cases of $n = 10^{19} cm^{-3}$ and $n = 10^{20} cm^{-3}$ with $m^* = 1.8\ m_e$ and $\omega_t(q)$ defined by eq.(6.5). Within the observed range of γ, T_c is not affected. This can be understood

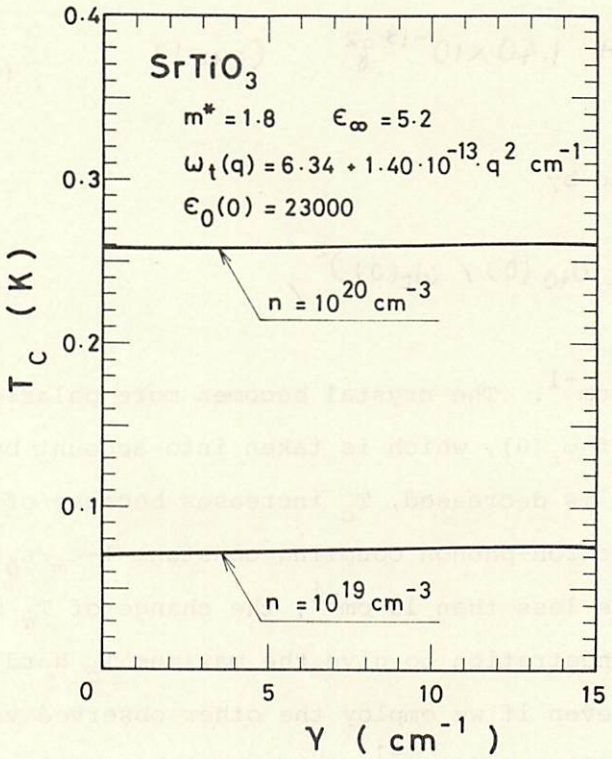

Fig.6.3. Dependence of T_c on the FE soft phonon damping width γ.

from the physics that the binding energy of the Cooper pair is unchanged, provided that the damping time of the mode is longer than the time during which the pair exchanges the mode virtually by the coherent oscillation.

6-3. Stress Effect

The effect of the stress on the superconductivity is investigated to make the importance of the FE soft mode clearer. As mentioned in 4-2.C, Pfeiffer and Schooley[85] observed a very curious behavior of T_c under uniaxial stresses and hydrostatic pressures. Since the volume of the crystal hardly changes with the stress of the order of 1 kb and neither does the electronic structure in the warped-band model of Mattheiss,[79] the change of the transition temperature ΔT_c cannot be explained by that of m*, or n. Thus, what remains to be considered is $\omega_t(q)$, or equivalently, $\varepsilon_0(q)$.

The change of $\omega_t(0)$ and $\varepsilon_0(0)$ with the stress was observed by several workers[72-75] and $\omega_t(0)$ softens to zero to bring about a ferroelectric state in case of the [100] and the [110] uniaxial stresses.[74,75] According to Uwe and Sakudo,[75] $\omega_y(0)$ vanishes at the stress of 1.6 kb in the [100] stress, while $\omega_z(0)$ vanishes at the stress of 5.6 kb in the [110] stress. The change of $\omega_t(0) \equiv (\omega_x(0)\omega_y(0)\omega_z(0))^{1/3}$ with the uniaxial stress is plotted in the bottom of Fig.6.4. The change of $\omega_t(0)$ with the hydrostatic pressure, denoted by H.P., is also shown, which is inferred from $\varepsilon_0(0)$ measured by Lowndess and Rastogi.[73]

Since there are no experimental results to estimate the change of the dispersion relation at present, we employ the same dispersion relation as in eq.(6.6). Under this assumption, only $\omega_t(0)$ is changed by the stresses. The change of $\omega_t(0)$ produces that of T_c, as shown in Fig.6.2 and the curve of ΔT_c as a function of the stress is depicted in Fig.6.4 for the two cases of $n = 2.5\times10^{19}\text{cm}^{-3}$ and $n = 6.3\times10^{19}\text{cm}^{-3}$. The parameters such as m* and ε_∞ are the same as those in Fig.6.2. For the [100] stress greater than 1.6 kb, ΔT_c is calculated under the assumption that the electronic structure in the ferroelectric state does not alter very much from that in the paraelectric state. The experimental points in Fig.6.4 are quoted from the work of Pfeiffer and Schooley[85] (Fig.4.2) without any distinction between the data for the Nb-doped samples and those for the reduced ones.

The difference in the behavior of ΔT_c with the [100] stress, the [110] stress and the hydrostatic pressure is explained quite well. In particular, the anomalous behavior of ΔT_c observed under the [100] stress near 1.6 kb is clarified to come from the ferroelectric transition. This seems to be a great support for the validity of the present theory.

6-4. Consideration of Other Mechanisms

Among various mechanisms suggested to account for the superconductivity in this material,[30,86-88] the model of Appel[86] and that of Zinamon[87] are consistent with the warped-band model with $g_v = 1$, although their treatments of the gap equation, in

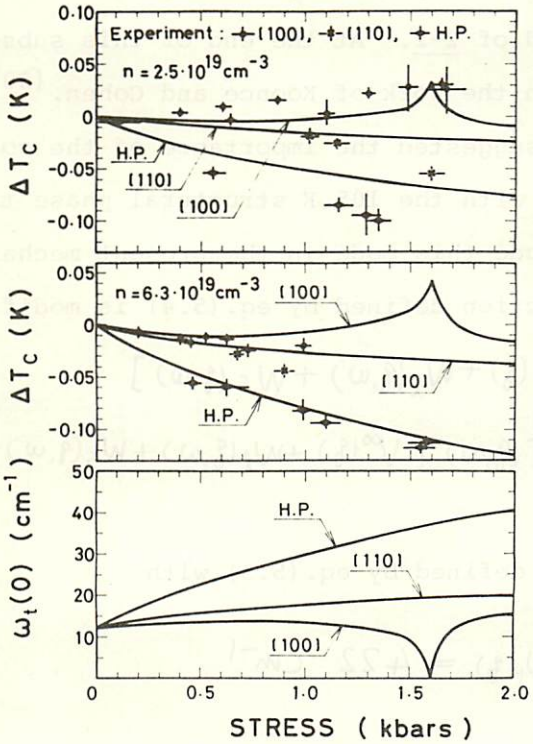

Fig.6.4. Calculated stress effects on T_c. Cases of the hydrostatic pressure, the uniaxial stresses along the [100] and the [110] directions are indicated by H.P., [100], and [110] respectively. Values of $\omega_t(0)$ under various stresses are illustrated in the bottom of the figure. The uppermost part of the figure treats the case of $n = 2.5\times10^{19}$ cm^{-3}, while the rest of it deals with the case of $n = 6.3\times10^{19}cm^{-3}$. Experimental points are quoted from those in Fig.4.2.

particular, of the Coulomb interaction were incomplete. Thus we consider these models by solving the gap equation with the use of the new method of 2-2. At the end of this subsection, we also make a comment on the work of Koonce and Cohen.[30]

Appel[86] suggested the importance of the soft phonon (A_{1g} mode) associated with the 105 K structural phase transition. In order to include this mode in the present mechanism, the effective interaction defined by eq.(5.4) is modified to be

$$V^R(q,\omega) = [\, V^\infty(q) + W_\ell(q,\omega) + W_S(q,\omega) \,] \Big/ [\, 1 + \Pi(q,\omega)\{ V^\infty(q) + W_\ell(q,\omega) + W_S(q,\omega)\} \,], \tag{6.8}$$

where $W_\ell(q,\omega)$ is defined by eq.(5.3) with

$$\omega_\ell = \sqrt{\frac{\varepsilon_0(q)}{\varepsilon_\infty}}\, \omega_t(q) = 422 \ \ cm^{-1}, \tag{6.9}$$

$\varepsilon_\infty = 5.2$, and $\varepsilon_0(q)$ given by eqs.(6.4) and (6.5). The interaction originated from the virtual exchange of the structural soft phonon $W_S(q,\omega)$ is obtained by

$$W_S(q,\omega) = \frac{\Xi_S^2 K^2}{2\rho_S \omega_S(q)} \cdot \frac{2\omega_S(q)}{\omega^2 - \omega_S^2(q) + i0^+}, \tag{6.10}$$

with the deformation potential Ξ_S, the reciprocal lattice vector of the R-point K, the density of the crystal ρ_S, and the energy of the A_{1g} phonon $\omega_S(q)$ given by

$$\omega_S(q) = 46.0 + 3.67\times10^{-14} q^2, \quad (cm^{-1}), \tag{6.11}$$

as was supposed by Appel. Taking $|K| = \sqrt{3}\pi/a$ with the lattice constant a = 3.9 A, ρ_s = 5.2 g/cm^3 and m*= 1.8 m_e, we can calculate T_c and the results for several values of Ξ_s are plotted in Fig.6.5. The behavior of all the curves is similar, but the value of T_c for Ξ_s= 1.0 eV becomes about three times as large as that for Ξ_s= 0 eV and the contribution of the A_{1g} phonon cannot be neglected. However, Ξ_s is of the order of 0.04 eV, as evaluated by Allen[92] with the use of the energy-band calculation of Mattheiss,[79] from which we cannot adopt this mechanism.

Next, we study the contribution of the acoustic phonons, which was emphasized by Zinamon.[87] The effective interaction in this mechanism is obtained by the replacement of $W_s(q,\omega)$ in eq.(6.8) by $W_a(q,\omega)$, defined by

$$W_a(q,\omega) = \frac{q^2}{2\rho_s c_a q}\left(\Xi_a + \frac{V^{1/2}(q)(\omega_l^2(q)-\omega^2)}{\omega_l^2-\omega^2}\,n\right)^2 \frac{2c_a q}{\omega^2 - c_a^2 q^2 + i0^+}, \quad (6.12)$$

where the acoustic mode has the dispersion relation of $c_a q$ with the sound velocity c_a, and Ξ_a is the deformation potential. Calculated T_c for several values of Ξ_a is shown in Fig.6.6, in which m* = 1.8 m_e, and $c_a = 7\times10^5$cm/sec are taken. When Ξ_s is chosen in the reasonable range, the effect of the acoustic phonon is not important.

Koonce and Cohen[30] applied Cohen's theory on the superconductivity in multi-valley semiconductors to this material and their treatment of the gap equation was much better than those of Appel and Zinamon. But they could not find out that the superconductivity in $SrTiO_3$ was due to the combination of

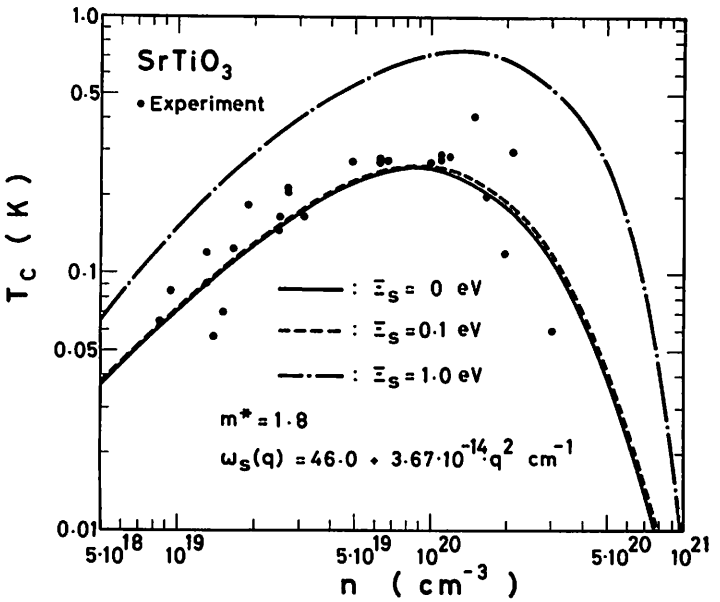

Fig.6.5. Effect of the structural soft phonon on T_c for several values of the deformation potential Ξ_s which couples electrons with the structural soft phonon. The result with Ξ_s=0 corresponds to the case of the complete neglect of the mode.

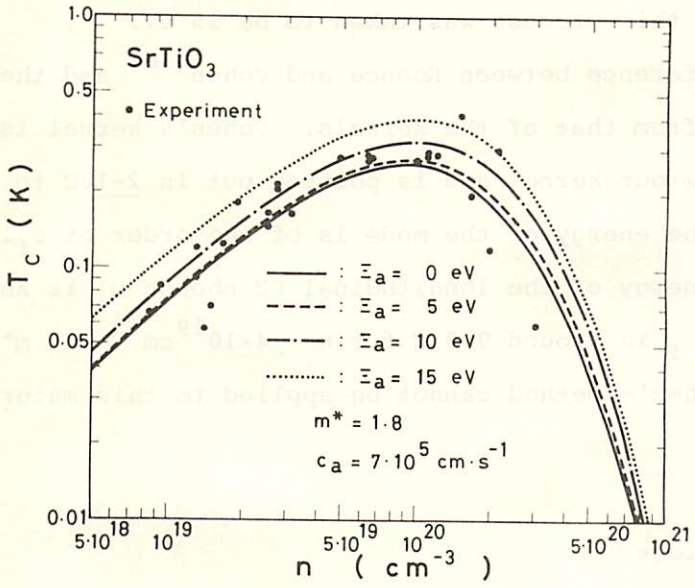

Fig.6.6. Estimation of the contribution of the acoustic phonons to the superconducting T_c for several values of the deformation potential Ξ_a.

the plasmon and the FE phonon. They adopted the multi-valley structure[78] and argued that the observed T_c could be explained by the inter-valley phonon scatterings, when the deformation potential for this process was taken to be 15 eV.

The difference between Koonce and Cohen[30] and the present theory stems from that of the kernels. Cohen's kernel is different from our kernel and is pointed out in 2-1.C to produce errors when the energy of the mode is of the order of ε_f. In $SrTiO_3$, the energy of the longitudinal FE phonon ω_ℓ is about 600 K, while ε_f is around 900 K for $n = 4\times10^{19}cm^{-3}$ and $m^* = 1.8\ m_e$. Therefore, Cohen's method cannot be applied to this material.

6-5. Discussions

A large number of experimental studies have been performed on pure and doped $SrTiO_3$ samples to determine various physical quantities. On the basis of the knowledge thus obtained, we have calculated T_c of this material from the first principles. The experimental results of T_c can be reproduced quite well, when we take the plasmon and the FE polar phonon into account. This suggests strongly that the mechanism of superconductivity in semiconducting $SrTiO_3$ is the plasmon-FE polar phonon one.

According to the discussions in chapter I, the plasmon plays an important role in superconductivity, when a system with a low carrier concentration is in the normal metallic state for $T > T_c$. This condition is just satisfied in semiconducting $SrTiO_3$ as shown in the following. For the dynamical process with the

frequency of the order of ω_p, the relevant dielectric constant is ε_∞, because ω_p is larger than ω_ℓ, defined by eq.(6.9), in $SrTiO_3$ for $n > 10^{19}$ cm^{-3}. Thus the r_s parameter should be defined with respect to ε_∞ and the value of $r_{s\infty}$, defined by eq.(5.10) with $m^* = 1.8\ m_e$, is larger than 6 for $n < 4\times10^{20} cm^{-3}$. In this way, the condition of the low carrier density is fulfilled. In order to investigate the electronic state in such a low-carrier-concentration system, Hall constant and electric mobility were measured at low temperatures. Even in a very low n, that is, $n \simeq 7\times10^{18} cm^{-3}$, these quantities were observed to be constant for $T < 10$ K.[30] At the same time, the system was found to be rather clean, because the mobility was of the order of $10^3 cm^2/Vsec$ and consequently, the impurity-scattering width was less than several degrees Kelvin. Accordingly, it is experimentally proved that the system is in the normal metallic state for $T > T_c$. Theoretically, however, it is rather difficult to understand the reason why the normal metallic state is present in such a low-carrier-concentration system. A possible explanation of this fact is that for the problem of the Anderson localization,[59] or the Wigner crystallization,[45] the static interaction rather than the dynamical interaction should be considered. The relevant r_s parameter, therefore, should be defined with respect to $\varepsilon_0(p_f)$, instead of ε_∞. The parameter r_{s0}, defined by

$$r_{s0} \equiv r_{s\infty}\, \epsilon_\infty / \epsilon_0(p_f), \tag{6.13}$$

is less than 0.2 in $SrTiO_3$, which excludes the possibility of

the transition into the nonmetallic state.

In any case, semiconducting $SrTiO_3$ is a normal metallic system with the $r_{s\infty}$ parameter larger than 6. Once such a system is obtained, the plasmon has a large contribution to superconductivity and besides, its contribution can be evaluated in the RPA quantitatively well. Thus, it is not so surprising that the calculated results of T_c in the RPA reproduce the observed T_c quite well in such a low-carrier-density system.

Although the main mechanism of superconductivity in $SrTiO_3$ seems to be determined by the present study, several additional investigations are necessary. The experiments on T_c [30,32] were performed before the technique to obtain the monodomain sample in the tetragonal phase was developed. Thus, T_c is expected to be reexamined in monodomain crystals. The stress effect should also be measured again from various reasons. When Pfeiffer and Schooley [85] made an experiment of the stress effect on T_c, they did not know the stress-induced ferroelectric transition and could not relate the anomaly of ΔT_c in Fig.4.2 to the softening of the FE mode. As a result, they did not pay attention to the [100] uniaxial stresses around 1.6 kb. More detailed study, then, is necessary for these values of the stresses and also for the [110] uniaxial stresses around 5.6 kb in order to confirm the present theory. This study of T_c under the stress will also shed light both on the effect of electrons on the stress-induced ferroelectric transition and on the electronic state in the ferroelectric state.

As to the sample preparation, there have been many discussions

on the difference between Nb-doped and self-reduced samples.[93,94] Experimentally, Nb-doped samples have higher T_c and the largest T_c of 0.41 K for $n = 1.5\times10^{20}\mathrm{cm}^{-3}$ in Fig.4.1 was obtained in this type of the samples. One explanation of this difference of T_c is that m*, or $\omega_t(0)$, or both of them may be different in each type of samples, because Unoki and Sakudo[64] and Jones *et al.*[93] suggested that compared with the Nb-doped samples, the self-reduced samples might have a smaller magnitude of the low-temperature distortion around the c-axis which is the origin of the cubic-to-tetragonal structural phase transition. The experiments of T_c for Nb-doped samples can be reproduced in the present theory, if m* is taken to be 2.5 m_e. However, there was also a suggestion[94] that the difference of T_c from the sample preparation might come from that of the number of paramagnetic centers in these samples. Thus, we cannot obtain the conclusive answer to the dependence of T_c on the sample preparation before we can make an estimation of the decrease of T_c due to the paramagnetic centers, ΔT_c, approximately given by[95]

$$\Delta T_c \sim \frac{\pi}{4}\cdot\frac{1}{\tau_s}\ , \qquad (6.14)$$

with the spin-flip scattering time τ_s, in each sample.

There is also the problem of anisotropy. Although we have treated all the quantities such as the effective mass and phonon energies to be isotropic, the actual system is anisotropic, as we have mentioned in 6-1. Thus the effect of anisotropy should be estimated, but it seems to be small for the s-wave coupling

of the Cooper pair, because the pair sees the quatities averaged over the angle.

According to the band calculation of Mattheiss,[79] the second-lowest conduction band at the Γ-point with a light effective mass (m* of the order of 0.6 m_e) is also occupied when n is larger than $2.5\times10^{19}cm^{-3}$. The ratio of the number of the "light" electrons n_ℓ to that of the "heavy" electrons in the lowest conduction band n_h is less than 0.1 for $n < 2\times10^{20}cm^{-3}$. Thus, we have to investigate the superconductivity in a two-carrier system. This problem constitutes the theme of chapter III. If we apply the results obtained in §8 to the present case, we can get the conclusion that the heavy carrier becoms superconducting and that the effect of the light carrier on the superconductivity of the heavy carrier is negligible. Therefore, the only change coming from the presence of the "light" electrons in the present system is that we should replot the theoretical curves of T_c in Figs.6.1,6.2,6.5, and 6.6 as a function of n_h instead of $n = n_\ell + n_h$. When such a treatment is done, T_c decreases steeper with the increase of n for $n > 10^{20}cm^{-3}$ and a better agreement with the experimental one can be obtained.

CHAPTER III

PREDICTION OF SUPERCONDUCTING TRANSITION TEMPERATURE OF MOS INVERSION LAYERS

Chapter III deals with an inversion layer formed at an MOS (Metal-Oxide-Semiconductor) structure. In §7, we describe the basic knowledge of this system. Special attention is paid to the two characteristics of the system, *i.e.*, the two-dimensionality and the carrier-density-controllability. In addition, a multi-carrier system is pointed out to be realized more easily in this system than in bulk systems. Further, an acoustic plasmon is shown to be made well-defined in this multi-carrier system. We give the calculated results of T_c in such a multi-carrier system in §8 in order to clarify the effect of the two-dimensional character of the plasmon on the superconductivity and also to investigate the role of the acoustic plasmon in the superconductivity. The interrelation between the plasmon and the acoustic plasmon is made clear. In the last part of §8, we apply this general theory to an inversion layer formed at the $Si(100)/SiO_2$ interface. In §9, we discuss the fluctuation effects and also make a speculation about the mechanism of superconductivity observed on the surface of a p-type InAs by Kawaji *et al.*[33]

§7. MOS Systems

7-1. Preliminaries

An n-channel inversion layer is realized in an MOS structure, when the electric field, applied perpendicularly to the surface of the p-type semiconductor by the gate voltage, is strong enough to bend the conduction band below the Fermi level. In this system, the motion of an electron perpendicular to the surface (the z-direction) is quantized and the electronic states form two-dimensional energy bands called electric subbands. Each subband is composed of a quantized motion in the z-direction and a continuum for motion in the plane parallel to the surface (the x-y plane). The carrier concentration of the system can be controlled over a wide range in a single sample by the gate voltage.

Owing to these two characteristics, that is, the quasi-two-dimensionality and the carrier-density-controllability, the MOS system has been regarded as an interesting system to reveal the quantum effect and the many-body effect and has been extensively studied both experimentally and theoretically. In particular, an n-channel inversion layer at the $Si(100)/SiO_2$ interface is the representative and also the most fundamental system in MOS physics and the electronic properties of this system have been studied for several years.[34] It is now well-established that in this system, many-body effects play important roles in determining various physical properties, such as the subband structure,[96,97] inter-subband optical transitions,[98] and the quasi-particle properties of the two-dimensional motion like the effective

mass,[96,97,99] and the g-factor.[96,99,100] It is also known that we can make a calculation of these physical properties in quantitative agreement with experimental results by taking account of the many-body effects in the RPA, or its refinement proposed by Hubbard.[48]

In this section, we present the calculated results of the subband structure of MOS systems formed on the surfaces of Si(100) and III-V compounds such as GaAs and InSb. A multi-carrier system is shown to be obtained more easily in MOS systems than in bulk ones. It is also shown that an acoustic plasmon, which can exist in a multi-carrier system in principle, can be made well-defined in MOS systems.[101]

7-2. N-Channel Inversion Layers at $Si(100)/SiO_2$ Interface under Uniaxial Stress along [001] Direction

At low temperatures, an n-channel inversion layer at the $Si(100)/SiO_2$ interface is usually composed of electrons in the ground subband formed at the two valleys in the [100] direction (*1*-valleys), since the effective mass perpendicular to the interface of these valleys m^*_{z1} is heavier than that of other valleys m^*_{z2}. (See, Fig.7.1.) The uniaxial stress along the [001] direction decreases the energy location of the two valleys in that direction (*2*-valleys) and transfers electrons from *1*- to *2*-valleys.[37] This change of the subband structure with the increase of the stress and the carrier concentration n_s is considered in this subsection.

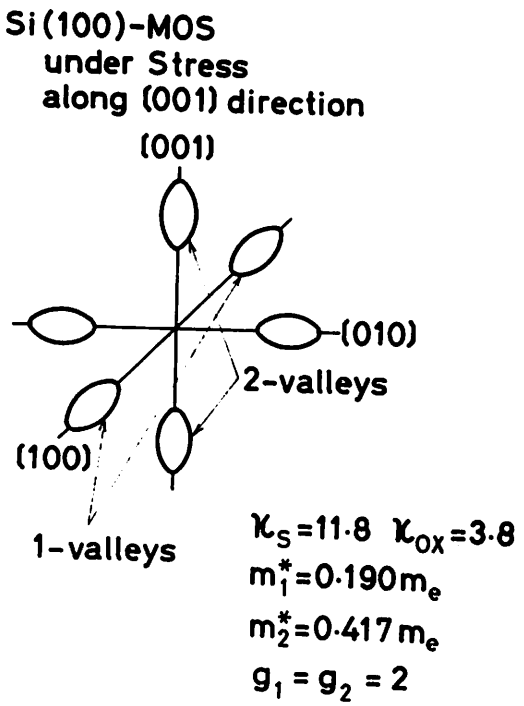

Fig.7.1. Constant energy surfaces of the conduction band of Si. These six valleys are equivalent in bulk systems, but the anisotropy of each valley makes them unequivalent at the (100) surface. In the n-channel inversion layer at the Si(100)/SiO_2 interface, all the electrons are in the *1*-st valleys in the absence of the stress, while the uniaxial stress along the [001] direction decreases the energy of the bottom of the *2*-nd valleys and transfers electrons into these valleys.

A. Hamiltonian

We treat the system composed of two kinds of valleys (1- and 2-valleys) and assume that only the lowest subband of each valley can be occupied by electrons. The Hamiltonian of the system is written as

$$H = H_K + H_S + H_{el\text{-}el}, \tag{7.1}$$

where H_S is the surface potential including the gate field, image potential, and the contribution from the depletion layer characterized by the total number of the negative charges in the layer per unit area, n_{dep}, and $H_{el\text{-}el}$ represents the Coulomb interaction between electrons. The kinetic energy, H_K, is written by

$$H_K = \sum_i \sum_\alpha \left\{ -\frac{1}{2m_{zi}^*}\frac{\partial^2}{\partial z^2} - \frac{1}{2m_i^*}\left(\frac{\partial^2}{\partial x^2}+\frac{\partial^2}{\partial y^2}\right) + s_i \right\}, \tag{7.2}$$

where m_{zi}^* and m_i^* are the effective masses of the i-th valley in the z-direction and in the x-y plane, respectively, and s_i is the energy location of the bottom of the i-th valley. Although 2-valleys are anisotropic in x-y plane, they are approximated to be isotropic and m_2^* is taken to be the density-of-states mass. We assume that the stress controls s_1-s_2 only, and neglect its effect on the effective masses, since it is very small.[102] When we apply the stress of 1 kb, the value of s_1-s_2 becomes about 7 meV in case of Si.

B. Variational method

We employ the variational method to determine the subband structure, that is, the number of electrons in the i-th valley, n_i, and the wave function of the ground subband in the valley, $\chi_i(z)$. As a trial function for $\chi_i(z)$, we use the following variational function:

$$\chi_i(z) = \sqrt{\frac{3}{2} b_i^3}\; z \exp\left\{ -\frac{(b_i z)^{3/2}}{2} \right\}, \tag{7.3}$$

where b_i is the variational parameter. This gives better results than the variational function proposed by Stern and Howard.[103] With the use of eq.(7.3), the expectation value of H is calculated as follows at T = 0 K:

$$\langle H \rangle = \langle H \rangle_{KE} + \langle H \rangle_{H} + \langle H \rangle_{F} + \langle H \rangle_{CORR}, \tag{7.4}$$

where the kinetic energy in x-y plane $\langle H \rangle_{KE}$ is written as

$$\langle H \rangle_{KE} = \sum_i \sum_{p\sigma} g_i \frac{1}{2m_i^*} p^2 n_{ip\sigma}, \tag{7.5}$$

with $p = (p_x, p_y)$. Here, g_i is the valley degeneracy, $n_{ip\sigma}$ is the distribution function of the electron of the i-th valley, momentum p, and spin σ. The Hartree energy $\langle H \rangle_H$ is given by

$$\begin{aligned}\langle H \rangle_H = \sum_i \sum_{p\sigma} g_i \Big\{ & s_i + \frac{5}{8}\Gamma\left(\frac{2}{3}\right) \frac{b_i^2}{2m_{zi}^*} + \frac{10}{9}\Gamma\left(\frac{2}{3}\right) \frac{4\pi e^2}{\kappa_s} \frac{n_{dep}}{b_i} \\ & + \frac{e^2}{12\kappa_s}\Gamma\left(\frac{1}{3}\right) \frac{\kappa_s - \kappa_{ox}}{\kappa_s + \kappa_{ox}} b_i \Big\} n_{ip\sigma} + \frac{1}{2} \sum_{ii'} \sum_{pp'\sigma\sigma'} \frac{10}{9}\Gamma\left(\frac{2}{3}\right) \frac{4\pi e^2}{\kappa_s} g_i g_{i'} \frac{1}{b_i} \\ & \times f_h\left[(b_{i'}/b_i)^{3/2} \right] n_{ip\sigma} n_{i'p'\sigma'},\end{aligned} \tag{7.6}$$

where $\Gamma(x)$ is the gamma function, κ_s and κ_{ox} are the dielectric constants of the silicon and the oxide, respectively, and $h(x)$ is defined by

$$h(x) = (3+11x+11x^2+3x^3)/3(1+x)^{11/3}. \qquad (7.7)$$

As mentioned in 7-1, the exchange and the correlation effects are important in this system and they are treated in $\langle H\rangle_F$ and $\langle H\rangle_{CORR}$, respectively. The Fock energy, $\langle H\rangle_F$, is calculated as

$$\langle H\rangle_F = -\frac{1}{2}\sum_{ii'}\sum_{pp'}\sum_{\sigma\sigma'} g_i V^0_{ii'}(|p-p'|)\, n_{ip\sigma}\, n_{i'p'\sigma'}\, \delta_{ii'}\,\delta_{\sigma\sigma'}$$

$$= -\sum_i \frac{1}{\sqrt{2}\,g_i}\left(\frac{n_i}{\pi}\right)^{3/2}\int_0^2 dz\, p_{fi} z\, V^0_{ii}(p_{fi} z)\cdot\left(\cos^{-1}\frac{z}{2} - \frac{z}{4}\sqrt{4-z^2}\right), \qquad (7.8)$$

with $n_i = \sum_p\sum_\sigma g_i n_{ip\sigma}$ and the Fermi wave number of the i-th subband $p_{fi} \equiv \sqrt{2\pi n_i/g_i}$, where the bare electron-electron interaction, $V^0_{ij}(q)$, is given by

$$V^0_{ij}(q) = V^0(q)\left[\frac{\kappa}{\kappa_s}\langle e^{-q|z-z'|}\rangle_{ij} + \frac{\kappa_s-\kappa_{ox}}{2\kappa_s}\langle e^{-qz}\rangle_i\langle e^{-qz}\rangle_j\right], \qquad (7.9)$$

with

$$V^0(q) \equiv 2\pi e^2/\kappa q, \quad \text{and} \quad \kappa = (\kappa_s+\kappa_{ox})/2. \qquad (7.10)$$

The form factors $\langle e^{-q|z-z'|}\rangle_{ij}$ and $\langle e^{-qz}\rangle_i$ are defined by

$$\langle e^{-q|z-z'|}\rangle_{ij} \equiv \int_0^\infty dz\, \chi_i(z)^2 \int_0^\infty dz'\, \chi_j(z')^2\, e^{-q|z-z'|}, \qquad (7.11)$$

and

$$\langle e^{-qz} \rangle_i \equiv \int_0^\infty dz\, \chi_i(z)^2\, e^{-qz}, \tag{7.12}$$

respectively. The contribution of the correlation effects $\langle H \rangle_{CORR}$ is calculated in the RPA and is given by

$$\langle H \rangle_{CORR} = \int_0^\infty \frac{dq}{2\pi} \int_0^\infty \frac{d\Omega}{2\pi} \left\{ \ln \varepsilon(q,i\Omega) - \mathrm{Tr}\left[\Pi(q,i\Omega) \mathbf{V}^0(q)\right] \right\}, \tag{7.13}$$

with

$$\varepsilon(q,i\Omega) \equiv \det \left(\mathbf{1} + \Pi(q,i\Omega)\, \mathbf{V}^0(q) \right). \tag{7.14}$$

Here, 1 is the unit matrix, $V^0(q)$ and $\Pi(q,i\Omega)$ are defined by

$$\mathbf{V}^0(q) = \left(V_{ij}^0(q) \right), \tag{7.15}$$

and

$$\Pi(q,i\Omega) = \left(\Pi_i(q,i\Omega)\, \delta_{ij} \right), \tag{7.16}$$

respectively, with the polarization function in the RPA, $\Pi_i(q,i\Omega)$, calculated at T = 0 K as

$$\Pi_i(q,i\Omega) = \frac{g_i m_i^*}{\pi} \left\{ 1 - \left[\frac{1}{2} \left(\sqrt{(\alpha_i^2 - \chi_i^2 + 1)^2 + 4\alpha_i^2 \chi_i^2} - \alpha_i^2 + \chi_i^2 - 1 \right) \right]^{1/2} / \chi_i \right\}, \tag{7.17}$$

with

$$\alpha_i = \frac{m_i^* \Omega}{p_{fi}\, q} \quad \text{and} \quad \chi_i = q / 2p_{fi}. \tag{7.18}$$

The realized state under the given n_s, n_{dep}, and the stress can be obtained as follows. Under some fixed $\{n_i\}$, the variational parameters, $\{b_i\}$, are determined by

$$\partial \langle H \rangle / \partial b_i = 0 , \tag{7.19}$$

and we substitute these values into <H> to get the total energy. Then we change $\{n_i\}$ to find the values to minimize <H>. In performing this procedure, we use the approximate forms for $\langle e^{-q|z-z'|} \rangle_{ij}$ and $\langle e^{-qz} \rangle_i$, for example, for $\langle e^{-q|z-z'|} \rangle_{11}$,

$$\langle e^{-q|z-z'|} \rangle_{11} = (1 + 0.4913 x) / (1 + 1.2870 x + 0.5941 x^2) , \tag{7.20}$$

with $x = q/b_1$, and for $\langle e^{-qz} \rangle_1$,

$$\langle e^{-qz} \rangle_1 = (1 + 0.1632 x) / (1 + 1.6678 x + 1.1202 x^2 + 0.3688 x^3 + 0.0544 x^4) , \tag{7.21}$$

with the same x as in eq.(7.20). These forms are obtained from the asymptotic behaviors of $\langle e^{-q|z-z'|} \rangle_{ij}$ and $\langle e^{-qz} \rangle_i$ at both $q \to \infty$ and $q \to 0$. The relative errors of these approximate values to the exact ones obtained by eqs.(7.11) and (7.12) with the wave function of eq.(7.3) are less than 0.01 for every q.

C. Calculated results

In case of the $Si(100)/SiO_2$ system, we can use the values, $\kappa_s = 11.8$, $\kappa_{ox} = 3.8$, $m^*_{z1} = 0.916\ m_e$, $m^*_{z2} = m^*_1 = 0.190\ m_e$, $m^*_2 = 0.417\ m$

and $g_1 = g_2 = 2$, where m_e is the mass of a free electron. An example of the calculated phase-diagram is shown in Fig.7.2 for the case of $n_{dep} = 10^{11}cm^{-2}$. The stress is characterized by $s_1 - s_2$. When $s_1 - s_2 < 6$ meV, all the electrons are in the *1*-st valleys for $n_s < 6\times10^{12}cm^{-2}$, while for $s_1 - s_2 > 13$ meV, electrons are in the *2*-nd valleys first and then begin to transfer to the *1*-st valleys with the increase of n_s. For the intermediate values of $s_1 - s_2$, the situation is a little complicated. As n_s is increased, electrons are in the *2*-nd valleys first and then all of them transfer into the *1*-st valleys. With the further increase of n_s, some electrons begin to enter into the *2*-nd valleys again.

The change of n_1/n_s with the increase of n_s is plotted in Fig.7.3 for several fixed values of the stress. The solid and the broken curves represent the cases of $n_{dep} = 10^{11}cm^{-2}$ and $n_{dep} = 10^{12}cm^{-2}$, respectively. The average depth of the i-th subband, $\langle z \rangle_i$, calculated by

$$\langle z \rangle_i = \frac{10}{9}\Gamma\left(\frac{2}{3}\right)/b_i, \qquad (7.22)$$

is also shown in the figure. It is the characteristic of this system that $\langle z \rangle_2$ is almost twice as large as $\langle z \rangle_1$. In any case, if we control the gate voltage and the stress properly, two kinds of valleys are simultaneously occupied by electrons and we can have an example of multi-carrier systems in MOS structures.

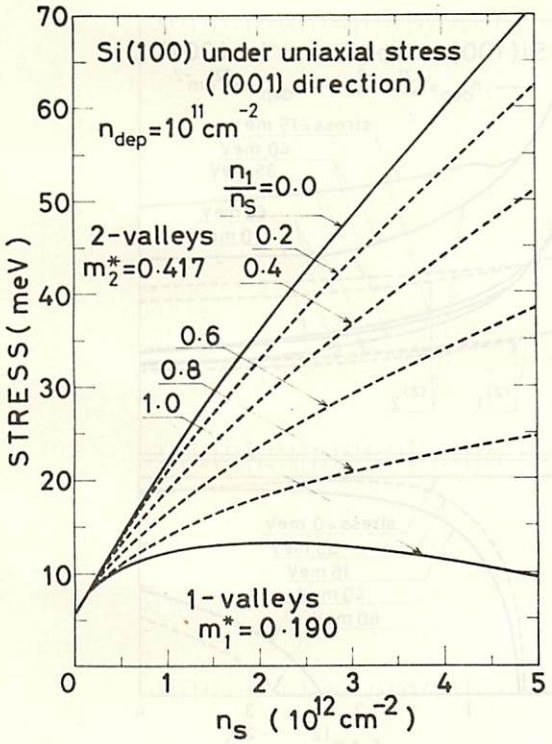

Fig.7.2. An example of the phase-diagram of the electron population in each kind of valleys calculated in the RPA. The ratio of the electrons in the *1*-st valleys to the total electrons, n_1/n_s, is indicated by the dashed lines. In the region indicated by "*1*-valleys", all the electrons are in the *1*-st valleys, while in the region of "*2*-valleys", they are in the *2*-nd valleys.

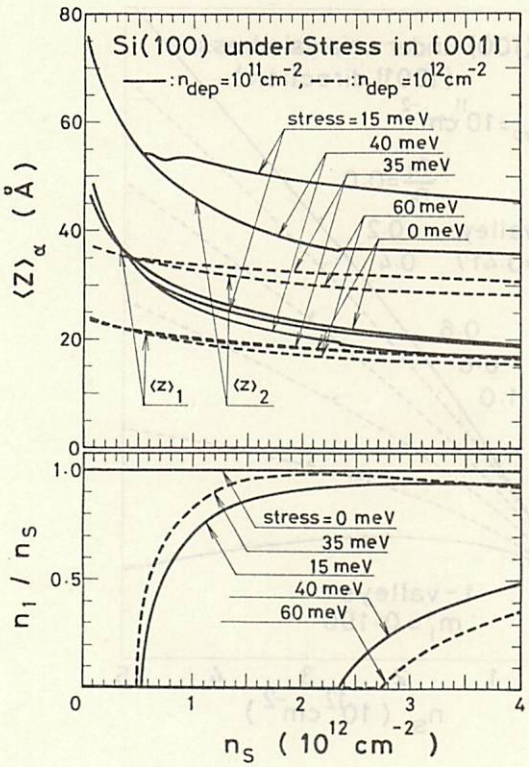

Fig.7.3. Calculated results of n_1/n_s, $\langle z \rangle_1$ and $\langle z \rangle_2$ as a function of n_s under several values of the stress characterized by $\varepsilon_1 - \varepsilon_2$. Solid and broken lines correspond to the results for the cases of $n_{dep} = 10^{11} cm^{-2}$ and $n_{dep} = 10^{12}$ cm^{-2}, respectively.

7-3. N-Channel Inversion Layers on III-V Compounds

Compared with the case of Si, the effective mass at the Γ-point in the conduction band is about one tenth in III-V compounds such as InAs and InSb. Thus, electrons in an n-channel inversion layer on these materials usually occupy more than two subbands, which is confirmed both experimentally and theoretically.[104] Moreover, when a gate voltage is strong, both Γ-valley with a light effective mass and the second minimum valleys (X- or L-valleys) with a heavy effective mass can be simultaneously occupied by electrons.[36]

Calculations of the subband structure can be done in a similar way to that in 7-2. In the present case, however, many-body effects are relatively small and can be neglected, while the effect of nonparabolicity of the Γ-valley should be considered.

Taking account of the nonparabolicity in the Kane's model,[105] we calculate the subband structure for several materials. An example of such calculations is shown in Fig.7.4, in which an n-channel inversion layer on the surface of a p-type GaAs is treated. The energy levels of the subbands in the Γ-valley, ε_i^{Γ}, those of the subbands in the second minimum valleys (X-valleys), ε_i^{X}, and the Fermi level μ are calculated as a function of n_s. The origin of energy is the top of the valence band at the interface. The subband structure changes with the increase of n_s as follows: First, all the electrons are in the ground subband formed at the Γ-valley. Then, some of them occupy the first-excited subband of the Γ-valley and a multi-carrier system is realized.

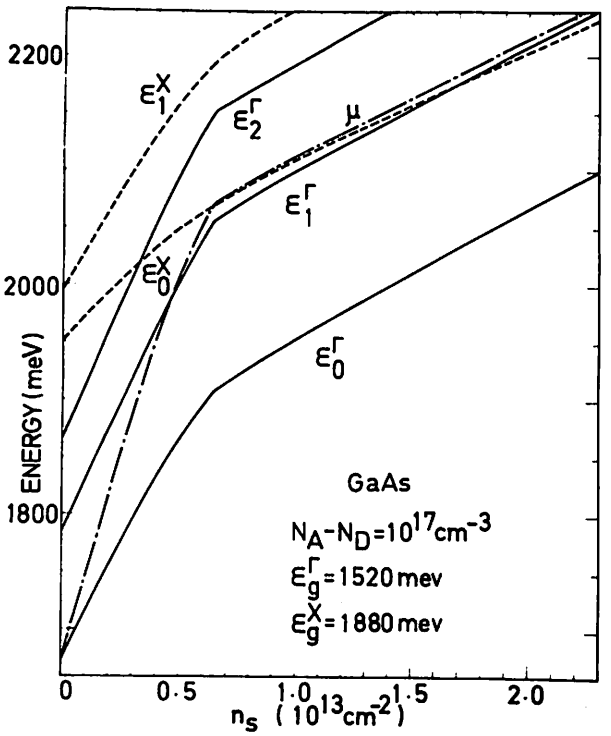

Fig.7.4. Energy levels of the subbands as a function of n_s in an n-channel inversion layer on the surface of a p-type GaAs whose dopant concentrations of acceptors and donors are N_A and N_D, respectively. The series of ε_0^Γ, ε_1^Γ, $\cdots$ shows the subband levels formed at the Γ-valley, while that of ε_0^X, ε_1^X, $\cdots$ shows these at the X-valleys. All the energies such as the Fermi energy μ and the energy location of the bottom of each valley, ε_g^Γ, or ε_g^X, are measured from the top of the valence band at the surface.

With the further increase of n_s, electrons begin to transfer to the ground subband in the X-valleys and a different kind of a multi-subband system is obtained. It must be noted here that ε_i^X increases more slowly than ε_i^Γ, because the effective mass of the X-valleys are much heavier than that of the Γ-valley. Thus, in MOS systems, the energy separation between the Γ-valley and the X-valleys is made smaller than that in bulk systems and the X-valleys are occupied by electrons more easily in MOS systems than in bulk ones.

7-4. Acoustic Plasmons in Two-Subband Systems

As we have seen in 7-2 and 7-3, MOS systems provide several kinds of multi-carrier systems. In such systems, there can be a collective mode other than the plasmon, that is, an acoustic plasmon (AP) in which electrons of each subband oscillate out of phase. Thus in this subsection, we investigate the AP in a two-subband system and study the conditions to make it a well-defined mode.

A. Hamiltonian in a second-quantized form

We consider the same system as that treated in 7-2. The Hamiltonian of this system can be written in a second-quantized form as

$$H = \sum_{ip\sigma} \varepsilon_{ip} C_{ip\sigma}^{+} C_{ip\sigma} + \frac{1}{2} \sum_{ij} \sum_{pp'\sigma\sigma'} \sum_{q\neq 0} V_{ij}^{0}(q)\, C_{ip\sigma}^{+} C_{jp'\sigma'}^{+} C_{jp'-q\sigma'} C_{ip+q\sigma} , \qquad (7.23)$$

where $C_{ip\sigma}$ is the anihilation operator of the electron with the momentum p and the spin σ in the i-th (i = 1, or 2) subband whose single-particle energy ε_{ip} is given by

$$\mathcal{E}_{ip} = p^2/2m_i^* - \epsilon_{fi} \tag{7.24}$$

with the Fermi energy of the i-th subband $\varepsilon_{fi} = \pi n_i/g_i m_i^*$. The number of electrons in this subband n_i and the wave function $\chi_i(z)$ are determined by the method described in 7-2. The interaction $V_{ij}^0(q)$ is defined in eq.(7.9). In eq.(7.23), we neglect the valley-exchange interactions, as usual, owing to the orthogonality of the Bloch functions.

B. Analytic continuation of the polarization function

The collective excitation modes are found in the form of zeros of the retarded dielectric function $\varepsilon^R(q,\omega)$, defined by eq.(7.14), in the lower ω-plane. The retarded polarization function $\Pi_i^R(q,\omega)$ in the lower ω-plane is obtained by the analytic continuation from the upper ω-plane. At T = 0, $\Pi_i^R(q,\omega)$ is calculated as

$$\Pi_i^R(q,\omega) = \frac{m_i^*}{2\pi}\left(z\chi_i + \sqrt{\alpha_i - \chi_i + 1}\sqrt{\alpha_i - \chi_i - 1} - \sqrt{\alpha_i + \chi_i + 1}\sqrt{\alpha_i + \chi_i - 1}\right)/\chi_i, \tag{7.25}$$

with x_i and α_i defined in eq.(7.18). The branch of $\sqrt{z}$ in the complex z-plane is so chosen that Im $\sqrt{z} \geq 0$ for the first, second and third quadrants and Im $\sqrt{z} < 0$ for the fourth quadrant for the case in which |Im ω| is much smaller than the Fermi energies,

ε_{f1} and ε_{f2}.

C. Analytic solution of the dispersion relation

In a two-subband system, an AP is the mode in which the plasma oscillation of the subband having the slower Fermi velocity is screened and Landau damped by electrons in the subband having the faster Fermi velocity. For the sake of simplicity, we assume here that the 1-st subband has the faster Fermi velocity. Then for small q, the AP is the mode in the following region in the excitation spectrum:

$$q v_{f2} < \omega < q v_{f1}, \tag{7.26}$$

where v_{fi} is the Fermi velocity of the i-th subband. In such a region, $\Pi_i^R(q,\omega)$ has the following approximate form:

$$\Pi_1^R(q,\omega) \simeq \frac{1}{V^0(q)} \cdot \frac{q_{TF1}}{q} \left(1 + i \frac{\omega}{q v_{f1}}\right), \tag{7.27}$$

and

$$\Pi_2^R(q,\omega) \simeq -\frac{1}{2} \cdot \frac{1}{V^0(q)} \cdot \frac{q \cdot v_{f2}^2 \cdot q_{TF2}}{\omega^2} . \tag{7.28}$$

Here, $V^0(q)$ is defined in eq.(7.10) and q_{TFi} is the inverse of the Thomas-Fermi screening length of the i-th subband given by

$$q_{TFi} = 2 e^2 m_i^* g_i / \kappa . \tag{7.29}$$

When eqs.(7.27) and (7.28) are put into $\varepsilon^R(q,\omega)$, we can solve

the equation of

$$\varepsilon^R(q, \omega_q - i\gamma_q) = 0, \tag{7.30}$$

as

$$\omega_q = v_{AP}\, q, \tag{7.31}$$

with

$$v_{AP} = \sqrt{q_{TF2}/2q_{TF1}} \cdot v_{f2} \cdot f_{AP}, \tag{7.32}$$

and

$$\gamma_q / \omega_q = \frac{1}{4}\sqrt{\frac{2q_{TF2}}{q_{TF1}}} \cdot \frac{v_{f2}}{v_{f1}} \cdot \frac{1}{f_{AP}}, \tag{7.33}$$

where f_{AP} is defined by

$$f_{AP} = \left\{1 + \frac{\kappa}{\kappa_S} q_{TF1} \left[2\langle|\vec{z}-\vec{z}'|\rangle_{12} - \langle|\vec{z}-\vec{z}'|\rangle_{11} - \langle|\vec{z}-\vec{z}'|\rangle_{22}\right]\right\}, \tag{7.34}$$

with

$$\langle|\vec{z}-\vec{z}'|\rangle_{ij} \equiv \int_0^\infty dz\, \chi_i^2(z) \int_0^\infty dz'\, \chi_j^2(z')\, |\vec{z}-\vec{z}'|. \tag{7.35}$$

To make the mode a well-defined one, ω_q in eq.(7.31) should satisfy the inequality (7.26) and γ_q/ω_q in eq.(7.33) should be small. Among these conditions, the most important one is whether the

sound velocity v_{AP} is greater than v_{f2} or not. This leads to the inequality for the presence of the well-defined AP as

$$g_2 m_2^* / 2 g_1 m_1^* > f_{AP}^{-2} . \tag{7.36}$$

Therefore, the larger value of f_{AP} is more advantageous for the AP. In addition, eq.(7.33) shows that the Landau damping is also reduced for the large f_{AP}. In order to see the physics of this condition, we consider the model case of

$$\chi_i^2(z) = \delta(z - z_i) , \quad \text{for } i=1 \text{ or } 2 . \tag{7.37}$$

Then f_{AP} is calculated to be

$$f_{AP} = \sqrt{1 + 2 q_{TF1} \frac{\kappa}{\kappa_s} |z_1 - z_2|} . \tag{7.38}$$

If the spatial separation of the two subband $|z_1 - z_2|$ is large, f_{AP} becomes large and the AP is well-defined. Physically, when the separation between two charged planes is much larger than the screening length, the plasma oscillation of one plane cannot be fully screened by the other one and the restoring force is strong enough to make the AP a well-defined mode. In bulk multi-carrier systems, the factor analogous to f_{AP} is $\sqrt{2/3}$ and it is more difficult for the AP to be a well-defined one. In this way, MOS systems have a great advantage for the presence of the AP.

D. Numerical calculation of the dispersion relation

In the previous discussion, we treat the case of the small q, but here we show the behavior of the AP in the whole (q,ω) plane by the numerical solution of eq.(7.30). An example of the calculated results is illustrated in Fig.7.5, in which we treat the case of a two-subband system, one in the Γ-valley and the other in the X-valleys, in GaAs. Besides the dispersion relation of the AP, that of the plasmon is also shown which is proportional to $\sqrt{q}$ for small q.[35] There are two kinks in the curve of ω_q. One is for $q \simeq p_{f1}$ and the other for $q \simeq 2.7p_{f1}$. They are due to the abrupt change in the screening of electrons in the *1*-st subband which comes from the existence of the Fermi surface. Thus this is just the same mechanism as Kohn anomaly in the phonon spectrum. This effect also causes the jump in γ_q.

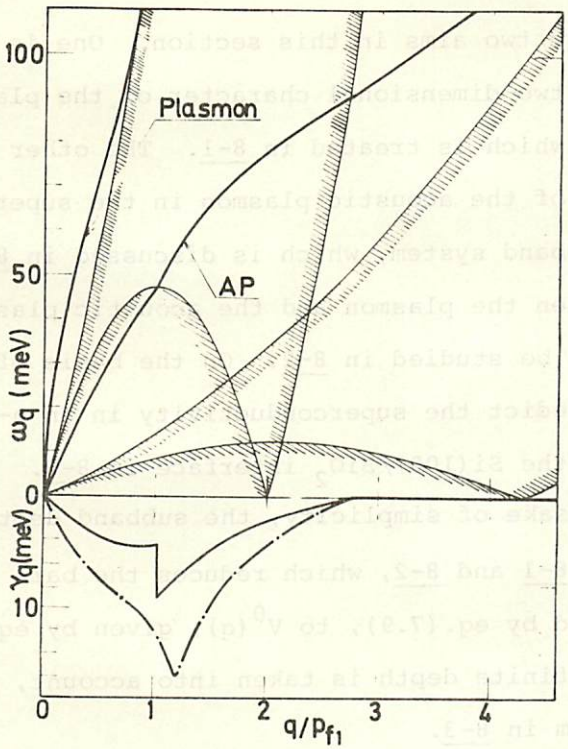

Fig.7.5. Dispersion relation ω_q and the Landau damping γ_q of the AP in a two-subband system which is expected to appear in the n-channel inversion layer on the surface of GaAs having ε_{f1}= 47.4 meV, ε_{f2}= 12.4 meV, m_1^* = 0.068 m_e, m_2^* = 1.2 m_e, g_1 = 1, g_2 = 3, $\langle z\rangle_1$= 19.1 Å and $\langle z\rangle_2$= 7.5 Å. The dot-dash line shows the width of the peak in the dynamical structure factor which corresponds to the AP. The hatched regions represent the regions of the intra-subband excitations. They are divided into two by the curve given by the relation of

$$\alpha_i + x_i = 1,$$

where α_i and x_i are defined in eq.(7.18).

§8. Superconductivity in MOS Inversion Layers

There are two aims in this section. One is to clarify the effect of the two-dimensional character of the plasmon on superconductivity, which is treated in 8-1. The other is to investigate the role of the acoustic plasmon in the superconductivity in a multi-subband system, which is discussed in 8-2. The interrelation between the plasmon and the acoustic plasmon is also the problem to be studied in 8-2. On the basis of these investigations, we predict the superconductivity in an n-channel inversion layer at the Si(100)/SiO_2 interface in 8-3.

For the sake of simplicity, the subband depth $\langle z \rangle_i$ is assumed to be zero in 8-1 and 8-2, which reduces the bare interaction $V^0_{ij}(q)$, defined by eq.(7.9), to $V^0(q)$, given by eq.(7.10). The effect of the finite depth is taken into account, when we treat the real system in 8-3.

8-1. Plasmon Mechanism of Superconductivity in Two-Dimensional Systems

A. Gap equation in a two-dimensional system

We consider the superconductivity in a single-subband system here and discuss the role of the plasmon whose dispersion relation is proportional to $\sqrt{q}$ for small q.[35] The Hamiltonian of the present system can be given by eq.(7.23), in which we take only the 1-st subband into account. The gap equation for the gap function of this subband $\Delta_1(\omega)$ in the weak-coupling theory at the transition temperature T_{c1} can be derived in an analogous

way to that in a three-dimensional system, given in 2-1, as

$$\Delta_1(\omega) = -\int_{-\epsilon_{f1}}^{\infty} \frac{d\omega'}{2\omega'} \tanh\frac{\omega'}{2T_{c1}} K_1(\omega,\omega')\Delta_1(\omega'), \tag{8.1}$$

where the kernel $K_1(\omega,\omega')$ is different from that in eq.(2.18) in the present two-dimensional system and is given by

$$K_1(\omega,\omega') = \frac{m_1^*}{2\pi}\cdot\frac{2}{\pi}\int_{|p-p'|}^{p+p'} \frac{q\,dq}{\sqrt{[(p+p')^2-q^2][q^2-(p-p')^2]}}\left[V_{11}^0(q)+\int_0^{\infty}\frac{2}{\pi}d\Omega\,\frac{\mathrm{Im}V_{11}^R(q,\Omega)}{\Omega+|\omega|+|\omega'|}\right]$$

$$= \frac{m_1^*}{\pi^2}\int_{|p-p'|}^{p+p'} \frac{q\,dq}{\sqrt{[(p+p')^2-q^2][q^2-(p-p')^2]}}\int_0^{\infty}\frac{2}{\pi}d\Omega\,\frac{|\omega|+|\omega'|}{\Omega^2+(|\omega|+|\omega'|)^2}V_{11}^R(q,i\Omega), \tag{8.2}$$

with $p = \sqrt{2m_1^*(\epsilon_{f1}+\omega)}$, $p' = \sqrt{2m_1^*(\epsilon_{f1}+\omega')}$, and the effective interaction $V_{11}^R(q,\Omega)$. Once the gap equation (8.1) is obtained, the numerical method to solve this equation is similar to that in 2-2. The only difference is in the calculation of K_{ij} defined by eq.(2.34), that is, eqs.(2.37) and (2.38) should be changed into

$$K_{ji} = K_{ij}, \tag{8.3}$$

and

$$K_{ij} = \frac{1}{4\pi}\cdot\frac{1}{\omega_{j+1}-\omega_j}\left[\mathrm{sgn}(P_{j+1}-\bar{P}_i)\int_0^{|P_{j+1}-\bar{P}_i|} - \mathrm{sgn}(P_j-\bar{P}_i)\int_0^{|P_j-\bar{P}_i|}\right.$$

$$\left. + \int_{P_j+\bar{P}_i}^{P_{j+1}+\bar{P}_i} + \frac{2}{\pi}\int_{|\bar{P}_i-P_j|}^{\bar{P}_i+P_j}\sin^{-1}\frac{q^2+\bar{P}_i^2-P_j^2}{2\bar{P}_i q} - \frac{2}{\pi}\int_{|P_{j+1}-\bar{P}_i|}^{P_{j+1}+\bar{P}_i}\sin^{-1}\frac{q^2+\bar{P}_i^2-P_{j+1}^2}{2\bar{P}_i q}\right] q\,dq \tag{8.4}$$

$$\times\int_0^{\infty}\frac{2}{\pi}d\Omega\,\frac{|\bar{\omega}_i|+|\bar{\omega}_j|}{\Omega^2+(|\bar{\omega}_i|+|\bar{\omega}_j|)^2}V_{11}^R(q,i\Omega),$$

respectively, where sgn(x) is defined in eq.(2.73).

In the following discussions of the present subsection, the subband suffix "*1*" will be supressed.

B. Analytic solution

As in the case of three-dimensional systems, we start from the plasmon-pole approximation, given by

$$\mathrm{Im}V^{R}(q,\omega) = -\pi\,\omega_p^2(q)\,\delta(\omega^2-\tilde{\omega}_p^2(q))\;V^{0}(q), \tag{8.5}$$

with

$$\omega_p(q) = \sqrt{2\pi e^2 n_s q/\kappa m^*}, \tag{8.6}$$

and

$$\tilde{\omega}_p(q) = \omega_p(q)/\sqrt{1-V^{R}(q,0)/V^{0}(q)}. \tag{8.7}$$

For the static interaction $V^{R}(q,0)$, we take the Thomas-Fermi approximation, given by

$$V^{R}(q,0) = 2\pi e^2/\kappa(q+q_{TF}), \tag{8.8}$$

with

$$q_{TF} = 2e^2 m^* g_v/\kappa, \tag{8.9}$$

where the valley degeneracy of the 1-st subband g_1 is rewritten into g_v here. When eq.(8.5) is put into eq.(8.2), the kernel can be calculated easily and an example of the calculated results is shown in Fig.8.1 by the solid line. Compared with Fig.3.1, this kernel varies more steeply near the Fermi surface. To see the origin of this difference, K(x,x') is calculated approximately for small $x \equiv \omega/\varepsilon_f$ and $x' \equiv \omega'/\varepsilon_f$ as

$$K(x,x') = \frac{1}{\pi g_v} \Lambda\left(\frac{2p_f}{q_{TF}}\right) + \frac{1}{4\pi g_v}\sqrt{\frac{q_{TF}}{p_f}}\, B\left(\frac{1}{4},\frac{1}{2}\right)\frac{|x|+|x'|}{\sqrt{|x-x'|}}, \tag{8.10}$$

where B(p,q) is the Beta-function and $\Lambda(x)$ is defined by

$$\Lambda(x) = \begin{cases} \cos^{-1}x/\sqrt{1-x^2}, & 0<x<1, \\ \ln\left(x+\sqrt{x^2-1}\right)/\sqrt{x^2-1}, & x>1. \end{cases} \tag{8.11}$$

The square-root singularity at $x = x' \neq 0$ stems from the $\sqrt{q}$-dependence of $\omega_p(q)$.

Considering the behavior of K(x,x') in eq.(8.10), we take the function F(x) in the model kernel of eq.(2.50) as

$$F(x) = \frac{1}{4\pi g_v}\sqrt{\frac{q_{TF}}{p_f}}\, B\left(\frac{1}{4},\frac{1}{2}\right)\sqrt{|x|} = \frac{0.4963}{g_v^{1/4}}\sqrt{r_s}\sqrt{|x|}, \tag{8.12}$$

where r_s is defined as usual by

$$r_s = \frac{m^* e^2}{\varkappa}\cdot\frac{1}{\sqrt{\pi n}}. \tag{8.13}$$

The function F(x) in eq.(8.12) has a steeper behavior than that

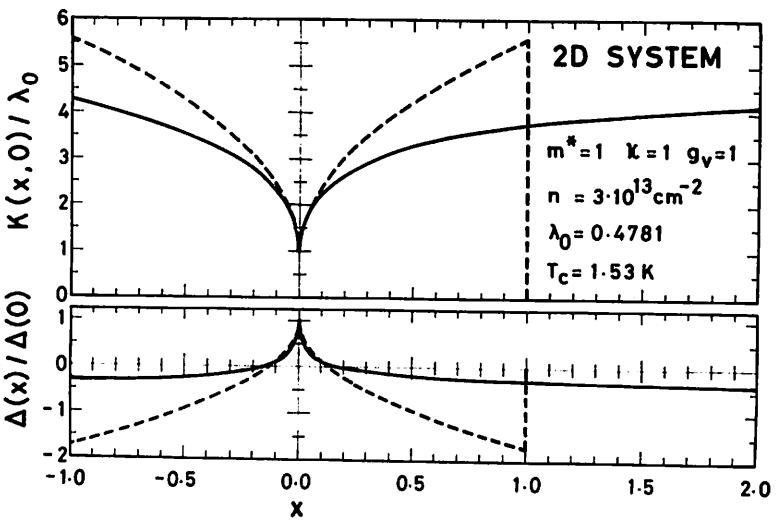

Fig.8.1. An example of the calculated kernel and the corresponing gap function in a two-dimensional system. Solid and broken lines are the results in the plasmon-pole approxmation, given by eqs.(8.5)-(8.8), and the model introduced in 2-3.B with the use of F(x) in eq.(8.12), respectively.

in eq.(3.7). The kernel in this model, *i.e.*, $K(x,0) \equiv \lambda_0 + F(x)$, and the corresponding gap function are plotted in Fig.8.1 by the broken lines. According to the discussions in 2-3.B, in particular, inequality (2.55), we notice that a two-dimensional system is more favorable for the presence of the plasmon mechanism of superconductivity than a three-dimensional one. In fact, the condition of (2.53) reads in the present case as

$$r_s \geq 1.5 , \quad \text{for} \quad g_v = 1 , \tag{8.14}$$

and the critical value of r_s is one fourth of that in a three-dimensional system, given by inequality (3.9).

C. Numerical results

Numerical results of T_c in this approximation, that is, with the use of the effective interaction given by eqs.(8.5)-(8.8), are shown in Fig.8.2 for several values of m*, κ, and g_v as a function of r_s. In order to see how T_c changes with the choice of the approximation to $\tilde{\omega}_p(q)$ in eq.(8.8), calculations are done with the other forms of $\tilde{\omega}_p(q)$: The Lundqvist's[43] form, given by

$$\tilde{\omega}_p(q) = \omega_p(q) \sqrt{1 + \left(1 + \frac{1}{2} \cdot \frac{q^2}{p_f^2}\right) \frac{q}{q_{TF}}} , \tag{8.15}$$

and that obtained by the RPA as

$$\tilde{\omega}_p(q) = \omega_p(q) \sqrt{1 + \frac{q}{q_{TF}} \cdot \frac{1}{1 - \theta(q-2p_f)\sqrt{1-(2p_f/q)^2}}} . \tag{8.16}$$

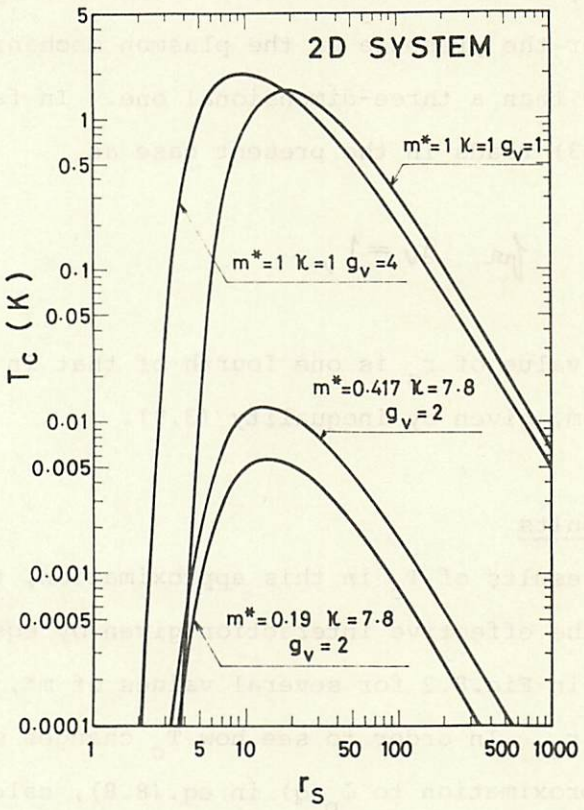

Fig.8.2. Calculated results of T_c in the plasmon mechanism as a function of r_s for several values of m*, κ, and g_v in a two-dimensional system.

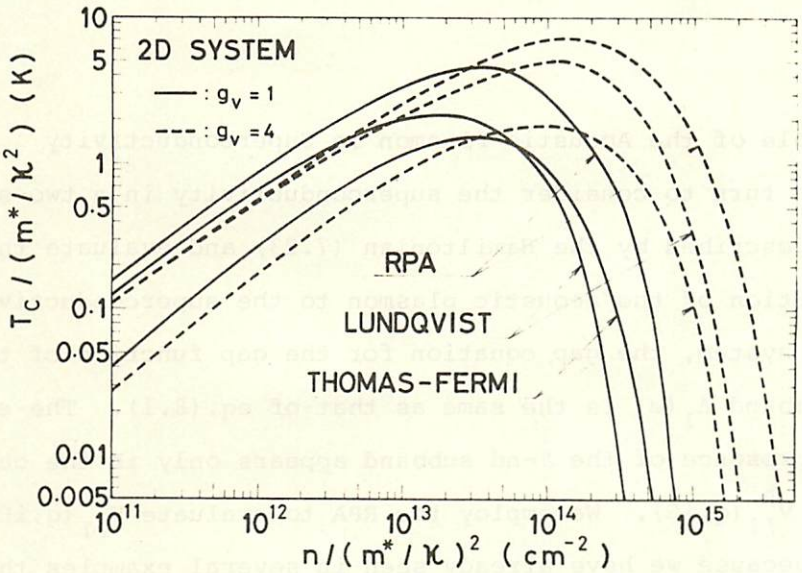

Fig.8.3. Calculated T_c scaled by the effective Rydberg as a function of the carrier concentration n scaled by the inverse of the effective Bohr radius squared, where m* is in the unit of m_e. The lines indicated by THOMAS-FERMI, LUNDQVIST, and RPA correspond to the results in the plasmon-pole approximation with the static interaction given by eqs.(8.8),(8.15) and (8.16), respectively.

These approximations have a correct behavior for very large q, that is, $\tilde{\omega}_p(q)$ approaches to $q^2/2m^*$ for $q >> p_f$. Results of T_c scaled by the effective Rydberg are shown in Fig.8.3 as a function of $n/(m^*/\kappa)^2$. The overall structure of T_c does not change very much with the choice of the effective interaction. This conclusion is the same as in the bulk systems in chapter I.

8-2. Role of the Acoustic Plasmon in Superconductivity

We turn to consider the superconductivity in a two-subband system described by the Hamiltonian (7.23) and evaluate the contribution of the acoustic plasmon to the superconductivity. In this system, the gap equation for the gap function of the *1*-st subband $\Delta_1(\omega)$ is the same as that of eq.(8.1). The effect of the presence of the *2*-nd subband appears only in the calculation of $V^R_{11}(q,i\Omega)$. We employ the RPA to evaluate $V^R_{11}(q,i\Omega)$, partly because we have already seen in several examples that this approximation gives rather good results of T_c and partly because various physical properties of the MOS system are explained well with the use of this approximation, as mentioned in 7-1. Thus $V^R_{11}(q,i\Omega)$ can be calculated as

$$V^R_{11}(q,i\Omega) = V^0(q)/[1+(\Pi_1(q,i\Omega)+\Pi_2(q,i\Omega))V^0(q)], \quad (8.17)$$

where $\Pi_i(q,i\Omega)$ is defined in eq.(7.17).

A. Contribution of the acoustic plasmon

Since $\langle z\rangle_i$ is taken to be zero here, the factor f_{AP}, defined

by eq.(7.34), becomes unity and the condition (7.36) for the presence of the acoustic plasmon becomes

$$g_2 m_2^* > 2 g_1 m_1^* , \tag{8.18}$$

so that for the time being, we consider only the cases in which the inequality (8.18) is satisfied. An example of the calculated T_{c1} as a function of n_2/n_1 is given in Fig.8.4. The carrier concentration of the 1-st subband n_1 is fixed and is so chosen as to give $r_{s1} = 3.6$, where r_{si} is defined by

$$r_{si} \equiv m_i^* e^2 / \kappa \sqrt{\pi n_i} . \tag{8.19}$$

At this carrier density of n_1, T_{c1} in the plasmon mechanism, *i.e.*, T_{c1} evaluated in the absence of the 2-nd subband, is less than $10^{-3} \times (m_1^*/\kappa^2)$ degrees Kelvin, where m_1^* is measured in the unit of m_e. Therefore, T_{c1} in this figure mainly comes from the contribution of the acoustic plasmon produced by electrons in the 2-nd subband.

In order to understand the physics involved in the curve of T_{c1} in Fig.8.4, let us evaluate the characteristic energy of the acoustic plasmon ω_0 which corresponds to the Debye energy of the phonon ω_D. The sound velocity of the acoustic plasmon v_{AP}, given in eq.(7.32), can be rewritten into the form of

$$v_{AP} = v_{f1} \sqrt{\frac{m_1^*}{2m_2^*} \cdot \frac{n_2}{n_1}} . \tag{8.20}$$

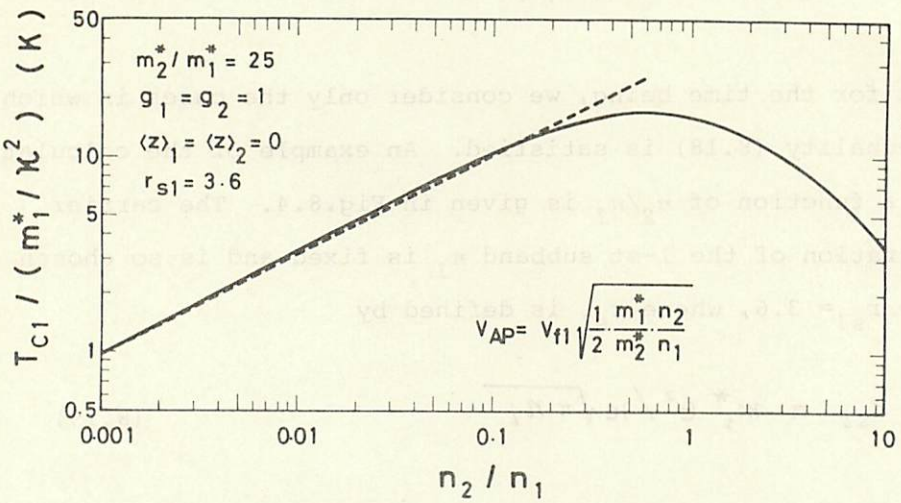

Fig.8.4. Change of $T_{c1}/(m_1^*/\kappa^2)$ with the increase of n_2/n_1. The broken straight line represents the relation of $T_{c1} \propto \sqrt{n_2/n_1}$.

With the use of this v_{AP}, ω_0 is estimated to be

$$\omega_0 \cong 2 p_{f1} v_{AP} = 4 \epsilon_{f1} \sqrt{\frac{m_1^*}{2m_2^*} \cdot \frac{n_2}{n_1}} . \qquad (8.21)$$

Thus, Fig.8.4 is considered to show the change of T_{c1} with the increase of the parameter $\omega_0/\varepsilon_{f1}$. When n_2/n_1 is less than 0.1 for $\omega_0/\varepsilon_{f1}$ to be smaller than about 0.2, T_{c1} increases in proportion to $\sqrt{n_2/n_1}$, that is, to ω_0, as indicated by the broken straight line in the figure. An analogous situation has been observed in the phonon mechanism of superconductivity in metals in which ω_D/ε_f is of the order of 0.01. In these metallic weak-coupling superconductors, T_c is proportional to ω_D, which is called the isotope effect. Therefore, the behavior of T_{c1} for the case of $n_2/n_1 \lesssim 0.1$ can be understood as an effect equivalent to the isotope effect in the phonon mechanism.

As n_2/n_1 and consequently $\omega_0/\varepsilon_{f1}$ are increased further, T_{c1} reaches its maximum at $n_1 \sim n_2$, namely, at $\omega_0/\varepsilon_{f1} \sim 0.4$ and then decreases rapidly. We can clarify this behavior, in particular, the decrease of T_{c1} for large n_2/n_1 by considering the range of the attractive interaction induced by the acoustic plasmon. Since the acoustic plasmon is the mode in which the plasma oscillation of carriers of one kind is screened by carriers of another kind, no charges are produced by the excitation of the acoustic plasmon in the system on the average, in contrast with the case of the plasmon. As a result, the acoustic plasmon does not couple with electrons for small q and brings about a short-range attractive potential, as phonons do. In such a short-range attractive

potential, it is difficult to form the Cooper pair, if $\omega_0/\varepsilon_{f1}$ is larger than unity for the kernel in the gap equation not to have a steep change near the Fermi surface. This is the reason why T_{c1} becomes small rapidly for large n_2/n_1.

In this connection, we will comment briefly on how the differnce in the range of the attractive potential works in the shape of the kernel in the gap equation. In case of a long-range attractive potential, only the kernel near the Fermi surface has a large effect of the attractive potential, even if the potential is induced by the mode having the energy larger than the Fermi energy, as mentioned in 3-2.C. This is due to the fact that only the scatterings with small momentum changes are important in such a long-range potential. In case of a mode which produces a short-range attractive potential, on the other hand, the momentum changes have no such restrictions, so that the kernel within the range of the energy of the mode has a large effect of the attractive potential. Consequently, when the energy of the mode is larger than the Fermi energy, the changing rate of the kernel near the Fermi surface becomes small. This makes the appearance of the superconductivity difficult, as we have learned in 2-3.B. Thus, when the energy of a mode is larger than the Fermi energy, it is preferable to the occurrence of superconductivity for the mode to induce a long-range attractive potential.

In any case, the acoustic plasmon mechanism of superconductivity bears a strong resemblance to the phonon mechanism. In a sense, the phonon mechanism may be regarded as a kind of the acoustic plasmon mechanism, because in the jellium approximation

to the system of ions, the phonon is nothing but the acoustic plasmon of the ions in the electron-ion system. Accordingly, we can consider that Fig.8.4 shows the overall behavior as to how the contribution of the phonon to superconductivity changes with the increase of the parameter ω_D/ε_f.

B. Interrelation between the plasmon and the acoustic plasmon

Now, we investigate the interrelation between the plasmon and the acoustic plasmon in the superconductivity. This study will clarify how the Cooper pair is formed in the system where the short-range attractive potential and the long-range one exist simultaneously. As we have seen in 8-2.A, T_{c1} as a function of n_2/n_1 has a maximum at $n_1 \sim n_2$. We have also calculated several other cases and have always obtained the result in which T_{c1} reaches its maximum at $n_1 \sim n_2$. In the following calculations, therefore, we treat the case of $n_1 = n_2$ mainly.

Figure 8.5 shows the examples of the calculated results of T_{c1} as a function of n_1 in a two-subband system. Every curve in the figure behaves in a similar way: For low n_1, *i.e.*, for the case of $r_{s1} \gtrsim 20$, T_{c1} is almost the same as that in the plasmon mechanism, that is, T_{c1} in the single-subband system with the same n_1, indicated by the broken curve, irrespective of the value of m_2^*/m_1^*. When n_1 is increased, T_{c1} increases first, reaches its maximum at $r_{s1} = 4 \sim 5$ and then decreases. It is also shown in the figure that a large m_2^*/m_1^* is preferable to obtain a large contribution of the acoustic plasmon.

In order to study this behavior a little minutely,

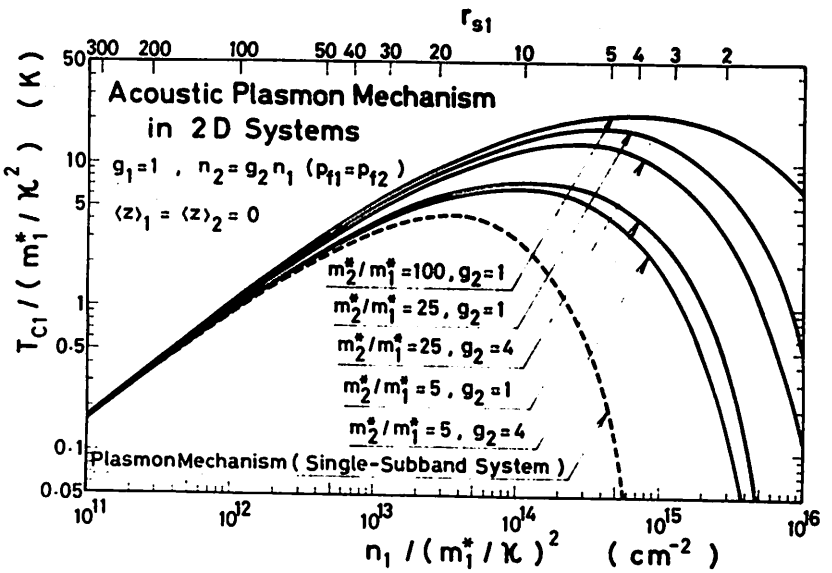

Fig.8.5. Transition temperature $T_{c1}/(m_1^*/\kappa^2)$ as a function of $n_1/(m_1^*/\kappa)^2$ for several values of m_2^*/m_1^* and g_2 in two-subband systems calculated in the RPA, where m_1^* is in the unit of m_e. The broken curve represents the result in the plasmon mechanism, that is, the result in the absence of the 2-nd subband.

we give an approximate kernel for the case of $g_1 = g_2 = 1$, $n_1 = n_2$, *i.e.*, $p_{f1} = p_{f2} \equiv p_f$, and $m_1^* \ll m_2^*$ by extending the idea of the plasmon-pole approximation to the present two-subband system as follows. First, we change eq.(8.5) into the form of

$$\mathrm{Im}\, V_{11}^{R}(q,\Omega) = -\pi V^0(q) \left\{ \omega_p^2(q)\, \delta(\omega^2 - \tilde{\omega}_p^2(q)) + \frac{q}{q+q_{TF1}}\, \omega_{AP}(q)^2\, \delta(\omega^2 - \tilde{\omega}_{AP}^2(q)) \right\}, \tag{8.22}$$

with

$$\omega_p(q) = \sqrt{2\pi e^2 q \left(\frac{n_1}{m_1^*} + \frac{n_2}{m_2^*}\right)/\kappa}\,, \tag{8.23}$$

$$\tilde{\omega}_p(q) = \omega_p(q)\sqrt{1 + q/q_{TF1}}\,, \tag{8.24}$$

$$\omega_{AP}(q) = \frac{p_f q}{m_2^*}\sqrt{q_{TF2}/2(q_{TF1}+q)}\,, \tag{8.25}$$

and

$$\tilde{\omega}_{AP}(q) = \omega_{AP}(q)\sqrt{(q + q_{TF1} + q_{TF2})/q_{TF2}}\,, \tag{8.26}$$

where q_{TFi} is defined in eq.(7.29). In eq.(8.22), the first term represents the contribution of the plasmon and the second one that of the acoustic plasmon. The frequencies of $\omega_p(q)$ and $\omega_{AP}(q)$ are calculated by an analogous way in 7-4.C, while other factors

like $\tilde{\omega}_p(q)/\omega_p(q)$ and $\tilde{\omega}_{AP}(q)/\omega_{AP}(q)$ are determined so as to give the correct strength of the coupling constant with electrons. The calculated kernel in this approximation reproduces the kernel calculated in the RPA well.

For small $x \equiv \omega/\varepsilon_{f1}$, $K_1(x,0)$ has the form of

$$K_1(x,0) = \frac{m_1^*}{m_1^*+m_2^*}\cdot\frac{1}{\pi}\Lambda\left(\frac{2p_f}{q_{TF1}+q_{TF2}}\right) + F_p(x) + F_{AP}(x), \tag{8.27}$$

with

$$F_p(x) = \frac{1}{4\pi}\sqrt{\frac{q_{TF1}}{p_f\left(1+\frac{m_1^*}{m_2^*}\right)}}\, B\left(\frac{1}{4},\frac{1}{2}\right)\sqrt{|x|}, \tag{8.28}$$

and

$$F_{AP}(x) = \frac{1}{4\pi}\cdot\frac{m_2^*}{m_1^*+m_2^*}\cdot\frac{m_2^*}{m_1^*}\sqrt{\frac{2(p_f+q_{TF1})}{q_{TF1}+q_{TF2}}}\,|x|\ln\frac{8}{|x|}, \tag{8.29}$$

where $\Lambda(x)$ is defined in eq.(8.11).

When the carrier density is low and p_f is small, the contribution of the plasmon $F_p(x)$ dominates that of the acoustic plasmon $F_{AP}(x)$. Therefore T_{c1} is determined almost only by the plasmon in this region of n_1. Physically, when a carrier concentration is low enough for the plasmon to have a large effect on the superconductivity, the wave function of the relative motion of the Cooper pair has a character convenient for the long-range attractive potential induced by the plasmon. The acoustic plasmon, on the other hand, shows only a small effect in this

region, because this mode induces a short-range attractive potential, as mentioned in 8-2.A.

When n_1 is increased, the contribution of the plasmon, $F_p(x)$, decreases, while that of the acoustic plasmon, $F_{AP}(x)$, increases. As a result, there is an optimum r_{s1} value at which the system makes full use of both contributions. With the further increase of n_1, T_{c1} is almost determined only by the acoustic plasmon and decreases gradually, but even in very small r_{s1}, the superconducting state can be brought about by the contribution of the acoustic plasmon $F_{AP}(x)$.

C. T_c of the whole system

In the foregoing calculations, we have devoted ourselves to the calculation of T_{c1}. However, in a two-subband system, the 2-nd subband has also the possibility to become superconducting and the transition temperature of it, T_{c2}, should be calculated. The transition temperature of the whole system T_c, therefore, cannot be given until the higher temperature between T_{c1} and T_{c2} is known.

Calculations of T_{c2} are done by the exchange of the roles of the two subbands in the previous calculations of T_{c1}. Examples of calculated T_c are shown in Fig.8.6. Since m_2^*/m_1^* plays an important role in the acoustic plasmon mechanism of superconductivity, as we have seen in 8-2.B, T_c is plotted as a function of m_2^*/m_1^* for the two cases of $r_{s1}= 2$ and $r_{s1}= 19$, in which only the case of $m_2^*/m_1^* \geq 1$ is treated. When m_2^*/m_1^* is not so large, in particular, when it is less than two or three, the contribution

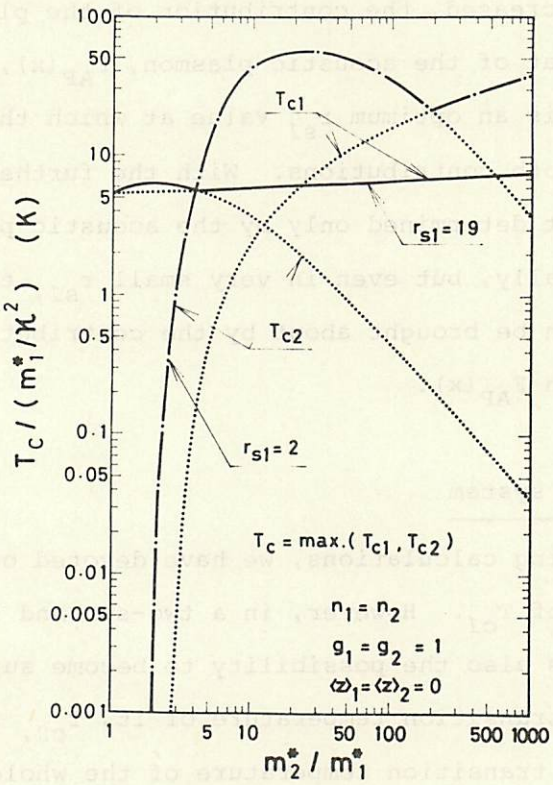

Fig.8.6. Dependence of T_c on m_2^*/m_1^*. The solid and the dot-dash lines correspond to the cases of $r_{s1}= 19$ and $r_{s1}= 2$, respectively. The transition temperature of the whole system T_c is given by the higher temperature between T_{c1} and T_{c2}.

of the acoustic plasmon is rather small, so that both T_{c1} and T_{c2} are mainly determined by the contribution of the plasmon. In such a case, the subband having a heavier effective mass is more advantageous. This leads us to the result of $T_c = T_{c2}$ for both cases of $r_{s1} = 2$ and $r_{s1} = 19$.

For the case of very large m_2^*/m_1^*, on the other hand, the acoustic plasmon has a considerable contribution to T_{c1} and makes T_{c1} high, in particular, for the case of small r_{s1}. As for the 2-nd subband, however, $\omega_{AP}(p_{f2})/\varepsilon_{f2}$ is so large that the acoustic plasmon does not contribute to T_{c2}. The change of T_{c2} comes from that of $r_{s2} = m_2^*/m_1^* \times r_{s1}$ in the plasmon mechanism. In this way, T_c becomes equal to T_{c1} for very large m_2^*/m_1^* owing to the difference of the contribution of the acoustic plasmon to T_{ci}.

D. Summary

To sum up the results obtained in the present subsection, there are two restrictions in order for the acoustic plasmon to play the main role in the superconductivity in a two-carrier system. First, the carrier concentration of the superconducting carrier should be nearly equal to that of the other carrier and at the same time, it should be high enough to provide the r_s parameter smaller than five. Secondly, the effective mass of the superconducting carrier should be much smaller than that of the other carrier. If these conditions are not fulfilled, there are other mechanisms such as the plasmon one to play the most important role in the superconductivity, even though the acoustic plasmon

has always some help for the system to become superconducting.

If we regard the phonon in a metal as an acoustic plasmon in an electron-ion system, the above two conditions are satisfied. Thus we can have an explanation why the phonon mechanism of superconductivity is realized in metals.

8-3. Application to $Si(100)/SiO_2$ Interface under Uniaxial Stress along [001] Direction

We explore the possibility of the superconductivity in an n-channel inversion layer at the $Si(100)/SiO_2$ interface which is the most typical and fundamental MOS structure. As pointed out in 7-2, a two-carrier system can be obtained even in this material by the control of the uniaxial stress along the [001] direction, but according to the results in 8-2.C, the acoustic plasmon will not give an important contribution to the superconductivity, because the parameter m_2^*/m_1^* is about 2.2 in this case. In order to see this, an example of the calculated T_{ci} is shown in Fig.8.7 as a function of n_1/n_s. In this figure, the total carrier concentration n_s is fixed to be $5\times10^{11}cm^{-2}$, while n_1 can be controlled by the application of the stress. As in the case of Fig.8.4, the maximum T_{ci}, which will be denoted by T_{ci}^{max}, appears at $n_1 \sim n_2$. When we compare T_{ci}^{max} with T_{ci}^{p} which is defined by T_{ci} in the plasmon mechanism, that is, T_{ci} in the single-subband system ($n_i = n_s$), T_{c2}^{max} is only 1.5 times as large as T_{c2}^{p} and T_{c1}^{max} is larger than T_{c1}^{p} by a factor of 5. Therefore the effect of the acoustic

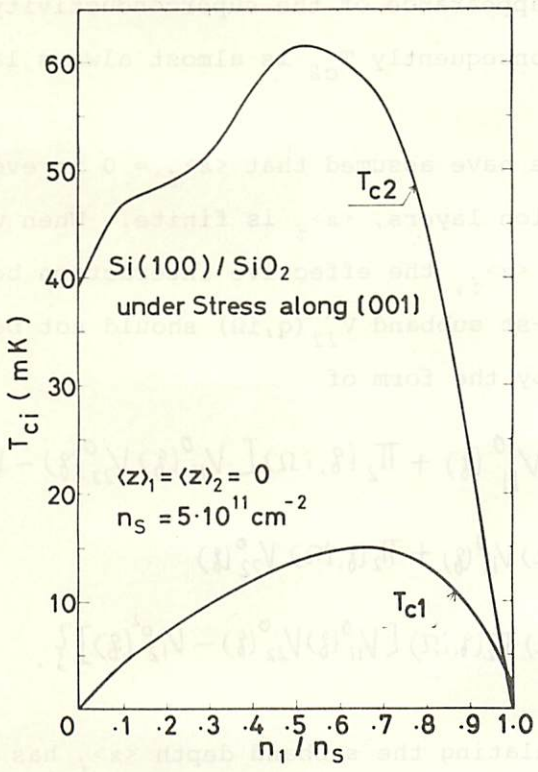

Fig.8.7. An example of the calculated T_{ci} as a function of n_1 for the case of $n_s = 5 \times 10^{11}$ cm^{-2} in an n-channel inversion layer at the Si(100)/SiO_2 interface under the uniaxial stress along the [001] direction. The ratio n_1/n_s can be controlled by the stress.

plasmon is found to be small for both T_{c1} and T_{c2}. In such a case as this, the subband having a heavier effective mass is preferable to the appearance of the superconductivity, as shown in 8-2.C. Consequently T_{c2} is almost always larger than T_{c1}.

Until now, we have assumed that $\langle z \rangle_i = 0$ in every case, but in real inversion layers, $\langle z \rangle_i$ is finite. When we treat the case of finite $\langle z \rangle_i$, the effective interaction between electrons in the 1-st subband $V_{11}^R(q, i\Omega)$ should not be calculated by eq.(8.17), but by the form of

$$V_{11}^R(q, i\Omega) = \left\{ V_{11}^0(q) + \Pi_2(q, i\Omega)\left[V_{11}^0(q) V_{22}^0(q) - V_{12}^{02}(q) \right] \right\}$$
$$/ \left\{ 1 + \Pi_1(q, i\Omega) V_{11}^0(q) + \Pi_2(q, i\Omega) V_{22}^0(q) \right.$$
$$\left. + \Pi_1(q, i\Omega)\Pi_2(q, i\Omega)\left[V_{11}^0(q) V_{22}^0(q) - V_{12}^{02}(q) \right] \right\}. \qquad (8.30)$$

The method of calculating the subband depth $\langle z \rangle_i$ has already been described in 7-2.B and the examples of the calculated results of $\langle z \rangle_i$ are given in Fig.7.3. According to this figure, the subband depth $\langle z \rangle_i$ can be controlled rather widely by the total number of the negative charges in the depletion layer per unit area n_{dep}, or equivalently, by the application of the substrate bias.

Using these results of the subband depth as a function of n_s, n_{dep}, and the stress, we can calculate T_{ci} as a function of these parameters from the first principles. An example of the calculated results is shown in Fig.8.8, in which T_{ci} is

plotted as a function of n_s for several values of n_{dep} and the stress is assumed to be so controlled as to give $n_1 = n_2 = n_s/2$. The transition temperature of the whole system is always given by T_{c2} and is at most 10 mK. It is also shown that T_c depends strongly on n_s and n_{dep}. This feature will provide a great help to confirm the present theory by the experiment.

Besides the present mechanism, the contribution of the acoustic phonons is also estimated in this system just as the same way as in 6-4 and we obtain the conclusion that the relative error of the results with the phonons to those without them is always within a few per cent, when the deformation potentials, Ξ_u and Ξ_d, are taken to be usually accepted values. (Ξ_u= 9.0 eV and Ξ_d= -6.0 eV[106])

In conclusion, the plasmon has the main effect on T_c in the present system and the acoustic plasmon works only subsidiarily. Thus, the main role of the stress is considered not to make the system to be a two-carrier system, but simply to transfer electrons into the 2-nd subband having a heavier effective mass. Accordingly, this system is not an interesting system from a point of the acoustic plasmon mechanism of superconductivity. Compared with this system, n-channel inversion layers on the surface of III-V compounds seem to satisfy the requirements for the acoustic plasmon mechanism, because the effective mass of the second minimum valleys is about from ten to fourty times as large as that in the Γ-valley. From such a reason, investigations into these materials are highly expected, although they are far behind from those into SiMOS structures at present, both experimentally and theoretically.

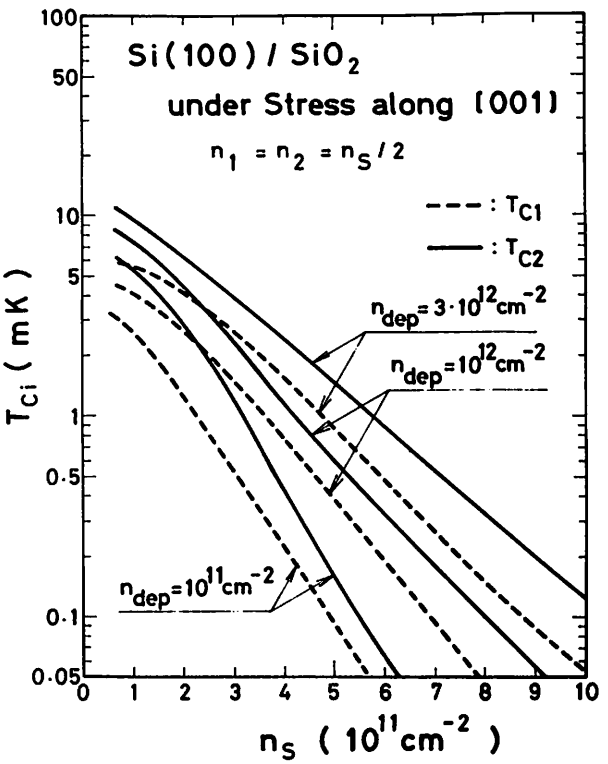

Fig.8.8. Calculated T_{ci} as a function of n_s for the cases of n_{dep}= $10^{11}cm^{-2}$, $10^{12}cm^{-2}$ and $3\times10^{12}cm^{-2}$ in an n-channel inversion layer on the Si(100) surface under the stress along the [001] direction. The stress is assumed to be so controlled as to give n_1= n_2= $n_s/2$. In this system, T_{c2} is always larger than T_{c1}.

§9. Discussions

9-1. Summary of Chapter III

A large amount of works have been done on an n-channel inversion layer at the $Si(100)/SiO_2$ interface, mainly because various quantities of this system such as n_s and $\langle z \rangle_i$ can be controlled easily by the change of the gate voltage and the substrate bias and also by the application of the uniaxial stress. The knowledge obtained in this way permits us to perform the first-principle calculation of T_c. From such a study of T_c, this system is predicted to show the superconducting behavior at the temperatures around 1 mK. The superconductivity is due mainly to the plasmon. Compared with the bulk systems, the two-dimensional character of the plasmon is shown to be preferable for the superconductivity. Although the predicted transition temperature is extremely low, it is within the observable range and besides, it will be the first direct proof of the plasmon mechanism of superconductivity, if the superconductivity is really observed and the calculated dependence of T_c on n_s, n_{dep} and the stress is assured experimentally.

9-2. Fluctuation Effect

Although we have discussed T_c in the mean-field approximation until now, we cannot neglect the effects of fluctuation in a two-dimensional system. However, even if there is no true transition to the superconducting phase,[107] the system has

superconducting behaviors near T_c. The excess conductivity σ', coming from the Cooper pairs which are created thermally in the normal phase, can reduce the resistivity so much that the system may be seen to be superconducting. In fact, in the range of the temperatures where the interactions between thermally activated Cooper pairs can be neglected, *i.e.*, in the classical range, one of the contributions to σ' is given by

$$\sigma'/\sigma_n = \frac{\pi}{16} \cdot \frac{g_1}{\sum_i g_i \tau_i \varepsilon_{fi}} \cdot \frac{T_{c1}}{T - T_{c1}} , \qquad (9.1)$$

where we have assumed that T_{c1} is much larger than T_{c2}, σ_n is the normal conductivity, and τ_i is the relaxation time of the i-th subband. In deriving eq.(9.1), we have assumed the dirty limit condition, that is, $\tau_1 T_{c1} \ll 1$. Equation (9.1) is similar to that obtained by Aslamazov and Larkin (AL)[108] for a thin metal, which was written by

$$\sigma'/\sigma_n = \frac{3\pi^2}{32} \cdot \frac{1}{\tau \varepsilon_f} \cdot \frac{1}{p_f d} \cdot \frac{T_c}{T - T_c} , \qquad (9.2)$$

where p_f, ε_f, τ, and d are the Fermi wave number, the Fermi energy, the relaxation time and the depth of the metal, respectively. The physics in eqs.(9.1) and (9.2) is the same and the difference is only in the numerical factor. This can be understood readily, because the result of AL can be reproduced by the time-dependent Ginzburg-Landau theory[109] and it does not matter whether the motion of electrons perpendicular to the surface is quantized as in MOS systems, or not as in thin metals. Another

contribution to σ' comes from the Maki term, which also gives the same result as that in a thin metal[110] except the same numerical factor. The same is applied to the critical range of the temteratures and we can obtain all the results of the superconducting fluctuation effects in MOS systems by changing the numerical factor in the corresponding results in thin metals.

9-3. Comment on the Kawaji's Experiment on the Superconductivity on the surface of InAs

Kawaji *et al.*[33] observed superconducting fluctuation effects on the surface of a p-type InAs in contact with SiO_2 experimentally. They also indicated that the phenomena were in the n-channel inversion layer. In the system, however, they could not control n_s by the gate voltage, so that they controlled n_s by the amount of N_a^+ ion diffused into the oxide part of the system. The observed transition temperatures, estimated with the use of the AL term, that is, eq.(9.1), or eq.(9.2), were given in Fig.9.1 for several samples with different n_s.[111] We have tried to explain the mechanism of the superconductivity, but the results in §8 shows that T_c becomes at most $10\times(m^*/\kappa^2)$ degrees Kelvin, calculated to be 10^{-3}K, if we use the values of κ = 14.3 and m*= 0.025 of InAs. Thus at present, we cannot account for the experiment of Kawaji *et al.* at all.

However, the behavior of T_c in this experiment is quite similar to those in Figs.8.3 and 8.5. In addition, we can reproduce their result of T_c in the plasmon mechanism quantitatively

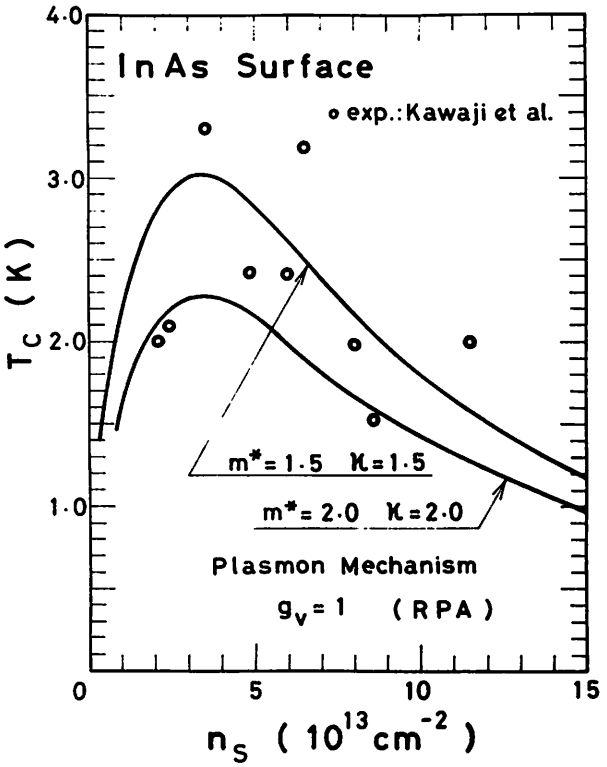

Fig.9.1. Experimental results of T_c on the surface of InAs observed by Kawaji *et al.* They are represented by open circles, while the solid lines show the results of T_c in the plasmon mechanism in a two-dimensional system calculated in the RPA. The curves of m* and κ are so chosen as to explain the experiment well.

if we use the values of m* and κ of the order of unity. This is indicated in Fig.9.1 by the solid lines. These values of m* and κ, however, differ very much from those of InAs. As to the difference in the value of m*, there are a few possible explanations. One is to assume that the superconductivity is in the electrons in the second minimum valleys at L-points whose effective mass is known to be of the order of unity.[112] Another is to assume that there is a surface state with a heavy effective mass and that the electrons in this state are responsible for the superconductivity. The value of κ is rather difficult to be explained. But we should remember that the relevant κ in the plasmon mechanism is the dynamic one with the energy of the order of ε_f, as we have learned often in this thesis. In the present case, ε_f becomes of the order of 400 meV, that is, the energy gap between the conduction and the valence bands of InAs, if we take m* $\sim$ 1 and n_s of the order of 10^{13}cm^{-2}. Therefore, if we take the dynamical effect of the valence electrons into account, κ may be of the order of unity, in contrast with the static value of 14.3. It must be noted here that the treatment of such a dynamical effect is just the same as to take the exciton effect into account.[23] In this sense, Kawaji's experiment might be explained by the combination of the plasmon and the exciton. But we have to solve many problems, both experimentally and theoretically, to confirm this speculation, which will be one of the main problems to be solved in the future.

9-4. Problem about the High T_c Superconductor

In the last part of the present thesis, we make a highly speculative discussion on the problem of the high T_c superconductor. In all the mechanisms treated in this thesis, T_c is at most of the order of $10\times(m^*/\kappa^2)$ degrees Kelvin with m^* in the unit of m_e and hence T_c/ε_f is almost always less than 0.001. Since this is the case with the phonon mechanism in usual metallic superconductors and also in ^{3}He in which paramagnon plays an important role, it seems to be a common feature of the superconductivity and the superfluidity. In fact, this may be explained physically as follows. The superconducting state is characterized by a pair coherent state and the conservation of the total number of particles is broken. This means that there should be a very large number of particles within the range of the coherence length ξ_0. Thus, ξ_0 should be much larger than the interparticle spacing r_0. Because of $r_0/\xi_0 \sim T_c/\varepsilon_f$, T_c/ε_f is always small in the pair condensed state.

If we take these results into account, it seems very difficult to obtain a superconductor with T_c larger than 100 K, if the carrier of the system is an electron. One possible way to have a high T_c superconductor is to make a system of carriers with a much heavier mass than that of electrons, for example, a system of proton-gas, superconducting. But this kind of systems seems very difficult to be obtained here on our earth.

SUMMARY

In the present thesis, a new method of calculating the superconducting transition temperature T_c is developed. This method is applicable to any kind of materials, provided that the weak-coupling approximation is satisfied. In addition, no adjustable parameters are introduced and we can make a first-principle calculation of T_c. With the use of this method, we can determine the mechanism of superconductivity in a given material, if its normal properties are known well.

There are various systems to which we would like to apply this method, but in this thesis, we have treated low-carrier-density systems such as degenerate semiconductors and investigate the roles of the Coulomb interaction in superconductivity, mainly because the contribution of the Coulomb interaction, in particular, that of the plasmon, has never been appreciated enough.

In chapter I, we have discussed the possibility of superconductivity in the electron-gas system with the aid of the plasmon and reduced the problem of the occurrence of the plasmon mechanism of superconductivity to the problem what is the ground state of an electron assembly in the jellium model, in case the superconductivity is not considered at all. If the ground state of the system having r_s larger than six is normal metallic one

with a well-defined Fermi surface, the plasmon mechanism of superconductivity appears. We also find that T_c can be evaluated well in the RPA.

In chapter II, the superconductivity in an n-type semiconducting $SrTiO_3$ has been investigated as an example of the real system in which the plasmon plays an important role. The observed results of the carrier-density-dependent T_c and also of the stress effects on T_c are explained quantitatively in the plasmon-ferroelectric soft phonon mechanism of superconductivity.

As a possible system to become superconducting only with the aid of the plasmon, we have treated an n-channel inversion layer at the $Si(100)/SiO_2$ interface in chapter III. This system is predicted to show the superconducting behavior at the temperatures around 1 mK for the carrier density of the order of $10^{11} cm^{-2}$.

The investigations in chapters II and III have also given us a knowledge about the interrelation between the plasmon and other modes such as phonons and acoustic plasmons in superconductivity. When the carrier density is very low and consequently every mode has an excitation energy larger than the Fermi energy, only the plasmon which induces a long-range attractive potential between the Cooper pair contributes to superconductivity. As the carrier density is increased, other modes begin to play a role in superconductivity, while the role of the plasmon decreases. As a result, superconductivity in a high-carrier-density system is brought about mainly with the aid of the modes such as phonons and acoustic plasmons which give rise to a short-range attractive potential between the Cooper pair.

REFERENCES

[1] H.K. Onnes, Comm. Phys. Lab. Univ. Leiden. Nos.119, 120, 122 (1911).

[2] W. Meissner and R. Ochsenfeld, Naturwiss. 21, 787 (1933).

[3] F. London, Proc. Roy. Soc. (London) A152, 24 (1935); Phys. Rev. 74, 562 (1948).

[4] V.L. Ginzburg and L.D. Landau, Zh. Eksperim. i. Teor. Fiz. 20, 1064 (1950).

[5] B.D. Josephson, Phys. Letters 1, 251 (1962); Advan. Phys. 14, 419 (1965).

[6] J. Bardeen, L.N. Cooper, and J.R. Schrieffer, Phys. Rev. 108, 1175 (1957).

[7] L.N. Cooper, Phys. Rev. 104, 1189 (1956).

[8] E. Maxwell, Phys. Rev. 78, 477 (1950); C.A. Reynolds, B. Serin, W.H. Wright, and L.B. Nesbitt, Phys. Rev. 78, 487 (1950).

[9] J.R. Schrieffer, D.J. Scalapino, and J.W. Wilkins, Phys. Rev. Letters 10, 336 (1963); D.J. Scalapino, J.R. Schrieffer, and J.W. Wilkins, Phys. Rev. 148, 263 (1966); W.L. McMillan and J.M. Rowell, Phys. Rev. Letters 14, 108 (1965); W.L. McMillan and J.M. Rowell, Superconductivity, ed. by R.D. Parks (Marcel Dekker, Inc., New York, 1969) Vol.1, Chapter 11.

[10] D. Pines and P. Nozieres, The Theory of Quantum Liquids (W.A. Benjamin, Inc., New York, 1966) Vol.1, p.53 and p.320; M.L. Cohen and P.W. Anderson, Superconductivity in d- and f-Band Metals, ed. by D.H. Douglass (AIP, New York, 1972) p.17.

[11] N.N. Bogoliubov, V.V. Tolmachev, and D.V. Shirkov, New Method in the Theory of Superconductivity (Consultants Bureau, New York, 1959).

[12] P. Morel and P.W. Anderson, Phys. Rev. 125, 1263 (1962).

[13] G.M. Eliashberg, Soviet Physics – JETP 38, 966 (1960); 39, 1437 (1960).

[14] Y. Nambu, Phys. Rev. 117, 648 (1960).

[15] J.R. Schrieffer, Theory of Superconductivity (W.A. Benjamin, Inc., New York, 1964).

[16] D.J. Scalapino, Superconductivity, ed. by R.D. Parks (Marcel Dekker, Inc., New York, 1969) Vol.1, Chap.10.

[17] W.L. McMillan, Phys. Rev. 167, 331 (1968).

[18] A.B. Migdal, Soviet Physics – JETP 7, 996 (1958).

[19] E.G. Batyev and V.L. Pokrovskii, Soviet Physics – JETP 19, 181 (1964); V. Heine, P. Nozières, and J.W. Wilkins, Phil. Mag. 13, 741 (1966); R.E. Prange and S. Sachs, Phys. Rev. 158, 672 (1967).

[20] W.A. Little, Phys. Rev. 134, A1416 (1964); J. Polym. Sci. 29C, 17 (1970); D. Davis, H. Gutfreund, and W.A. Little, Phys. Rev. B13, 4766 (1976).

[21] I.E. Dzyaloshinskii and E.I. Kats, Soviet Physics - JETP 28, 178 (1969).

[22] V.L. Ginzburg, Contemp. Phys. 9, 355 (1968); Soviet Phyiscs - Uspekhi 13, 335 (1970).

[23] D. Allender, J.Bray, and J. Bardeen, Phys. Rev. B7, 1020 (1973); J.C. Phillips, Phys. Rev. Letters 29, 1551 (1972); J.C. Inkson, and P.W. Anderson, Phys. Rev. B8, 4429 (1973).

[24] James W. Garland, Jr., Phys. Rev. Letters 11, 111 (1963); 114 (1963).

[25] V. Radhakrishnan, Phys. Letters 16, 247 (1965).

[26] H. Fröhlich, J. Phys. C1, 544 (1968); A. Rothwarf, Phys. Rev. B9, 3560 (1970).

[27] B.T. Geilikman, Soviet Physics - Uspekhi 16, 17 (1973).

[28] É.A. Pashitskii, Soviet Physics - JETP 28, 1267 (1969); É.A. Pashitshkii and V.M. Chernousenko, Soviet Physics - JETP 33, 802 (1971).

[29] M.L. Cohen, Phys. Rev. 134, A511 (1964); Rev. Mod. Phys. 36, 240 (1964); Superconductivity, ed. by R.D. Parks (Marcel Dekker, Inc., New York, 1969) Vol. 1, Chap. 12.

[30] C.S. Koonce, M.L. Cohen, J.F. Schooley, W.R. Hosler and E.R. Pfeiffer, Phys. Rev. 163, 380 (1967).

[31] P.B. Allen and M.L. Cohen, Phys. Rev. 177, 704 (1969).

[32] J.F. Schooley, W.R. Hosler, and M.L. Cohen, Phys. Rev. Letters 12, 474 (1964).

[33] S. Kawaji, S. Miki, and T. Kinoshita, J. Phys. Soc. Japan 39, 1631 (1975).

[34] F. Stern, CRC critical Rev. in Solid State Sci. 5 499 (1974); G. Dorda, Festkörperprobleme (Advances in Solid State Physics), ed. by H.J. Queisser (pergamon Vierweg, 1973) Vol. 13, p.215; Y. Uemura, Proc. 2nd ICSS, Japan, J. Appl. Phys. Suppl. 2, Part 2, 17 (1974); G. Landwehr, Festkörperprobleme (Advances in Solid State Physics), ed. by H.J. Queisser (Pergamon Vierweg 1975) Vol. 15, p.49; J.F. Koch, ibid., p.79; Y.Uemura, Surface Sci. 58, 1 (1976); J.F. Koch, Surface Sci. 58, 104 (1976);

T. Ando, Electronic Properties of Two-Dimensional Systems, ed. by G. Dorda and P.J. Stiles (North-Holland Pub. Company, Amsterdam, 1978) p.1.

[35] F. Stern, Phys. Rev. Letters 18, 546 (1967).

[36] Y. Takada and Y. Uemura, J. Phys. Soc. Japan 43, 139 (1977).

[37] Y. Takada and T. Ando, J. Phys. Soc. Japan 44, 905 (1978).

[38] D.A. Kirzhnits, E.G. Maksimov, and D.I. Khomskii, J. Low. Temp. Phys. 10, 79 (1973).

[39] D.N. Zubarev, Soviet Physics - Uspekhi 3, 320 (1960).

[40] M.L. Cohen, C.S. Koonce and M.Y. Au-Yang, Phys. Letters 24A, 582 (1967); M.L. Cohen, Superconductivity, ed. by R.D. Parks (Marcel Dekker, Inc., New York) Vol. 1, Chap. 12, P.659.

[41] A. Layzer and D. Fay, Intern. J. Magnetism 1, 135 (1971); S. Nakajima, Prog. Theor. Phys. 50, 1101 (1973); P.W. Anderson and W.F. Brinkman, Phys. Rev. Letters 30, 1108 (1973).

[42] D. Bohm and D. Pines, Phys. Rev. 82, 625 (1951); 85, 338 (1952); 92, 609 (1953); 92, 626 (1953).

[43] B.I. Lundqvist, Phys. kondens. Materie 6, 206 (1967); L. Hedin and S. Lundqvist, Solid State Physics, ed. by F. Seitz, D. Turnbull, and H. Ehrenreich (Academic Press, New York and London, 1969) Vol. 23, P.84.

[44] A.W. Overhauser, Phys. Rev. B3, 1888 (1970).

[45] E.P. Wigner, Phys. Rev. 46, 1002 (1934); Trans. Faraday Soc. 34, 678 (1938).

[46] D. Pines, Phys. Rev. 109, 280 (1958).

[47] J. Lindhard, Kgl. Danske Videnskab. Selskab. Mat. fys. Medd. 28, 8 (1954).

[48] J. Hubbard, Proc. Roy. Soc. (London) A243, 336 (1957); T.M. Rice, Ann. Physics (New York) 31, 100 (1965).

[49] B.B.J. Hede and J.P. Carbotte, Canad. J. Phys. 50, 1756 (1972); H. Yasuhara, J. Phys. Soc. Japan 36, 361 (1974); D.N. Lowy and G.E. Brown, Phys. Rev. B12, 2138 (1975).

[50] K.S. Singwi, M.P. Tosi, R.H. Land, and A. Sjölander, Phys. Rev. 176, 589 (1968); K.S. Singwi, A. Sjölander, M.P. Tosi, and R.H. Land, Phys. Rev. B1, 1044 (1970).

[51] P. Vashishta and K.S. Singwi, Phys. Rev. B6, 875 (1972).

[52] N.F. Berk and J.R. Schrieffer, Phys. Rev. Letters 17, 433 (1966); S. Doniach and S. Engelsberg, Phys. Rev. Letters 17, 750 (1966).

[53] P. Nozières and D. Pines, Phys. Rev. 111, 442 (1958); R.A. Coldwell-Horsfall and A.A. Maradudin, J. Math. Phys. 1, 395 (1960); W.J. Carr, Phys. Rev. 122, 1437 (1961); N.F. Mott, Phil. Mag. 6, 287 (1961); F.W. de Wette, Phys. Rev. A135, 287 (1964); H.M. van Horn, Phys. Rev. 157, 342 (1967); B. Pietrass, Phys. stat. sol. 24, 571 (1967); S.F. Edwards and A.J. Hillel, J. Phys. C1, 61 (1968); A. Ishihara, Phys. Letters A39, 313 (1972); see also the review article written by C.M. Care and N.H. March, Adv. Phys. 24, 101 (1975).

[54] A.A. Kugler, Ann. Phys. 53, 133 (1969).

[55] S.G. Brush, H.L. Sahlin and E. Teller, J. Chem. Phys. 45, 2102 (1966); H.M. van Horn, Phys. Letters A28, 706 (1969); J.P. Hansen, Phys. Letters A41, 213 (1972); E.L. Pollock and J.P. Hansen, Phys. Rev. A8, 3110 (1973); H. Totsuji and S. Ichimaru, Progr. Theor. Phys. 52, 42 (1974).

[56] A. Bagchi, Phys. Rev. 178, 707 (1969).

[57] S. Misawa, Phys. Rev. 140, A1645 (1965); A.K. Rajagopol and S.D. Mahenti, Phys. Rev. 158, 353 (1967).

[58] Y. Osaka, J. Phys. Soc. Japan 22, 1513 (1967).

[59] P.W. Anderson, Phys. Rev. 109, 1492 (1958).

[60] See for example, D. Pines and P. Nozières, The Theory of Quantum Liquids (Benjamin, Inc., New York, 1966) p.193; and also, K.L. Kliewer and R. Fuches, Phys. Rev. 181, 552 (1969).

[61] P.W. Anderson, Phys. Chem. Solids 11, 26 (1959).

[62] V.L. Gurevich, A.I. Larkin, and Y.A. Firsov, Soviet Physics – Solid State 4, 131 (1962).

[63] J.A. Noland, Phys. Rev. 94, 724 (1954); M.Cardona, Phys. Rev. 140, A651 (1965); W.S. Beer, Phys. Rev. 144, 734 (1966); J. Phys. Chem. Solids 28, 667 (1967); Y.T. Sihvonen, J. Appl. Phys. 38, 4431 (1967); M.I. Cohen and R.F. Blunt, Phys. Rev. 168, 929 (1968); M. Capizzi and A. Frova, Phys. Rev. Letters 25, 1298 (1970); Nuovo Cimento 5, 181 (1971); K.W. Blazey, Phys. Rev. Letters 27, 146 (1971); D. Redfield and W. Burke, Phys. Rev. Letters 28, 435 (1972).

[64] H. Unoki and T. Sakudo, J. Phys. Soc. Japan 23, 546 (1967); P.A. Fleury, J.F. Scott, and J.M. Worlock, Phys. Rev. Letters 21, 16 (1968); H. Thomas and K.A. Müller, Phys. Rev. Letters 21, 1256 (1968); G. Shirane and Y. Yamada, Phys. Rev. 177, 858 (1969).

[65] H.E. Weaver, J. Phys. Chem. Solids 11, 274 (1959).

[66] T. Sakudo and H. Unoki, Phys. Rev. Letters 26, 851 (1971).

[67] P.W. Anderson, Proc. Conf. on the Physics (Academy of Science, U.S.S.R. Moscow, 1958), p.290; W. Cochran, Adv. Phys. 9, 387 (1960).

[68] R.A. Cowley, Phys. Rev. 134, A981 (1964); W.G. Stirling, J. Phys. C5, 2711 (1972); W.G. Stirling and R. Currat, J. Phys. C9, L519 (1976); M. Iizumi, K. Gesi and J. Harada, J. Phys. C6, 2031 (1973).

[69] A.S. Barker, Phys. Rev. 145, 391 (1966).

[70] P.A. Fleury and J.M. Worlock, Phys. Rev. 174, 613 (1968).

[71] Y. Yamada and G. Shirane, J. Phys. Soc. Japan 26, 396 (1969).

[72] B. Pietrass and E. Hegenbarth, J. Low Temp. Phys. 7, 201 (1972); G. Martin and E. Hegenbarth, J. Low Temp. Phys. 18, 101 (1975).

[73] R.P. Lowndes and A. Rastogi, J. Phys. C6, 932 (1973).

[74] Y. Fujii, H. Uwe, H. Unoki, and T. Sakudo, Acta Cryst. A28, S230 (1970); W.J. Burke and R.J. Pressley, Solid State Commun. 9, 191 (1971).

[75] H. Uwe and T. Sakudo, Phys. Rev. B13, 271 (1976).

[76] H.W. Gandy, Phys. Rev. 113, 795 (1959); A.E. Paladino, L.G. Rubin, and J.S. Waugh, J. Phys. Chem. Solids 26, 391 (1965).

[77] H.P.R. Frederikse, W.R. Thurber, and W.R. Hosler, Phys. Rev. 134, A442 (1964).

[78] A.H. Kahn and A.J. Leyendecker, Phys. Rev. 135, A1321 (1964).

[79] L.F. Mattheiss, Phys. Rev. B6, 4718 (1972); B6, 4740 (1972).

[80] T.F. Soules, E.J. Kelly, D.M. Vaught, and J.W. Richardson, Phys. Rev. B6, 1519 (1972); T. Wolfram, E.A. Kraut and F.J. Morin, Phys. Rev. B7, 1677 (1973).

[81] H.P.R. Frederikse, W.R. Hosler, and W.R. Thurber, J. Phys. Soc. Japan, Suppl. 21, 32 (1966); Phys. Rev. 143, 648 (1966); Phys. Rev. 147, 583 (1966); E. Ambler, J.H. Colwell, W.R. Hosler, and J.F. Schooley, Phys. Rev. 148, 280 (1966); H.P.R. Frederikse, W.R. Hosler, W.R. Thurber, J. Babiskin, and P.G. Siebermann, Phys. Rev. 158, 775 (1967); O.N. Tufte and E.L. Stelzer, Phys. Rev. 173, 775 (1968).

[82] Z. Sroubek, Phys. Rev. B2, 3170 (1970).

[83] O.N. Tufte and E.L. Stelzer, Phys. Rev. 141, 675 (1966).

[84] F. Kucher and P. Frankus, Solid State Commun. 16, 185 (1975); Phys. Rev. B16, 874 (1977).

[85] E.R. Pfeiffer and J.F. Schooley, Phys. Rev. Letters 19, 783 (1967); J. Low Temp. Phys. 2, 333 (1970).

[86] J. Appel, Phys. Rev. Letters 17, 1045 (1966); Phys. Rev. 180, 508 (1969).

[87] Z. Zinamon, Phil. Mag. 21, 347 (1970).

[88] D.N. Eagles, Phys. Rev. 178, 668 (1969); W. Klose, H. Schuster, Solid State Commun. 6, 89 (1968); K.L. Ngai, Phys. Rev. Letters 32, 215 (1974).

[89] R.H. Lyddane, R.G. Sachs, and E. Teller, Phys. Rev. 59, 673 (1941); A.S. Barker, Phys. Rev. 136, A1290 (1964).

[90] F.W. Lytle, J. Appl. Phys. 35, 2212 (1964).

[91] W.G. Spitzer, R.C. Miller, D.A. Kleinman, and L.E. Howarth, Phys. Rev. 126, 1710 (1962).

[92] P.B. Allen, Solid State Commun. 13, 411 (1973).

[93] C.K. Jones and J.K. Hulm, Phys. Letters 26A, 182 (1968).

[94] N.E. Phillips, J.C. Ho, D.P. Woody, J.K. Hulm, and C.K. Jones, Phys. Letters 29A, 356 (1969).

[95] A.A. Abrikosov and L.P. Gor'kov, Soviet Physics – JETP 12, 1243 (1961).

[96] T. Ando, Phys. Rev. B13, 3468 (1976); Surface Sci. 58, 128 (1976).

[97] B. Vinter, Phys. Rev. B13, 4447 (1976); F.J. Ohkawa, Surface Sci. 58, 326 (1976).

[98] T. Ando, Solid State Commun. 21, 133 (1977); 21, 801 (1977).

[99] C.S. Ting, T.K. Lee, and J.J. Quinn, Phys. Rev. Letters 34, 870 (1975).

[100] J.F. Janak, Phys. Rev. 178, 1416 (1969); K. Suzuki and Y. Kawamoto, J. Phys. Soc. Japan 35, 1456 (1973); T. Ando and Y. Uemura, J. Phys. Soc. Japan 37, 1044 (1974).

[101] Y. Takada, J. Phys. Soc. Japan 43, 1627 (1977).

[102] J.C. Hensel, H. Hasegawa and M. Nakayama, Phys. Rev. 138, A225 (1965).

[103] F. Stern and W.E. Howard, Phys. Rev. 163, 816 (1967).

[104] N. Kotera, Y. Katayama, and K.F. Komatsubara, Phys. Rev. B5, 3065 (1972); A. Dearr, J.P. Kotthaus, and J.F. Koch, Solid State Commun. 17, 455 (1975); T. Kuroda and S. Narita, J. Phys. Soc. Japan 37, 1325 (1974).

[105] E.O. Kane, J. Phys. Chem. Solids 1, 249 (1957).

[106] K. Murase, K. Enjouji and E. Otsuka, J. Phys. Soc. Japan 29, 1248 (1970).

[107] P.C. Hohenberg, Phys. Rev. 158, 383 (1967).

[108] L.G. Aslamazov and A.I. Larkin, Soviet Physics – Solid State 10, 875 (1968).

[109] A. Schmid, Z. Phys. 215, 210 (1968); H. Schmidt, Z. Phys. 216, 336 (1968); E. Abrahams and J.W.F. Woo, Phys. Rev. Letters 27A, 117 (1968).

[110] K. Maki, Progr. Theor. Phys. 40, 193 (1968).

[111] S. Kawaji, private communication.

[112] J.R. Chelikowsky and M.L. Cohen, Phys. Rev. B14, 556 (1976).